ATL

[redacted]

ASTRONAUTICS
ELECTRONICS
MECHANICS
ATOMICS

GPO PRICE $ _____

CFSTI PRICE(S) $ _____

Hard copy (HC) 3.00

Microfiche (MF) .75

ff 653 July 65

ADVANCED TECHNOLOGY LABORATORIES

A DIVISION OF

AMERICAN-Standard

AMERICAN RADIATOR & STANDARD SANITARY CORPORATION

Final Report

RESEARCH ON DIFFUSION OF HYDROGEN THROUGH PALLADIUM-SILVER ALLOY

PHASE 3

ATL Job 1230502

ATL-D-1306 31 May 1965

for
National Aeronautics and Space Administration
Western Operations Office
Contract No. NAS7-118
Covering work performed from
April 1964 through May 1965

Submitted by:
R. C. Bachmann

Approved by:
R. W. Towle
J. T. Chambers

American Radiator & Standard Sanitary Corporation
ADVANCED TECHNOLOGY DIVISION
369 Whisman Road
Mountain View, California

CONTENTS

CONTENTS
(concl.)

LIST OF ILLUSTRATIONS

LIST OF ILLUSTRATIONS
(cont.)

LIST OF ILLUSTRATIONS
(concl.)

LIST OF TABLES

SUMMARY

This program was directed toward the advancement of knowledge in the field of hydrogen-gas diffusion through palladium-silver (Pd-Ag) alloy. Primary emphasis was placed on generating both experimental and analytical information that will describe the characteristics of the hydrogen-diffusion valve (static-flow-control) principle when electrical current is applied.

Diffusion elements were fabricated from various lengths (24 to 36 inches) of 0.045" ID × 0.003" wall palladium-silver-alloy tubing (75 wt.% Pd-25 wt.% Ag). The magnitude of the hydrogen diffusion was measured by causing the diffused hydrogen to flow into a vacuum chamber of known volume for a given time interval. Hydrogen-flow-rate measurements were generated as functions of the mean diffusion-element temperature, the dc power required to maintain the temperature, and the hydrogen pressure differential across the diffusion element. Correlation of data was favorable in that unit flow-rate trends were found to be generally repeatable when using a single element tested at different time intervals, different elements possessing the same length, and different elements possessing different lengths. The dynamic range of the measured flow rates was 10^3 for the mean-element-temperature interval (75 to 700°F) tested.

Utilizing the data above, an empirical equation was determined; this equation was used to predict the hydrogen-diffusion unit flow rates for specific test conditions.

Both physical and chemical contamination of the diffusion element occurred during the fabrication and data-collection processes. This contamination caused a considerable reduction in the attainable flow rate. Procedures were established to reduce the possibility of element contamination during fabrication and to insure effective decontamination of the element during data collection.

Metallurgical studies of various sections of diffusion elements indicated that both annealed and unannealed diffusion elements were used during data collection. Although the two types of elements differed significantly in physical properties, no variation was detected in the hydrogen-diffusion capabilities.

With a view to utilizing the hydrogen-diffusion principle in a low-thrust-producing device for satellite attitude-control applications, attainable thrust

levels for different thruster operating conditions were estimated and possible power-input optimization techniques were studied. Representative results of this analytical study indicate that a thruster device containing a 40-inch diffusion element at a temperature of 350°F can produce a 100-micropound thrust and that 3 watts of power would be required.

Based on the information derived from this study, three breadboard thruster models were fabricated and delivered to NASA/WOO for evaluation.

INTRODUCTION

As present and projected space payloads become increasingly sophisticated, the need grows for highly reliable thrusters that generate low thrust levels. These devices must be able to resolve extremely small angular displacements and produce minute control torques for correcting attitude errors and for compensating for external forces (gravitational and planetary oblateness, solar pressure, orbital imperfections, etc.). Control systems often call for the continuous application of thrust forces of approximately the magnitude of the prevailing disturbing forces. In addition, thrusters must possess wide dynamic range, small size and weight, low-power consumption, good response, high reliability, and long life.

Early investigations conducted at Advanced Technology Division (ATD) indicated that a static-flow-control valve based on temperature-regulated hydrogen diffusion (ref. Appendix A) through a small-diameter thin-wall palladium tube was potentially capable of satisfying the above requirements. Phase 1 of the current program was undertaken to further this investigation. The diffusion-rate characteristics of hydrogen through pure-palladium tubing were experimentally evaluated. During this investigation,[1] it was determined that because of tubing deterioration during formation of the β-phase, pure palladium would not be satisfactory as a practical static-flow-control device. Subsequent studies, however, indicated that palladium-silver alloy (75 wt. % Pd-25 wt. % Ag) does not suffer from such deterioration. Therefore, the potential use of this alloy as a static-flow-control device appeared promising.

Phase 2 of the program was initiated to obtain detailed knowledge of the parameters controlling hydrogen diffusion through a palladium-silver alloy.[2] The results of this phase provided information for defining a) the effects of tubing resistivity, b) the transient-response characteristics, and c) the effects of aging of tubing.

Upon completion of Phase 2, it was concluded that the feasibility of utilizing the hydrogen-diffusion process as a practical method of static-flow control had been established. In addition, preliminary analytical work indicated that, based on the

---

1. Superscripts indicate items in References.

measured hydrogen flow rates, the hydrogen-diffusion-valve principle could be potentially employed in an attitude-control device capable of initiating and maintaining micropound thrust levels.

Before embarking on the actual design of flight-type hardware, it was necessary to investigate other vital parameters that describe hydrogen diffusion through palladium-silver alloy. For example, certain mechanisms of diffusion flow were not well understood, nor were analytical methods available for accurate prediction of hydrogen-diffusion flow rates.

Phase 3 of the program was introduced with the following objectives:

a) Establish hydrogen-flow-rate characteristics for various lengths of palladium-silver-alloy diffusion elements operating between ambient and 400°F.

b) Develop, using data generated, empirical relationships that can be employed to predict diffusion flow rates for given operating conditions.

c) Conduct a design study directed toward defining a preliminary diffusion-valve thruster configuration and the thrust levels it would achieve.

d) Fabricate three thruster breadboard models for submission to NASA/WOO for experimental evaluation of thrust levels.

I. FORMULATION OF APPARATUS AND EXPERIMENTAL TECHNIQUES

A. Test Apparatus

The test apparatus shown schematically in Figure 1 was simular to that employed in the previous two phases.[1,2] The basic test apparatus (Figure 2) consisted of tubing and accessories to monitor hydrogen flow at two distinct levels. The high-pressure system guides and controls the flow of ultra-pure bottled hydrogen gas to the interior of the palladium-silver-alloy diffusion element; the low-pressure system guides and measures hydrogen-gas flow diffused through the element.

The high-pressure system consisted of a hydrogen supply (impurity content, air, is less than 2 ppm), a high-pressure regulator valve, a low-flow fine-control pressure regulator valve, a safety shut-off valve, a diffusion canister to house the element, and a high-pressure bleed line downstream from the diffusion canister.

The low-pressure system consisted of a cold trap; a pressure tap leading to a McLeod gage and to a collection vessel with a capacity of approximately 1 ft^3 and a pressure tap leading to a second McLeod gage and a thermocouple gage; a vapor trap; and a mechanical vacuum pump with a free-air capacity of 375 liter/min. A bypass line was positioned between the vacuum-pump inlet and the high-pressure system to permit evacuation of the interior of the palladium-silver-alloy diffusion element. A second smaller mechanical pump was used in conjunction with the McLeod pressure gages.

The diffusion elements used for hydrogen-flow-rate measurements consisted of varying lengths (between 24 and 36 inches) of 0.045" ±0.005" OD × 0.003" ±0.0003" wall palladium-silver-alloy tubing (75 wt. % Pd-25 wt. % Ag). It was planned to use only fully annealed palladium-silver-alloy tubing. However, metallurgical studies revealed that some of the diffusion elements were unannealed.

Diffusion elements were formed by winding the palladium-silver-alloy tubing into the desired cyclindrical helical shape (Figure 3). The element was separated from the baseplate of the diffusion canister by Type 304 stainless-steel tubing (3" × 0.062" OD × 0.008" wall). Since the thermal diffusivity of stainless steel is much lower than that of palladium-silver, the stainless steel minimized conductive heat losses from the element and promoted a more uniform temperature distribution.

The stainless-steel tubing passes through the diffusion-canister baseplate by means of two electrically insulated feed-throughs. One feed-through connects to the ultra-pure hydrogen source; the other leads to the downstream bleed-off valve. The diffusion element is heated by the direct passage of electric current, accomplished by connecting power leads of a variable power supply to the stainless-steel tubing.

A minimum of five iron/Constantan thermocouples was used to measure the diffusion-element temperature distribution. The leads of the butt-welded thermocouples were connected to a precision potentiometer by insulated terminals passing through the diffusion-canister baseplate. Initially, the thermocouples were attached to the element with a ceramic cement (Figure 3). This method, however, was replaced by a spot-welding technique that resulted in slightly higher and generally more consistent temperature measurements.

During the experimental portion of the program, a new diffusion canister to house the diffusion element was fabricated from stainless steel. The new canister had the same basic dimensions as the previous aluminum canister. Stainless steel was employed to further inhibit conductive heat losses and to eliminate the possibility of oxygen outgassing from the canister during the high-temperature oxygen-regeneration process (ref. Section II.B.3.).

Power measurements were made utilizing a digital voltmeter to measure the voltage drop across the diffusion element and a precision resistor (0.1 ± 0.005 ohms) in series with the element.

B. Test Procedure and Data Reduction

After proper functioning of the instrumentation was verified, permeability characteristics of the diffusion element were experimentally evaluated by generating hydrogen-diffusion flow-rate data as functions of mean tubing temperature and power input. The test procedure for the data-collection sequence is described below.

The entire low-pressure system is evacuated to approximately 5×10^{-3} torr (normal condition during the absence of hydrogen flow). At a desired pressure, hydrogen is allowed to enter the high-pressure system and is momentarily bled through the diffusion element to flush away contaminants. The dc power supply is adjusted to give the desired diffusion-element tubing temperature. When this

temperature is stable, the hydrogen diffusion through the palladium-silver element will be stable. The pressure drop across the orifice plate (situated at the entrance of the collection tank) is measured with two McLeod gages to verify steady flow. The diffused hydrogen gas is then allowed to collect in the collection tank by closing a valve between the tank and the vacuum pump. Simultaneously, the time of gas collection is measured and a sample of the diffused gas is captured in the McLeod gage that is connected to the collection vessel. Collection time varies from 30 seconds to 10 minutes, depending on the anticipated flow rate. The temperatures of the collection vessel and McLeod gage are also recorded. The valve between the collection vessel and the vacuum pump is then opened, and the system is pumped down and prepared for another test.

The temperature, volume, original and final pressures, and collection time of the captured gas are now known. The perfect gas law is used to calculate the total hydrogen flow rate. The total flow rate is converted to a unit flow rate in order to compare data obtained with different diffusion-element lengths. A sample calculation for one test is presented in Appendix B.

The measured temperature distribution of the diffusion element is converted to a mean temperature by mechanically integrating, over the diffusion-element length, the locally measured temperatures. The use of a mean temperature facilitates data presentation for the various diffusion elements tested.

II. EXPERIMENTAL STUDIES

A. Hydrogen-Flow-Rate Results

1. General

Hydrogen-flow-rate measurements were made with a number of diffusion elements. Effective diffusion lengths varied between 24 and 36 inches; hydrogen-supply pressures varied between 24.7 and 99.7 psia. Since the hydrogen gas is diffused into a vacuum, the pressure differential across the element (diffusion driving potential) is essentially the supply pressure. The majority of data collected is presented in the form of unit hydrogen flow rate as a function of mean tubing (diffusion-element) temperature and the power input required to maintain the temperature.

2. Effect of Diffusion-Element Temperature Distribution

A comparison of typical data obtained during Phase 2 with the experimental data collected during the first test series of the current phase is presented in Figure 4. The data indicate that for the same mean tubing temperatures, hydrogen flow rates obtained during the current phase with diffusion element 10 are approximately 30 to 35% higher than those obtained during Phase 2 with diffusion element 9. This difference was investigated by comparing the local temperature distributions of the two diffusion elements (see Figure 5), recognizing that the local diffusion rate is an exponential rather than a linear function of tubing temperature. Even though the mean tubing temperatures of two diffusion elements are identical, the element possessing the most uniform local temperature distribution should produce the largest unit flow rate because of the exponential temperature dependency described above. Using the available theory and empirical correlations,[3,4] local diffusion rates were calculated for the temperature distributions indicated in Figure 5. The rates were then integrated over the lengths of diffusion elements 9 and 10 and converted to average unit diffusion rates. A comparison of the resultant unit rates confirmed that for the same mean tubing temperature, diffusion element 10 should exhibit a higher unit flow rate than element 9, although the calculated increase in flow rate (17%) was not as large as the 30 to 35% measured increase.

The measured relationship between hydrogen flow rate and power input for element 10 is shown in Figure 6. As shown, element 10 required approximately 10 to

15% less power to achieve a given flow rate than did element 9. This reduction in power input is supported by typical temperature distributions measured along elements 9 and 10. The temperature-distribution curves (see Figure 5) indicate that while both diffusion elements had approximately equal mean tubing temperatures, element 10 had much smaller temperature gradients and maintained end-point temperatures of 50 and 120°F higher than element 9. The above conditions promoted lower heat losses and a corresponding smaller power input for element 10.

3. Effect of Diffusion-Element Length

Data were collected with test element 11 (effective diffusion length = 24 inches) at hydrogen supply pressures of 49.7, 64.7, and 99.7 psia. The results are presented in Figures 7 and 8 in terms of unit hydrogen flow rates as functions of mean effective tubing temperature and power input. Generally, the results exhibit favorable correlation with Phase 2 data (see Figures 9 and 10) in that both sets of data suggest similar trends.

The data scatter in Figure 7 is greater than that shown in Figure 8. This is reasonable since the tubing temperature is determined by calculating the mean temperature from the temperature distribution measured over the test element, while the power input is measured directly, using a digital voltmeter and a precision resistor. Thus the margin of uncertainty is reduced when the hydrogen flow rates are presented in terms of dc power input. It is also encouraging to note that, in general, the degree of data scatter in the current phase was less than that of the previous phases.[1,2]

Data collected with diffusion element 12 (effective diffusion length = 30 inches) at hydrogen supply pressures of 49.7, 64.7, and 99.7 psia are presented in Figures 11 and 12. Note that the different pressure levels did not produce a family of curves for the measured hydrogen flow rates, whereas data obtained with previous elements clearly indicated trends dependent upon the hydrogen supply pressure. This discrepancy is believed to result from inaccurate flow-rate determination attributable to improper instrumentation and measurement techniques. The problem was alleviated by improving the power-measurement technique and assuring that both the mercury and the glass components used in the McLeod pressure gages were clean and free from contaminants.

Figures 13 and 14 compare partial data obtained using elements 10 and 12. Both these elements have an effective diffusion length of 30 inches. The data obtained using element 10 is believed to be most representative of hydrogen flow rate through a 30-inch diffusion element for the indicated conditions, because the collection of this data did not meet with the instrumentation difficulties described above.

Initial data collected with a 36-inch diffusion element (13) are shown in Figures 15 and 16. During data collection, a leak was detected at one end of the brazed joints connecting the palladium-silver tubing to the stainless-steel tubing. The leak significantly altered the measured flow rates (see Figures 15 and 16). Data collection was therefore temporarily discontinued to allow necessary repairs. Because of these repairs, the effective diffusion length of the diffusion element was reduced to 34 inches.

Upon resumption of testing, a number of flow-rate measurements for a hydrogen supply pressure of 24.7 psia were made to determine whether this lower pressure would produce any significant change in the flow-rate trends previously measured for the higher supply pressures (49.7, 64.7, and 99.7 psia). Results are presented in Figures 17 and 18. Data for the 24.7-psia hydrogen supply pressure indicated that an inflection point occurs in the flow-rate trends at a tubing temperature in the vicinity of 320°F and a power input of 11.2 watts. This point suggests an upper operating limit (24.7-psia pressure differential) beyond which increased flow can be obtained only at unreasonably large expenditures of power. The flow rates measured for the hydrogen supply pressures of 49.7 and 64.7 psia suggest similar trends, but the inflection points are displaced to higher temperatures.

Based on the above results, an additional test series was initiated to confirm and further investigate the nature of the observed inflection point in the hydrogen-flow-rate data. A new element with a 24-inch diffusion length (diffusion element 15) was utilized for this study. A length of 24 inches was chosen in the hopes of establishing the presence of the observed inflection points when using different diffusion elements and the repeatability of data when using different elements of the same effective diffusion length. The experimental results presented in Figures 19 and 20 indicate an inflection point occurring in the hydrogen-flow-rate trend at a mean effective tubing temperature

of approximately 360°F and a power input of 11.7 watts. Note that the pressure differential across the element is 64.7 psia. Beyond this inflection point, the rate of increase in the hydrogen flow rate declines appreciably with increasing temperature (power) to a tubing temperature of 420°F and a power input of 14.5 watts. However, a further increase in tubing temperature (power) promotes a significant increase in the hydrogen flow rate, and the trend of the data approaches the form previously exhibited at the lower temperatures (below approximately 350°F). The form of the inflection points shown in Figures 19 and 20 is different from that suggested by either Figures 17 and 18 or the results of Phase 2. They are, however, similar to the inflection-point characteristics of the diffusion elements in Phase 1.

Results obtained with element 15 further indicate that within the applicable ranges, the data shown in Figures 19 and 20 compare favorably with results previously obtained with a 24-inch element (11). In particular, the flow-rate trends are basically identical when the comparison is made in terms of power input, thereby indicating that repeatable data are obtained when using different elements of the same diffusion length. However, with regard to tubing temperature, repeatability of the flow-rate data is not as impressive, although identical trends are clearly indicated for elements 11 and 15. The apparent nonrepeatable nature of the flow-rate data as a function of temperature for these two dimensionally identical elements was caused by the difficulties in measuring the tubing temperature during testing of element 15. Many thermocouples near the two termination points of this element were found to short out against the diffusion canister. Consequently, the mean tubing temperature indicated by the remaining thermocouples, i.e., those near the center of the element, was representative only of the center portion of the element. Therefore, the actual mean tubing temperature of element 15 at a given flow rate is lower than that indicated in Figure 19.

A comparison of Phase 3 data with portions of Phase 2 results is shown in Figures 21 and 22. Note the excellent repeatability of the flow-rate data for a 24-inch element shown in Figure 22. Results shown in these figures suggest that the employment of diffusion elements of varying length will produce identical trends in the flow-rate data and, generally, repeatable results. Maximum data scatter in Figure 22 is about 20%.

4. Ambient Diffusion Rates

A test series was conducted to determine the presence of hydrogen diffusion at mean tubing temperatures in the 75 and 100°F temperature ranges. A 24-inch element (15) was used. The flow-rate-measurement procedure employed was identical to that previously used, but the collection time was increased from 30 seconds to 10 minutes. Since the magnitude of the hydrogen-flow-rate measurements would be small, it was necessary to estimate the magnitude of the gas pressure rise in the collection vessel that occurred independently of the diffused-hydrogen-gas flow. This pressure rise is essentially due to the gas leakage from the atmosphere into the collection system and the outgassing in the collection system. The results of these tests are presented in Tables I, II, and III.

The flow rates presented in Table I were obtained using the rates of pressure rise (also shown in Table I) measured in the collection system when the diffusion element was subjected to a 64.7-psia hydrogen supply pressure (effectively a 64.7-psia pressure differential across the diffusion element) and to the indicated temperatures. These flow-rate calculations were based on the assumption that the pressure rise (given in Table I) in the collection system was entirely due to hydrogen diffusion through the element and not associated with either leakage or outgassing. The resulting average unit hydrogen flow rate is 3.9×10^{-10} lbm/sec-in.^{2}/0.001 in. for element temperatures of approximately 75°F and an average rate of 5.3×10^{-10} lbm/sec-in.^{2}/0.001 in. at an average temperature of 104°F.

Table II compares the measured rates of pressure rise in the collection vessel for the indicated diffusion-element temperatures with the indicated pressure differentials across the diffusion element: 64.7 psia (hydrogen supply pressure used in determining results in Table I) and 10×10^{-3} torr (effective hydrogen supply pressure of zero psia). A comparison of the rates of pressure rise for these two conditions indicates that they are of the same order of magnitude and are approximately the same value. This immediately suggests that the leakage and outgassing in the experimental apparatus become quite prominent if the apparatus is utilized in measuring hydrogen flow rates at diffusion-element temperatures in the ambient range. Table II further indicates that the assumption discussed above (see preceding paragraph) is

TABLE I

PARTIAL RESULTS OF HYDROGEN-GAS FLOW-RATE MEASUREMENTS FOR A 24-INCH DIFFUSION ELEMENT AND THE INDICATED CONDITIONS

Diffusion-Element Temperature (°F)	Rate of Pressure Rise* (torr/minute)	Unit Mass Flow Rate (lbm/sec-in.^{2}/0.001 in.)
74	3.8×10^{-3}	3.2×10^{-10}
74	4.0×10^{-3}	3.3×10^{-10}
74	4.4×10^{-3}	4.0×10^{-10}
75	4.8×10^{-3}	4.3×10^{-10}
76	4.3×10^{-3}	3.8×10^{-10}
76	5.4×10^{-3}	4.9×10^{-10}
103	6.1×10^{-3}	5.2×10^{-10}
105	6.2×10^{-3}	5.4×10^{-10}

* Rate of pressure rise measured in the collection tank for a pressure differential of 64.7 psia across the diffusion element.

TABLE II

COMPARISON OF RATE OF HYDROGEN-GAS PRESSURE RISE IN THE COLLECTION VESSEL FOR A 24-INCH DIFFUSION ELEMENT SUBJECTED TO THE INDICATED CONDITIONS

Diffusion-Element Temperature	Rate of Pressure Rise (torr/minute)	
(°F)	$\dot{P}_{vacuum}$ *	$\dot{P}_{64.7\ psia}$ **
74	3.0×10^{-3}	3.8×10^{-3}
74		4.0×10^{-3}
74		4.4×10^{-3}
75	4.6×10^{-3}	4.8×10^{-3}
76	2.5×10^{-3}	4.3×10^{-3}
76	3.7×10^{-3}	5.4×10^{-3}
80	3.1×10^{-3}	
102		6.1×10^{-3}
103	3.2×10^{-3}	6.2×10^{-3}
105	3.3×10^{-3}	

* $\dot{P}_{vacuum}$ = rate of pressure rise measured in the collection tank for a pressure differential of less than 10×10^{-3} torr across the diffusion element.

** $\dot{P}_{6.47\ psia}$ = rate of pressure rise measured in the collection tank for a pressure differential of 64.7 psia across the diffusion element.

TABLE III

PERTINENT RESULTS OF HYDROGEN-GAS FLOW-RATE MEASUREMENTS FOR A 24-INCH DIFFUSION ELEMENT AT 75°F AND 64.7-PSIA HYDROGEN SUPPLY PRESSURE - BASED ON THE RESULTS OF SIX TESTS

Average Diffusion-Element Temperature	Rate of Pressure Rise (torr/minute)		Average Unit Mass Flow Rate (lbm/sec-in.^{2}/0.001-in.)		
(°F)	$\dot{P}_{vacuum}$ *	$\dot{P}_{64.7\ psia}$ **	$\dot{M}_{Cor}$ †	$\dot{M}_{Uncor}$ ††	$\dot{M}_{Calc}$ ‡
75	3.4×10^{-3}	4.5×10^{-3}	1.1×10^{-10}	3.9×10^{-10}	3.5×10^{-10}

* $\dot{P}_{vacuum}$ = rate of pressure rise measured in the collection tank for a pressure differential of less than 10×10^{-3} torr across the diffusion element.

** $\dot{P}_{64.7\ psia}$ = rate of pressure rise measured in the collection tank for a pressure differential of 64.7 psia across the diffusion element.

† $\dot{M}_{Cor}$ = average unit mass flow rate based on laboratory measurements which account for leakage and outgassing effects.

†† $\dot{M}_{Uncor}$ = average unit mass flow rate based on laboratory measurements which do not account for leakage and outgassing effects.

‡ $\dot{M}_{Calc}$ = unit mass flow rate calculated for test conditions using results in Section II. D.

questionable; consequently, the actual diffusion rates resulting from the hydrogen-diffusion process at an element temperature of 75°F are significantly less than those presented in Table I.

The diffusion rates exhibited by the element subjected to a 64.7-psia hydrogen supply pressure and a mean temperature in the 75 and 100°F ranges can be more realistically estimated by recognizing the leakage and outgassing effects (see Table III). Note that in the 75°F temperature range, the average rate of pressure rise in the collection tank for a 64.7-psia pressure differential across the diffusion element is 4.5×10^{-3} torr/minute. The corresponding average pressure rise for a 10×10^{-3} torr pressure differential (effectively no pressure differential) is 3.4×10^{-3} torr/minute. Therefore, the indicated pressure rise caused purely by hydrogen diffusion is approximately 1.1×10^{-3} torr/minute, which results in a hydrogen flow rate of 1.1×10^{-10} lbm/sec-in.^{2}/0.001 in. This is approximately 75% lower than the values indicated in Table I.

Using equation 1 (ref. Section II.D), a predicted value of the hydrogen-diffusion rate was determined for the test conditions (64.7-psia pressure differential across the diffusion element at 75°F). This value, 3.5×10^{-10} lbm/sec-in.^{2}/0.001 in., exhibits encouraging agreement with measured results.

B. Diffusion-Element Contamination

1. Effects of Contamination

The initial unit hydrogen flow-rate data obtained using diffusion elements 11 and 13 and previous results are compared in Figure 23 as a function of mean effective tubing temperature. Element 11 had an effective diffusion length of 24 inches; element 13 had an initial length of 36 inches. For a given tubing temperature, the indicated flow rates do not immediately suggest any direct correlation between the various diffusion lengths tested.

However, a comparison of the flow rates determined for element 13 on 7-31-64 with those of 8-3-64 suggests the basis of this discrepancy. After the data of 7-31-64 were collected, a leak was detected in the stainless-steel transition tubing of element 13. During repair, the surface of the element was accidentally brought into contact with hydrocarbon impurities. When the test series was resumed

on 8-3-64, it became apparent that the previous unit flow rates of 7-31-64 could not be duplicated because of this contamination.

Figure 24 shows the unit flow rate as a function of the power necessary to heat the test element to a desired mean temperature. The results, similar to those presented in Figure 23, suggest that since the power input and mean tubing temperature are measured independently, the experimental measurement procedure does not promote the discrepancies noted in the data for elements 10, 11, and 13.

The actual flow-rate data for element 13 are shown in Figure 25. These data indicate that within a given series, the measured flow-rate trends are generally consistent in that a minimum of scatter is exhibited and the rates can be easily represented by a single curve.

The McLeod pressure gages used in determining hydrogen flow rates were cleaned and checked periodically throughout the experimental work; therefore, a relatively high degree of confidence can be placed in this instrumentation. It was therefore concluded that the low flow rates measured for elements 11 and 13 were related to contamination of the test elements.

2. Cause of Contamination

The presence of contamination of a palladium-alloy diffusion element is not a problem that is unique only to this experimental study. Contamination of a hydrogen-diffusion membrane appears to be the rule rather than the exception, and reported hydrogen-permeation rates vary accordingly. The actual contamination is a result of both element poisoning, a chemical effect, and element asphyxiation, a physical effect.[5]

Element poisoning at the tubing temperatures encountered in this test program can usually be attributed to unsaturated hydrocarbons, hydrogen sulfide (sulfur-bearing gases), chlorine-bearing gases, and mercury. Diffusion-element asphyxiation is due to the stagnant layer of foreign gas that builds up in the interior of the diffusion element. This stagnant gas cuts the partial pressure difference of the hydrogen and, thus, the driving force necessary for diffusion.

It is evident that contamination of a hydrogen-diffusion element can exert significant influence on the magnitude of the resultant diffusion rates. Methods to

eliminate its detrimental effect must be devised before other hydrogen-diffusion characteristics can be validly evaluated. Therefore, an intensive study was conducted to establish a standard laboratory procedure that would reduce the possibility of diffusion-element contamination during fabrication and to insure proper decontamination of the element during data collection. The procedure is described in succeeding paragraphs.

3. Reduction and Control

All diffusion elements are fabricated from 0.045" OD × 0.003" wall tubing of palladium-silver fully annealed alloy (75 wt.% Pd-25 wt.% Ag) certified by a certificate of compliance (see Section II.C.). Before the element is fabricated, the palladium-silver tubing is cleaned according to steps outlined in the Tube Laboratory Manual.[6] These steps consist of a rinse in acetone, a rinse in three changes of trichlorethylene, a rinse in two changes of methyl alcohol, and drying in warm air between 70 and 100°C. Polyethylene gloves are worn by all personnel throughout the cleaning and fabrication process.

The cleansed palladium-silver tubing is wound into the desired helical shape and then brazed to the stainless-steel tubing. A hydrogen flame is used for brazing to eliminate the impurities produced by an oxyacetylene system. The same hydrogen gas supply is used for brazing and for actual diffusion tests. The impurity content of the gas is certified to be less than 2 ppm. Brazing flux is applied to all portions of the diffusion-element surface that may come into contact with the flame, to further reduce the possibility of impurity formation. The brazed joints are scrubbed to remove the excess flux, after which the entire system is again cleaned according to the procedure noted above. The element is then mounted in the diffusion canister and the entire system is evacuated.

After proper functioning of the instrumentation is verified, the diffusion characteristics of the element are evaluated by generating data on unit hydrogen flow rate as a function of mean effective tubing temperature. If the data indicate low flow rates that are traceable to a contaminated element, a decontamination process is initiated.

Asphyxiation can be easily eliminated by attaching a bleed valve to the diffusing system. Any stagnant gas can then be removed by flushing the diffusion element with the ultra-pure hydrogen gas used for diffusion.

Removal of chemical poisonong, however, is much more involved. Poisoning due to organic materials can be alleviated by regeneration treatments. Regeneration is usually accomplished by exposing the element to air at a high temperature and then re-introducing hydrogen after removing the air. The regeneration method found most effective in the present study, however, consists of exposing the entire surface area of the diffusion element to pure oxygen. This regeneration process is carried out at mean tubing temperatures of at least 700°F (regeneration temperatures as high as 1200°F have been employed) with an oxygen pressure of 20 psig for at least 15 minutes.

Other decontamination processes which produced noticeable but less significant results include continuous hydrogen diffusion for at least 24 hours at a tubing temperature of 500°F and cyclic hydrogen diffusion after the temperature of the element is raised to 700°F in vacuum. Figure 26 compares the relative merits of these decontamination methods.

C. Metallurgical Study

1. Diffusion-Element Deformation

Application of the high-temperature oxygen-regeneration process to the diffusion elements caused a number of them to deform noticeably. In fact, the deformation was often of such magnitude that the elements made contact with the stainless-steel transition tubing and/or diffusion canister and resulted in electrical shorting. In these extreme cases, the diffusion elements were rendered useless for further experimental work.

Methods to eliminate or reduce the element deformation were studied. The most successful solution to this problem was to reduce the thermal shock effects by eliminating large, sudden temperature changes during oxygen regeneration, and to support the diffusion element with thin braces fabricated from mica sheets. The

braces added substantial support to the diffusion-element coils and prevented them from shorting against each other, the stainless-steel transition tubing, or the diffusion-canister interior. Figure 3 shows a typical test element supported by three of the mica braces.

2. Metallurgical Comparison of Elements

The deformation problems described above were not present in all of the oxygen-regenerated diffusion elements. In fact, deformation characteristics were exhibited only by elements fabricated from the first of the two shipments of tubing received. The elements that did not warp during oxygen regeneration (shipment no. 2) were also found to possess several other properties absent from the deformed elements (shipment no. 1). For example, the tubing from shipment no. 2 was much easier to form into the desired diffusion-element shape. This shipment also exhibited a softer, smoother tubing-surface texture. Photomicrographs of various diffusion-element specimens, taken to further investigate differences between the two shipments, are shown in Figure 27. Although both shipments include a certificate of compliance stating that the tubing was fully annealed, the photomicrographs show that shipment no. 1 was not annealed and shipment no. 2 was annealed. Note that in Figure 27 there are no distinct equiaxial grain boundaries present in the unannealed tubing. Rather, the grain structure appears to be stretched and gives definite indications of cold working. The evident cold working is a result of the extrusion processes used during the formation of the tubing. When the elements fabricated from this shipment of tubing were regenerated, a certain amount of stress relieving probably occurred. However, actual recrystallization of the grain structure, which occurs during annealing, was not initiated. This is reasonable since the annealing temperature of palladium-silver alloy is approximately 1600°F. The results of the photomicrograph study were forwarded to the tubing supplier. They agreed that, based on Figure 27, shipment no. 1 had not been annealed as requested.

It is interesting to note that no difference was detected in the diffusion rates between the unannealed and the annealed diffusion elements. Nevertheless, the annealed tubing is desirable; elements fabricated from this tubing are easily shaped and will not readily deform under thermal shock.

D. Empirical Correlation of Data

The design of devices based on the diffusion-valve principle requires the capability to predict hydrogen flow rates with reasonable accuracy for given operating conditions. Generally, analytical techniques are not available and empirical data must be utilized. A brief study was therefore conducted to establish an equation relating unit hydrogen flow rate through palladium-silver-alloy tubing to tubing temperature, wall thickness, surface area, and pressure differential across the tubing. Utilization of the data collected for the 24-inch element (11) resulted in the following tentative equation.* The procedure for determining this equation is outlined in Appendix C.

$$\dot{M} = \frac{3.82 \times 10^{-2} \, A \, e^{-11,120/T} \sqrt{\Delta P}}{h} \quad . \tag{1}$$

Upon initiation of the above study, it was planned that subsequently compiled data would be employed to further define the magnitude of the constants in equation 1. However, as the program developed, it became evident that, due to the importance of the remaining tasks, additional work on this subject could not be carried out.

Typical comparisons of the diffusion rates predicted by equation 1 with measured values are shown in Figures 28 and 29.

* See Nomenclature for definition of all symbols.

III. THRUSTER DESIGN APPLICATION

The experimental work throughout this program clearly establishes the utility of the hydrogen-diffusion principle as a practical static-flow-control method. An additional feature of this concept is the capability to produce and maintain extremely small flow rates. Because of this capability, the diffusion-valve principle appears promising in fulfilling requirements associated with micropound-range thrusters.

A. Analysis of Flow Regime

With a view to the above thoughts, an estimate was made of the theoretical thrust levels that can be produced by measured hydrogen flow rates passing through an appropriately designed thrust chamber. Before preliminary design calculations could be made, however, it was necessary to describe the type of flow present in an orifice or nozzle operating at the low pressures and the flow rates encountered during the experimental portion of this program, and to affirm that viscous-flow relationships can be validly employed in the design calculations.

One criterion for the type of flow under low-pressure conditions is the Knudsen number, which is defined as the ratio of the mean free path to a characteristic dimension of the system. The mean free path of hydrogen can be determined from[7]

$$\lambda = \frac{\mu}{0.5\ U\ \rho} \quad . \tag{2}$$

The applicable characteristic dimension for the present experimental system is the orifice diameter (0.073 inch). It can be shown that the limits of the various flow regimes in terms of the Knudsen number are:

Viscous flow	$\lambda/D < 0.01$
Transition flow	$0.01 < \lambda/D < 1.00$
Molecular flow	$\lambda/D > 1.00$

Viscous flow denotes that intermolecular collisions predominate in determining the characteristics of the flow. Because of the large number of intermolecular collisions, the gas acts as a continuous or viscous medium. However, when the mean free path of the molecules is greater than the characteristic dimension, the flow is described by collisions between molecules and the wall, not by collisions between molecules alone.

Since there are comparatively few intermolecular collisions, each molecule acts independently of the others. This type of flow is called free-molecule flow. For an average pressure of 0.75 mm across the orifice, the Knudsen number was found to be 2.04×10^{-3}. This value clearly falls within the limits of viscous flow, as shown above. The operating condition corresponds to hydrogen diffusion through a 24-inch element at a tubing temperature equal to approximately 340°F.

Another criterion describes the boundaries of various flow regimes in terms of the Mach and Reynolds numbers:[8]

Molecular and transition flow	$M/Re = 3\text{-}10$
Transition and slip flow	$M/Re = 0.1$ for $Re < 1$
	$M/\sqrt{Re} = 0.1$ for $Re > 1$
Slip and viscous flow	$M/Re = 0.01$ for $Re < 1$
	$M/\sqrt{Re} = 0.01$ for $Re > 1$

The lack of precision in the definition of these boundaries is apparent, since the same order of magnitude is used for the regime boundaries defined by both M/Re and $M/\sqrt{Re}$.

The region of flow described as slip flow exists when the Reynolds number is too low for the boundary-layer theory to be completely valid but not low enough to permit viscosity effects to be neglected. Thus, it is necessary to demonstrate that the hydrogen flow experienced throughout the test program was either completely viscous or, if the flow was in the slip region, at least approached the slip viscous boundary.

The Mach number can be determined by

$$M = \frac{(K)\ Re}{\sqrt{\pi K/2}} \quad , \tag{3}$$

where

$$Re = \frac{4\dot{m}}{\pi \mu D} \quad . \tag{4}$$

$M/\sqrt{Re}$ was found to be 3.96×10^{-3} for an average pressure of 0.75 mm across the orifice. It is apparent, therefore, that viscous flow was present in the flow system. Thus, the standard viscous-flow relationships can be utilized in determining the various thrust parameters.

B. Analytical Estimation of Thrust Parameters

1. Thrust Calculations

An estimate was made of the theoretical thrust levels that could be produced by measured hydrogen flow rates and a convergent-nozzle configuration. The results were then utilized to generate a family of curves illustrating the thrust levels as functions of different nozzle throat diameters and various lengths of 0.045" OD × 0.003" wall palladium-silver tubing diffusing hydrogen gas at temperatures between 160 and 400°F. A convergent-nozzle configuration was chosen instead of the convergent-divergent type because of the resulting simplicity of the analytical work and a consideration of the potential thruster application (see Section III.C.). The approach used to determine the thrust levels and construct the performance curves is described more fully in following paragraphs. The type of thruster system being analyzed is illustrated in Figure 30, where location 2 corresponds to the exit throat section of the nozzle.

The total mass flow rate that can be produced by a given tubing length at a given temperature can be easily calculated by utilizing the unit hydrogen flow rates previously determined for a hydrogen supply pressure of 64.7 psia (essentially the pressure drop across the Pd-Ag tubing lengths). These calculations were made for Pd-Ag tubing lengths of 10, 20, 30, 40, and 50 inches, diffusing hydrogen at temperatures between 160 and 400°F. An upper temperature limit of 400°F was chosen on the basis of the previously discussed inflection point, which occurred in the mass flow-rate trends at approximately 400°F for a hydrogen supply pressure of 64.7 psia.

Isentropic relations can be applied to the flow in the thruster nozzle (see Figure 30) by employing the usual simplifying assumptions of no friction effects and no heat transfer to the walls. Based on the potential use of the thruster, it can also be assumed that the working substance (diffused hydrogen) exhausts to a vacuum; thus, sonic flow conditions will exist in the nozzle throat section. It is further assumed that the temperature of the hydrogen gas in the thrust chamber is equal to the mean effective temperature of the Pd-Ag tubing. The mass flow rate, defined by

$$\dot{m} \doteq \rho V A \quad , \tag{5}$$

can also be expressed by

$$\dot{m} = \frac{A_t P_1}{\sqrt{T_1}} \sqrt{\frac{g_c \gamma}{R} \left(\frac{2}{\gamma + 1}\right)^{\frac{\gamma+1}{\gamma-1}}} \tag{6}$$

for flow through a nozzle with critical conditions existing in the throat section (choked flow).[9] Thus, for a given nozzle throat diameter, equation 6 can be used to calculate the chamber pressure for a given total hydrogen flow rate. Using the flow rates and the temperature range considered above, chamber pressures were calculated for nozzle throat diameters of 0.02, 0.04, 0.07, 0.10, and 0.13 inch. These chamber pressures were then utilized in calculating thrust levels.

An application of the momentum principle to the system shown in Figure 30 results in the following expression for the thrust produced:

$$F = \frac{\dot{m} V_2}{g_c} + (P_2 - P_3) A_2 \quad . \tag{7}$$

Equation 7 can be expanded and modified to

$$F = C_F P_1 A_t \quad , \tag{8}$$

where C_F, the ideal thrust coefficient, can be defined by[10]

$$C_F = \sqrt{\frac{2\gamma^2}{\gamma - 1} \left(\frac{2}{\gamma + 1}\right)^{\frac{\gamma+1}{\gamma-1}} \left[1 - \left(\frac{P_2}{P_1}\right)^{\frac{\gamma-1}{\gamma}}\right]} + \frac{P_2 - P_3}{P_1} \frac{A_2}{A_t} \quad , \tag{9}$$

which results in a value of 1.27 for a convergent sonic nozzle passing hydrogen gas into a vacuum.

However, because of the presence of a) low mass flow rate and Reynolds number and b) small nozzle diameters, the boundary layer on the nozzle wall could potentially fill the nozzle throat section. In this case, the frictional and pressure effects in the boundary layer can cause the ideal thrust coefficient to vary significantly from its predicted value. Research performed at NASA/Ames Research Center indicates that the thrust coefficient does indeed vary noticeably with nozzle

shape for regions of low mass flow rates.[11] The applicable results of this study are presented in Figure 31. Using these results and equation 8, thrust levels were calculated for the selected throat areas. Typical results are shown in Figure 32. The curves shown serve to illustrate the various thrust levels that can be attained through different combinations of effective palladium-silver-tubing diffusion lengths, diffusion temperature, and convergent-nozzle throat diameter. For example, a thruster chamber containing a 10-inch element at 300°F and exhausting through a 0.02-inch throat diameter to a vacuum would produce 10 micropounds of thrust. Similarly, a 50-inch element at 310°F exhausting through a 0.13-inch throat diameter to a vacuum could theoretically produce 100 micropounds of thrust. Note that the flow-rate magnitude measured at ambient condition (see Section II.A.4) would theoretically cause a thrust in the 0.02-micropound range.

Magnitudes of the thrust levels presented in Figure 32 generally correspond to the maximum values attainable for the indicated thrust-chamber configuration and the specific diffusion-element operating conditions. It should be emphasized that these thrust levels do not represent the maximum values for a thruster system employing the diffusion-valve principle and that the thrust-level magnitude can be increased in direct proportion to the increase in the hydrogen-gas flow rate.

Many potential diffusion-valve applications would, of course, benefit from increased hydrogen-gas flow. For a given diffusion element, the mass flow rate can be easily increased by raising the element temperature and/or the hydrogen supply pressure. However, caution is necessary in this respect, because experimental results show that the rate of increase of hydrogen-diffusion flow rate with element temperature can be strongly influenced by the gas-supply pressure. For example, an unfavorable inflection point in the flow-rate trend is exhibited by the data at an element temperature equal to approximately 400°F when the gas-supply pressure is 64.7 psia. This inflection point, however, is displaced to higher temperatures if larger supply pressures are utilized. This flow-rate characteristic is not unique in that it has been encountered by other investigators[12] who have measured hydrogen-diffusion rates using elements operating at 900°F and supply pressures of 800 psig. Measured flow rates as high as 30×10^{-7} lbm/sec were reported for a diffusion

element 1 foot in length. Thus, flow-rate and thrust-level magnitudes larger than those discussed in this report can be readily obtained if desired.

Note that based on equations 6 and 8, it can be initially assumed that the thrust is independent of the throat area. This is not true, however, because the thrust coefficient varies with the throat diameter. The effect of this variation on thrust levels can be seen in Figure 32. For a given mass flow rate, established by the selection of the diffusion-element length and temperature, different thrust levels can be produced. The magnitude of the thrust level will increase with the throat diameter in the same manner that the thrust coefficient increases with the throat diameter.

2. Specific-Impulse Evaluation

The specific impulse is also an important parameter in determining rocket performance. It is a characteristic of fuel economy and can be defined as the thrust level produced by a device with a propellant weight flow rate of unity. Specific impulse is usually expressed as

$$I_s = F/\dot{w} \quad , \tag{9}$$

which can be expanded to[10]

$$I_s = \frac{C_F \sqrt{T_1}}{\sqrt{\frac{g_c \gamma}{R} \left[\frac{2}{\gamma + 1}\right]^{\frac{\gamma+1}{\gamma-1}}}} \quad . \tag{10}$$

Using the above relation, specific-impulse magnitudes were determined for hydrogen gas exhausting through a convergent nozzle into a vacuum. The results are shown in Figure 33 as functions of gas temperature and nozzle throat diameter. Note that specific-impulse values for a hydrogen-diffusion thruster indicated in Figure 33 are quite high when compared to values for other gases and also compare favorably to values for chemical rocket systems. This result should not be surprising because specific impulse is inversely proportional to the square root of the molecular weight, and hydrogen has a small molecular weight.

C. Rarefied-Flow Nozzle Characteristics

An optimum nozzle design depends on a number of practical considerations. Primary among these considerations is a description of both the working substance (solid, liquid, gas, etc.) and the type of propulsive device (chemical, electrical, etc.). For example, in most rocket-propulsion applications, a very large stagnation pressure exists upstream of the nozzle. This pressure dictates a more critical design of the divergent portion of a nozzle than of the convergent portion, because when the high stagnation pressure expands through the divergent section, the resulting large kinetic energy of the expanding gas can promote significant momentum and energy losses.

However, for thruster applications involving nozzles that must pass very low-density gas (small stagnation pressure), different and often new nozzle design problems are encountered. Because of the growing interest in this type of nozzle application, a number of experimental and analytical studies have recently been conducted.[11-15] Typical results indicate that if a gas is flowing in the viscous regime but borders on the viscous-transition boundary, the variation of nozzle geometry between convergent, convergent-divergent, or sharp-edge orifice types will produce little change in some of the flow characteristics. In particular, for a low-density gas-flow (low stagnation pressure) application such as described in this report, the convergent-divergent nozzle appears to act as a convergent nozzle in that it allows for only minor pressure recovery; i.e., there is almost no pressure to recover.

Many problems encountered in low-density flow are caused by deviations from the "ordinary" description of viscous flow. Primary among these deviations is the effect of increased boundary-layer growth in the nozzle throat section. The detrimental effects of the boundary layer can be reduced by insuring that, although the throat section is extended to give the gas stream direction and stability, this extended length is not so large as to promote excessive boundary-layer growth. Excessive boundary-layer growth can also be caused by flow separation at the upstream end of the throat section. Such flow-separation effects can be checked by forming a symmetrical well-rounded nozzle entrance and a sharp-edged exit section.

D. Power-Requirement Study

1. Correlation of Power Input for Laboratory Diffusion System

The total power input required to produce a given thrust is one of the critical design parameters for a thruster application of the type described in this report. When applied to a thruster employing the diffusion-valve principle, the magnitude of the power input is controlled primarily by the heat-loss modes from the thruster package. Consequently, detailed knowledge of both the heat-loss mechanisms and their magnitudes is a prerequisite for an optimized thruster design. With this in mind, a study was undertaken to compare, for given laboratory operating conditions, the power input measured during collection of hydrogen-flow-rate data with the power input calculated by a heat-transfer analysis. The laboratory conditions consisted of hydrogen diffusion through a 24-inch element subjected to a pressure differential of 64.7 psia and a mean temperature of 400°F. The calculated power requirement is based on a steady-state heat balance applied to the appropriate portion of the laboratory test system. The end product of this analysis can then be potentially correlated to the actual measured results. Based on a resulting successful correlation, the analytical methods can be further applied to various potential thruster designs to generate a power-optimized thruster design.

Using the analytical approach presented in Appendix D, the theoretical power requirements for the described laboratory operating condition was calculated to be 15.4 watts, compared to the measured power input of approximately 16.5 watts. The analysis indicated that the power-input magnitude accounts for heat losses from the diffusion element to the interior of the thruster canister. The calculated power requirement (15.4 watts) was composed, in part, of a 6.5-watt radiant loss and a 7.8-watt natural convection loss. Conduction losses along the diffusion-element length were found to be negligible. The remaining power input, 0.77 watt, was required to increase the enthalpy of the hydrogen gas from ambient (storage) temperature to the diffusion temperature. This power requirement (0.77 watt) does not, of course, represent an actual heat loss; rather, it dictates the theoretical minimum power requirement that might result if the thruster system were perfectly insulated and therefore not subjected to heat-loss effects.

Results of the power-requirement study suggested that a number of significant parameters exist that have a pronounced effect on the heat-loss magnitudes and consequently on the power-input requirements for an extremely low-level thruster configuration. For example, certain of the equations (see Appendix D) indicate that optimization of a thruster design with respect to power would include holding the areas A_1 and A_2 to a minimum value while maintaining the ratio A_1/A_2 as close as possible to unity.

2. Power-Input Optimization

The favorable correlation exhibited by the two total power-input magnitudes (calculated versus measured) discussed above suggests that if the operating conditions are known, a meaningful estimate of the power input needed to produce a given thrust can be calculated for various thruster designs. Consequently, the heat-transfer analysis was repeated for thruster designs varying in insulative capabilities. The insulative conditions were generated by employing radiation shields between the diffusion element and the thruster body. Use of such shielding with various thermocouple arrangements is a popular means of reducing radiant-heat losses from thermocouples during convection gas-temperature measurement.[15] The shields are made of very thin high-conductivity and high-reflectivity material.

Note that in the previous power-requirement study (ref. Section III. D. 1), the dimensions of both the diffusion element and the thruster body were identical to diffusion element 10 and the laboratory diffusion canister (ref. Appendix D, Figure D-1). Results presented below are based on calculations made for this system with the addition of 1, 2, and 3 intermediate radiation shields evenly spaced between the element and the interior of the diffusion canister.

The analytical methods employed for the power-input-optimization study are described in Appendix D. It should be further noted that the evaluation of natural-conduction heat-transfer effects in this study utilized rarefied-gas-flow techniques rather than the conventional approach employed for the previous (laboratory diffusion system) natural-convection estimate. This method was also used, however, to evaluate the magnitude of the natural-convection heat transfer in the actual laboratory diffusion system, i.e., no intermediate shielding.

The significance and the results of the analyses are shown in Table IV and Figure 34. Results in Table IV reveal that the presence of the intermediate shielding produces an increase in the effective heat-sink temperature (shield surrounding the element) and thus causes a noticeable decrease in the temperature potential between the inner shield and the diffusion element. The resultant corresponding calculated reduction in radiant and convective heat-loss mechanisms and consequently in the power-input requirement gives clear evidence of the beneficial effects promoted by intermediate shielding.

A description of the trends one might expect in the reduction of power input as a function of the number of shields can also be seen in Figure 34. Note that as the number of shields is increased, the power-input requirement is reduced. However, the efficiency of the composite shielding system is also reduced.

A comparison of the power-input requirement for the laboratory system, (i.e., no intermediate shielding), based on measured and calculated results, is also shown in Figure 34. The calculated results utilized both conventional and rarefied-gas analysis techniques in estimating the natural-convection effects. Favorable agreement between the results obtained with these approaches is indicated; thus, their use is justified. Note that for the points in question (no intermediate shielding), the maximum deviation of the calculated power input from measured results is about 24%. This is considered well within the allowable limits for this type of heat-transfer analysis. These results suggest that noticeable reductions in the theoretical power-input requirement are possible through the proper use of radiation-shielding techniques. However, as is often the case, experience reveals that the actual observed decrease in heat loss may be noticeably less than the spectacular reduction indicated by the calculated values in Figure 34. This decreased shielding efficiency is a result of the heat-conduction mechanisms established between the shields. Since the shields are made of thin highly reflective metals, they unfortunately possess excellent thermal conductivity. Although these conduction effects can be minimized by inserting insulation material between the shields, the reduction in the heating requirement will still be somewhat lower than that predicted by analytical methods.

TABLE IV

PERTINENT RESULTS OF POWER CORRELATION AND OPTIMIZATION ANALYSIS FOR A 24-INCH DIFFUSION ELEMENT OPERATING AT 400°F AND 64.7-PSIA PRESSURE DIFFERENTIAL

Number of Intermediate Shields	Temperature of Shield Surrounding Element (°F)	Radiation Losses (watts)	Natural-Convection Losses (watts)	Enthalpy Increase (watts)	Total Power Requirement (watts)
Calculated Results:					
None*	130	6.5	7-8**	0.77	15.3
None	130	6.5	5.4†	0.77	12.7
1	256	3.54	1.13†	0.77	5.44
2	302	2.54	0.686†	0.77	4.00
3	324	2.02	0.49†	0.77	3.29
Measured Results:					
None	105	---	---	---	16.8

* Corresponds to actual laboratory diffusion-canister configuration.

** Evaluated using conventional continuum natural-convection heat-transfer techniques.

† Evaluated using rarefied-gas-analysis techniques.

Brief mention should be made of another approach capable of minimizing the power-input requirement. This method utilizes the large hydrogen-gas-supply-pressure range that can be applied to a diffusion element.[15] For example, proper balancing of a large hydrogen supply pressure with a low element temperature could produce the same diffusion flow rate as a low supply pressure and a high element temperature. However, the low element temperature would obviously dictate a lower power input.

IV. BREADBOARD THRUSTER MODELS

One of the objectives of this program involved the fabrication of three breadboard thruster models based on analytical and experimental results. The thruster designs were established by NASA/WOO. The essential configurations and compositions of the thrusters were identical to the diffusion canisters and applicable components utilized in the experimental portion of this study.

The first thruster package contained palladium-silver-alloy tubing (75% palladium-25% silver, ±2% mixture ratio) of approximately 50 inches in length with an outside diameter of 0.045 inch, a wall thickness of 0.003 inch, and an exhaust-orifice diameter of approximately 0.02 inch. The second package contained palladium-silver-alloy tubing (±2% mixture ratio) of approximately 40 inches in length with an outside diameter of 0.045 inch, a wall thickness of 0.003 inch, and an exhaust-orifice diameter of approximately 0.07 inch. The third thruster package contained palladium-silver-alloy tubing (±2% mixture ratio) of approximately 30 inches in length with an outside diameter of 0.045 inch, a wall thickness of 0.003 inch, and an exhaust-orifice diameter of approximately 0.13 inch. Note that each of the operating conditions should produce a thrust of approximately the same magnitude for a given element temperature (ref. Figure 32).

Details of the thruster designs are shown in ATL Dwgs. D-8782, D-8783, C-8784, and Figure 35. Fabrication procedures were similar to those employed during the experimental test program. All connections and joints were vacuum-checked using a Veeco mass spectrometer leak detector. The sensitivity of this instrument to detection of leaks is 5.12×10^{-5} micron ft^3/hr. Every effort was extended toward preventing diffusion-element contamination during fabrication, and the decontamination methods described in Section II.B.3. were employed during laboratory checkout of the thrusters. Upon verification of proper diffusion-element operation, the breadboard thruster models were submitted to NASA/WOO for evaluation.

V. CONCLUSIONS

1. The objectives of the Phase 3 investigation were successfully completed. The study produced favorable results.

2. The characteristics of hydrogen diffusion through palladium-silver-alloy tubing at temperatures between ambient and 700°F were established.

3. Measured flow-rate trends indicate repeatability, and a relationship was derived that can be used to predict these trends.

4. No variation in hydrogen flow rates was detected between annealed and unannealed elements. However, a significant dependency of physical properties upon the degree of element annealing was evident.

5. Methods to insure element decontamination were devised and their effect has proved permanent.

6. Analytical studies based on experimental results showed that the utilization of the hydrogen-diffusion-valve principle with an appropriate thruster configuration can produce and sustain micropound thrust levels requiring a minimum power input. For example, preliminary empirical and analytical results indicated that a thruster containing a 40-inch diffusion element at an element temperature of 350°F could produce a 100-micropound thrust and a power input of 3 watts would be required. The measured dynamic range (flow rate) of such a device is 10^3.

VI. RECOMMENDATIONS

It is highly recommended that, based on the experimental measurements of thrust levels on the breadboard thruster models submitted to NASA/WOO, an effort be initiated to correlate the experimental results with the analytical predictions of the thrust levels presented in this report.

Although breadboard thruster models employing hydrogen-diffusion operation have been fabricated and submitted to NASA/WOO for evaluation, the design of these items for specific application has not been undertaken. Based on current attitude-control system requirements and the favorable results of this program, it is recommended that a design study be initiated immediately to arrive at an optimized hydrogen-diffusion thrust-control system. The initial portion of the proposed design study would involve a detailed analysis aimed at the general evaluation and optimization of the following important performance parameters:

a) Gas storage conditions.

b) Effect of system weight on specific impulse.

c) Power-input requirements.

d) Applicability to specific mission requirements.

e) Reliability analysis.

A thorough ground-test evaluation could then be conducted on breadboard models to substantiate the design effort. Some of the guidelines for this investigation are indicated in this report.

ILLUSTRATIONS

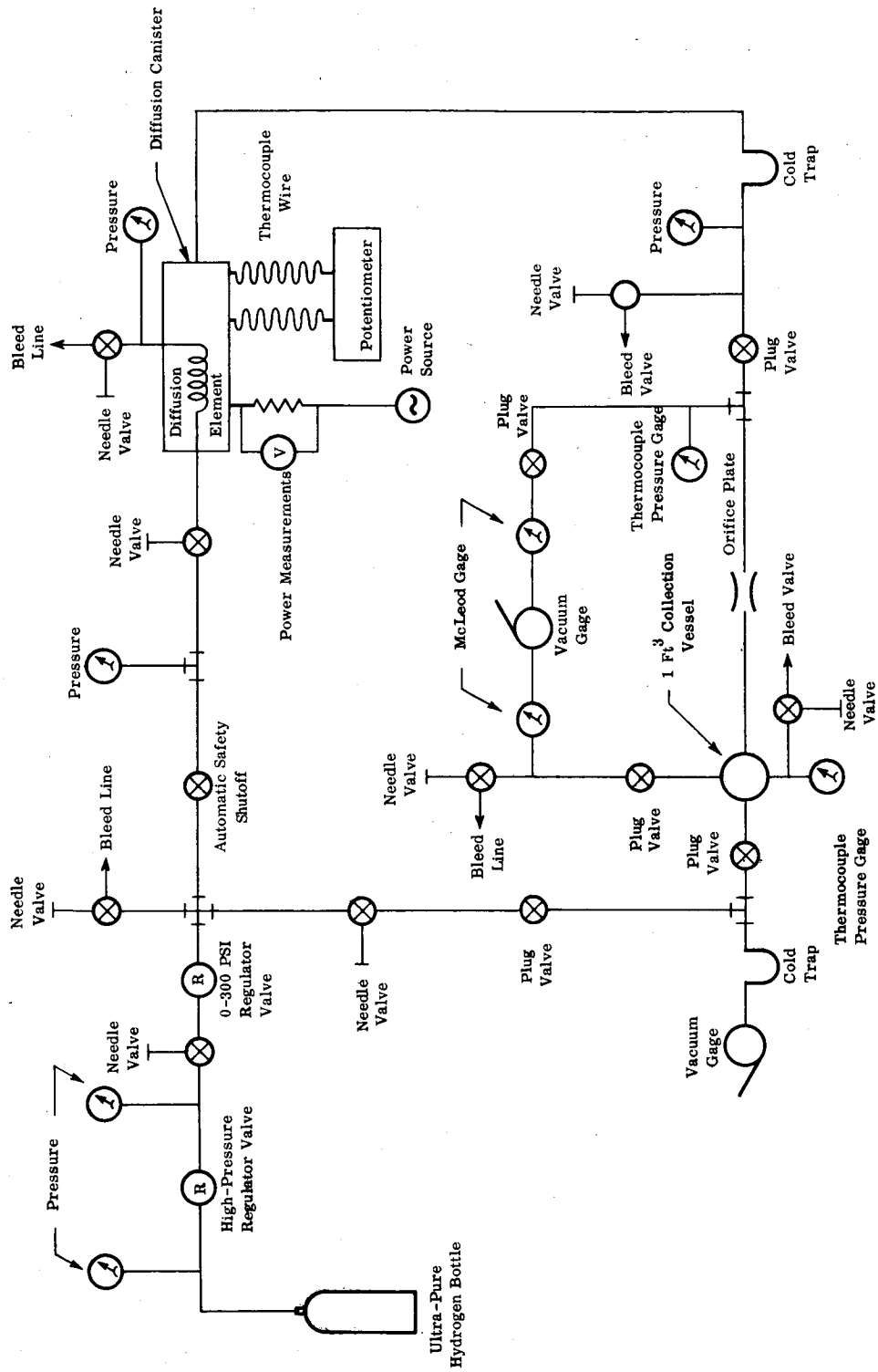

SCHEMATIC OF TEST APPARATUS
HYDROGEN VERSUS PALLADIUM-SILVER-ALLOY PERMEABILITY STUDY

FIGURE 1

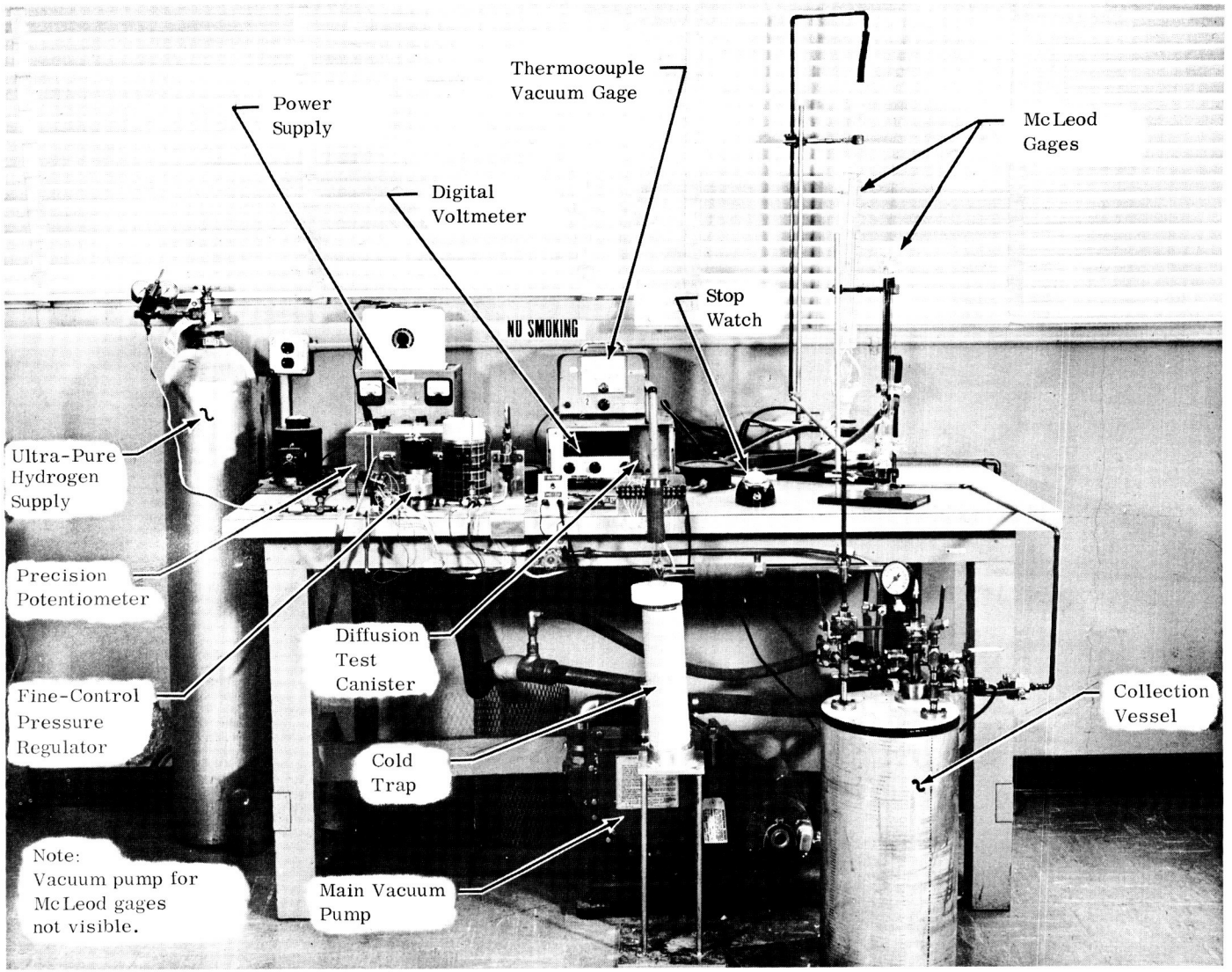

BASIC TEST APPARATUS
HYDROGEN VERSUS PALLADIUM-SILVER-ALLOY PERMEABILITY STUDY

FIGURE 2

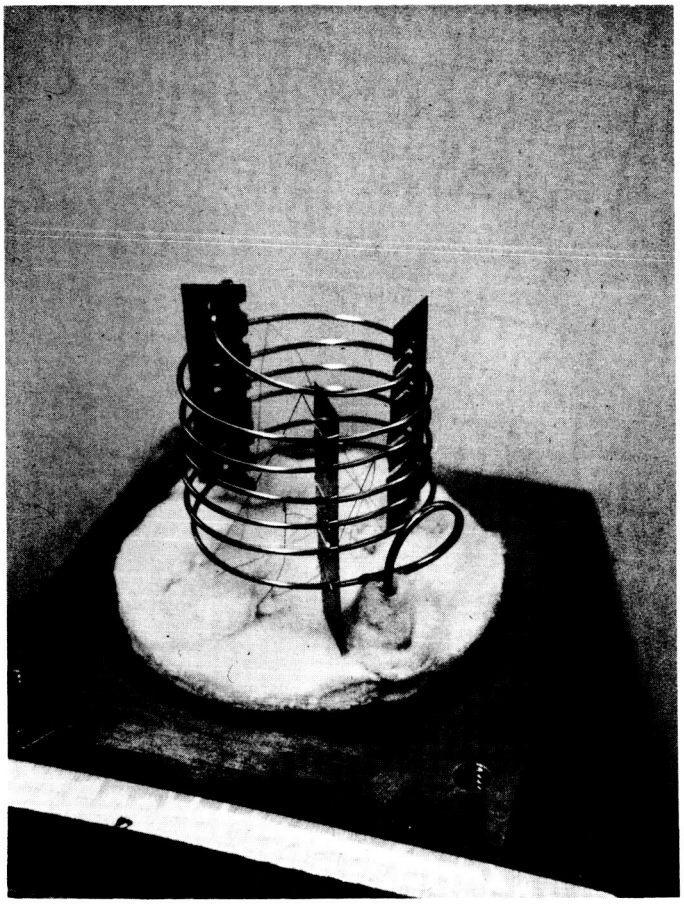

TYPICAL DIFFUSION ELEMENT SHOWING
THERMOCOUPLE WIRES AND MICA SUPPORTS

FIGURE 3

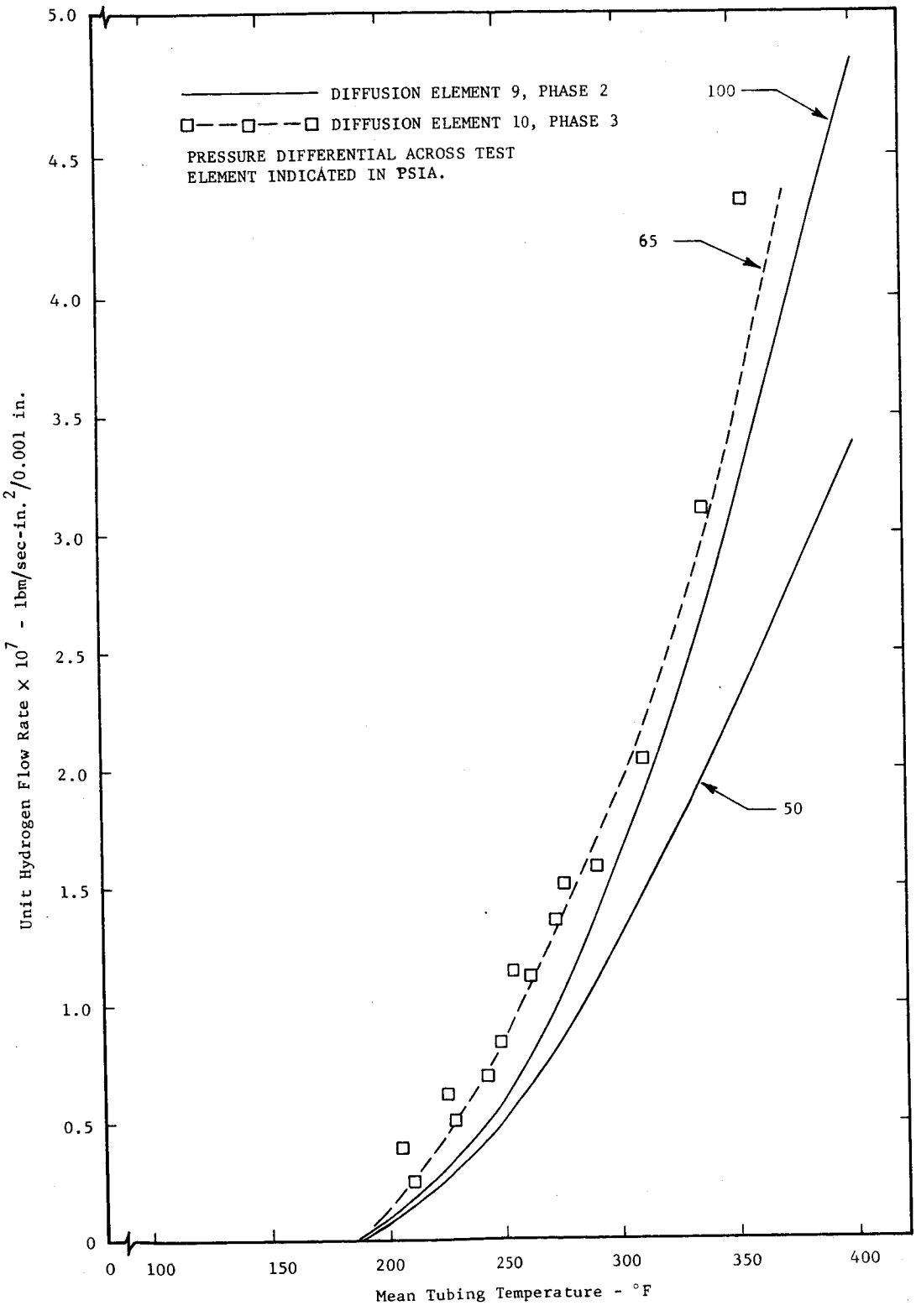

EFFECT OF MEAN TUBING TEMPERATURE ON HYDROGEN FLOW RATE FOR DIFFUSION ELEMENTS 9 AND 10

FIGURE 4

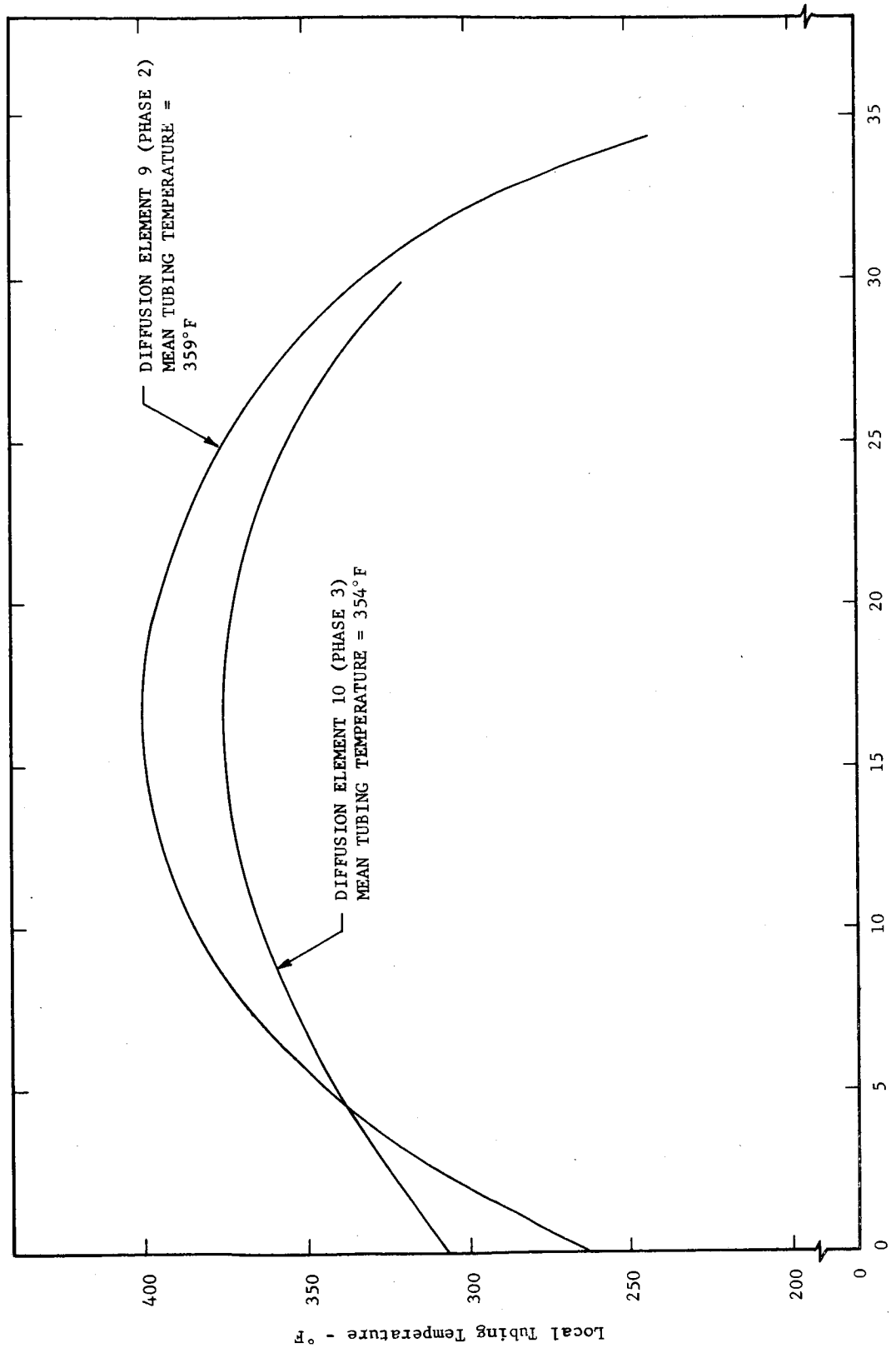

COMPARISON OF LOCAL TUBING-TEMPERATURE DISTRIBUTIONS OF DIFFUSION ELEMENTS 9 AND 10

FIGURE 5

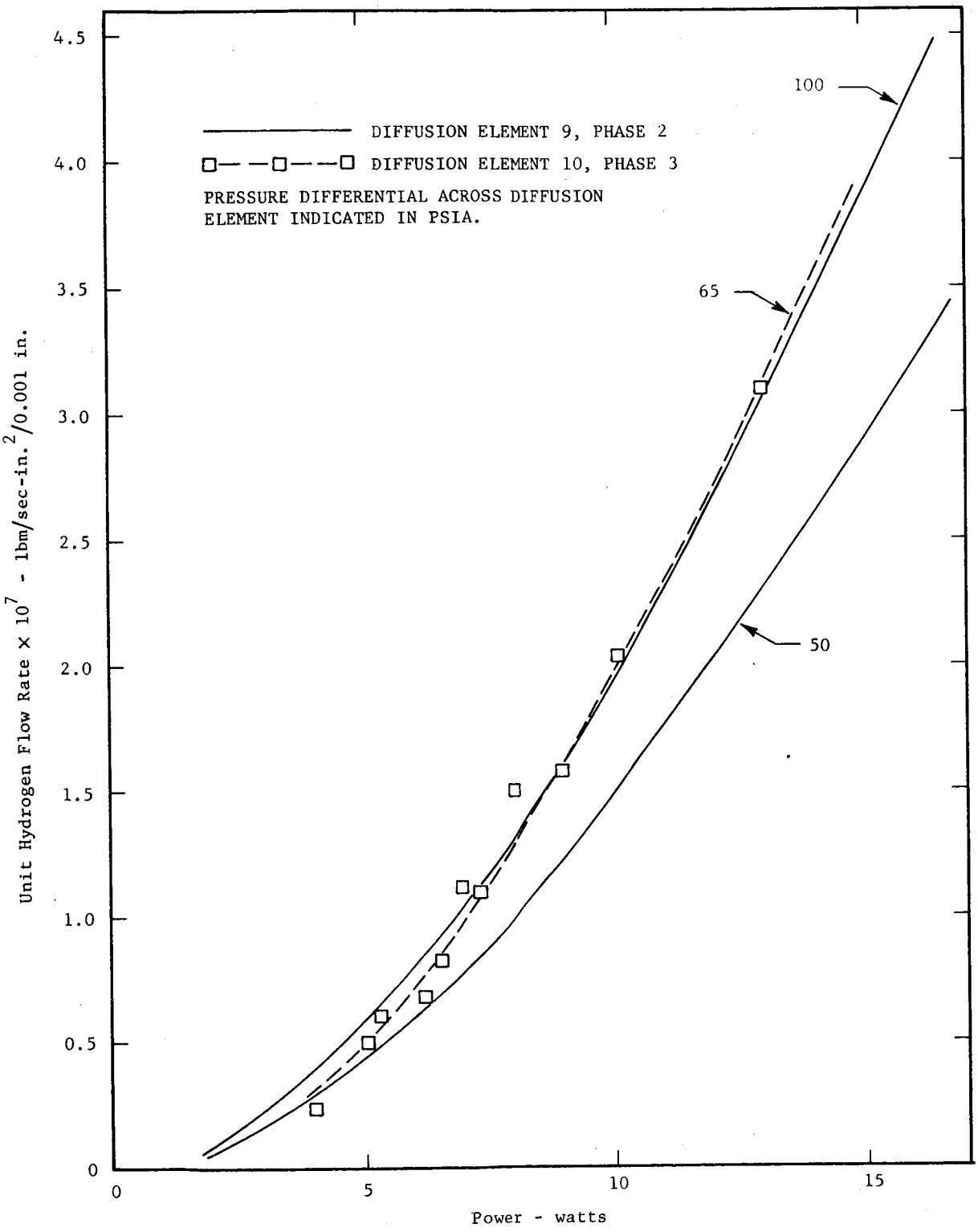

EFFECT OF DC POWER INPUT ON HYDROGEN FLOW RATE FOR DIFFUSION ELEMENTS 9 AND 10

FIGURE 6

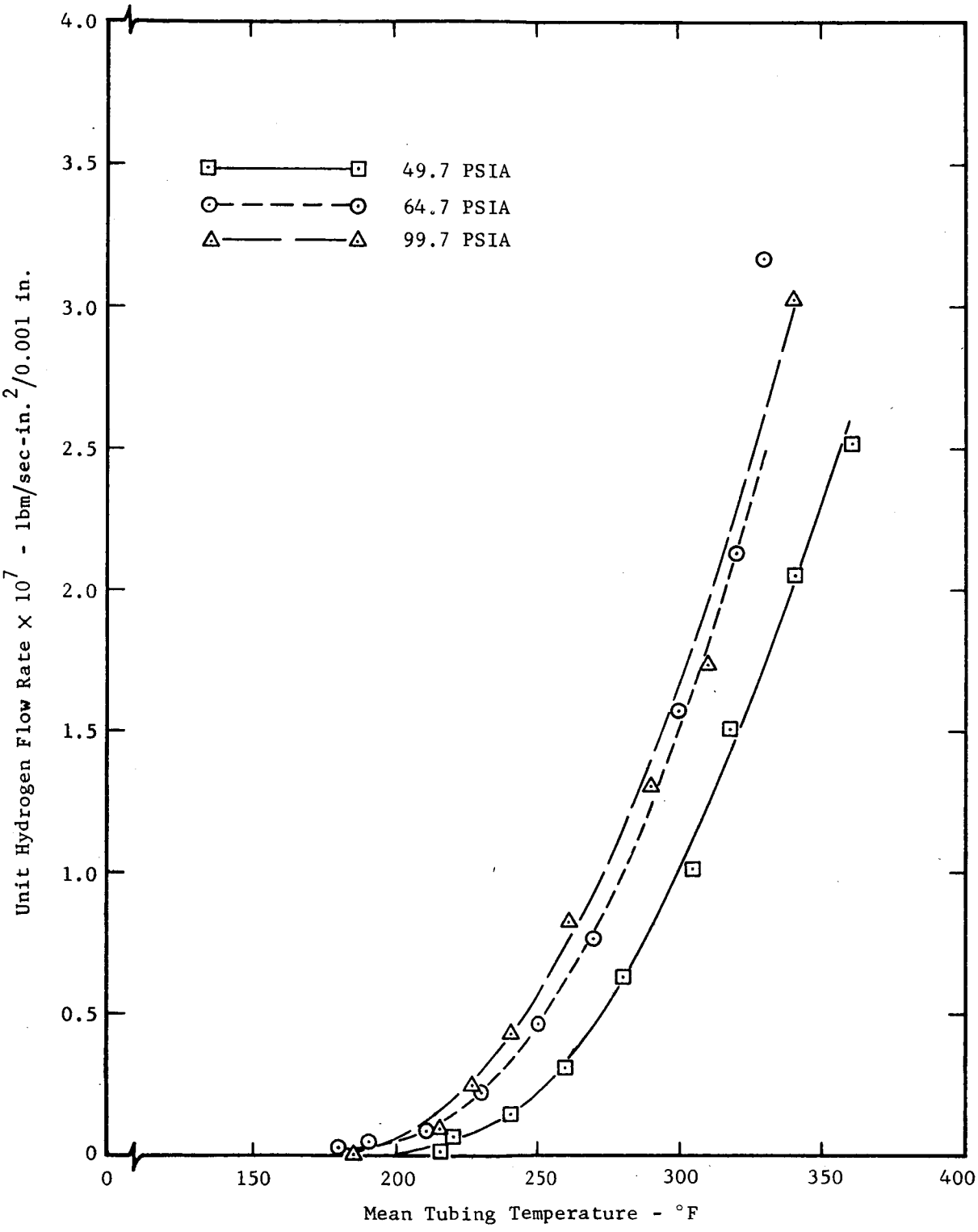

EFFECT OF MEAN TUBING TEMPERATURE ON HYDROGEN FLOW RATE AT INDICATED PRESSURE DIFFERENTIALS FOR 24-INCH DIFFUSION ELEMENT 11

FIGURE 7

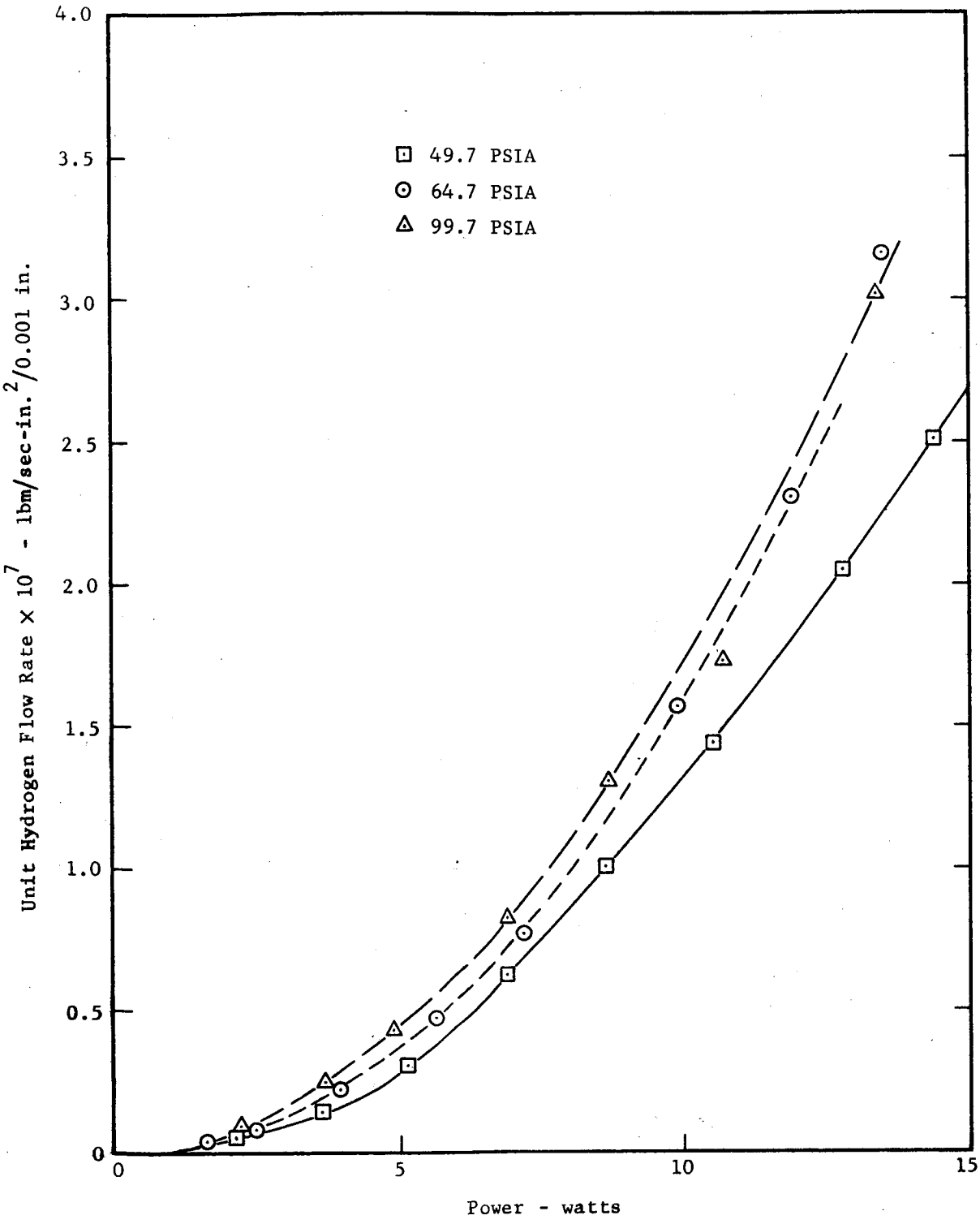

EFFECT OF DC POWER INPUT ON HYDROGEN FLOW RATE
AT INDICATED PRESSURE DIFFERENTIALS FOR 24-INCH DIFFUSION ELEMENT 11

FIGURE 8

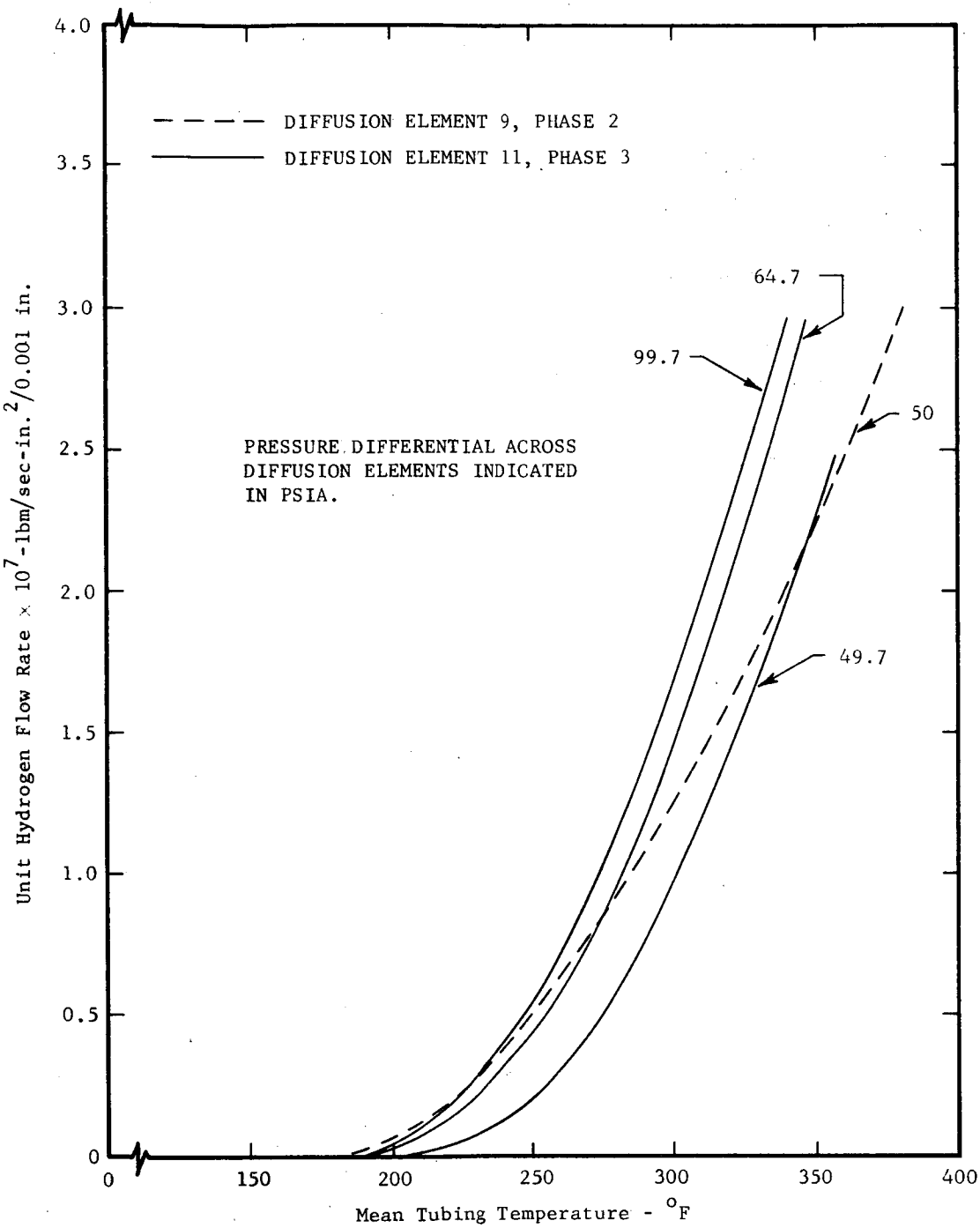

EFFECT OF MEAN TUBING TEMPERATURE ON HYDROGEN FLOW RATES FOR DIFFUSION ELEMENTS 9 AND 11

FIGURE 9

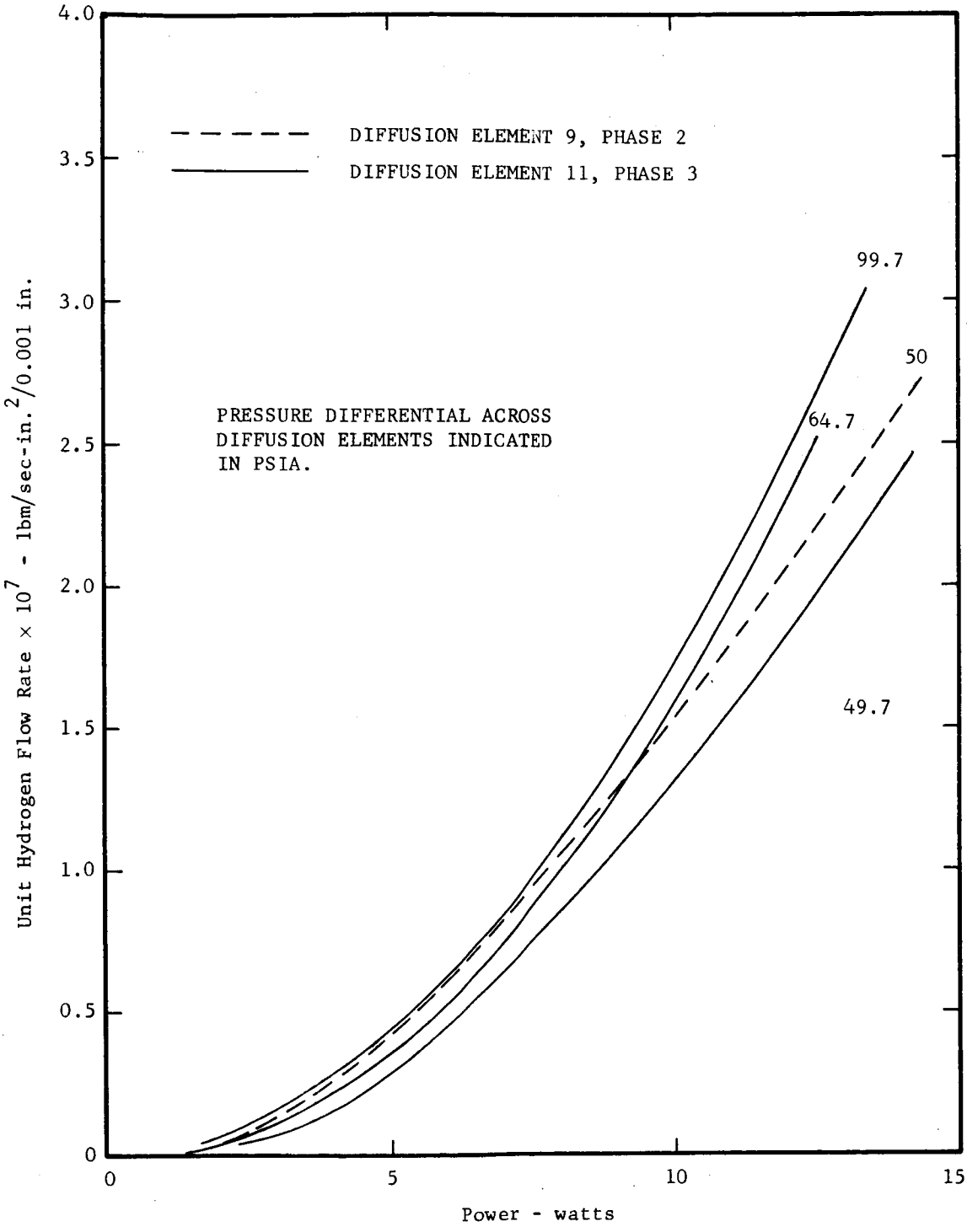

EFFECT OF DC POWER INPUT ON HYDROGEN FLOW RATE FOR DIFFUSION ELEMENTS 9 AND 11

FIGURE 10

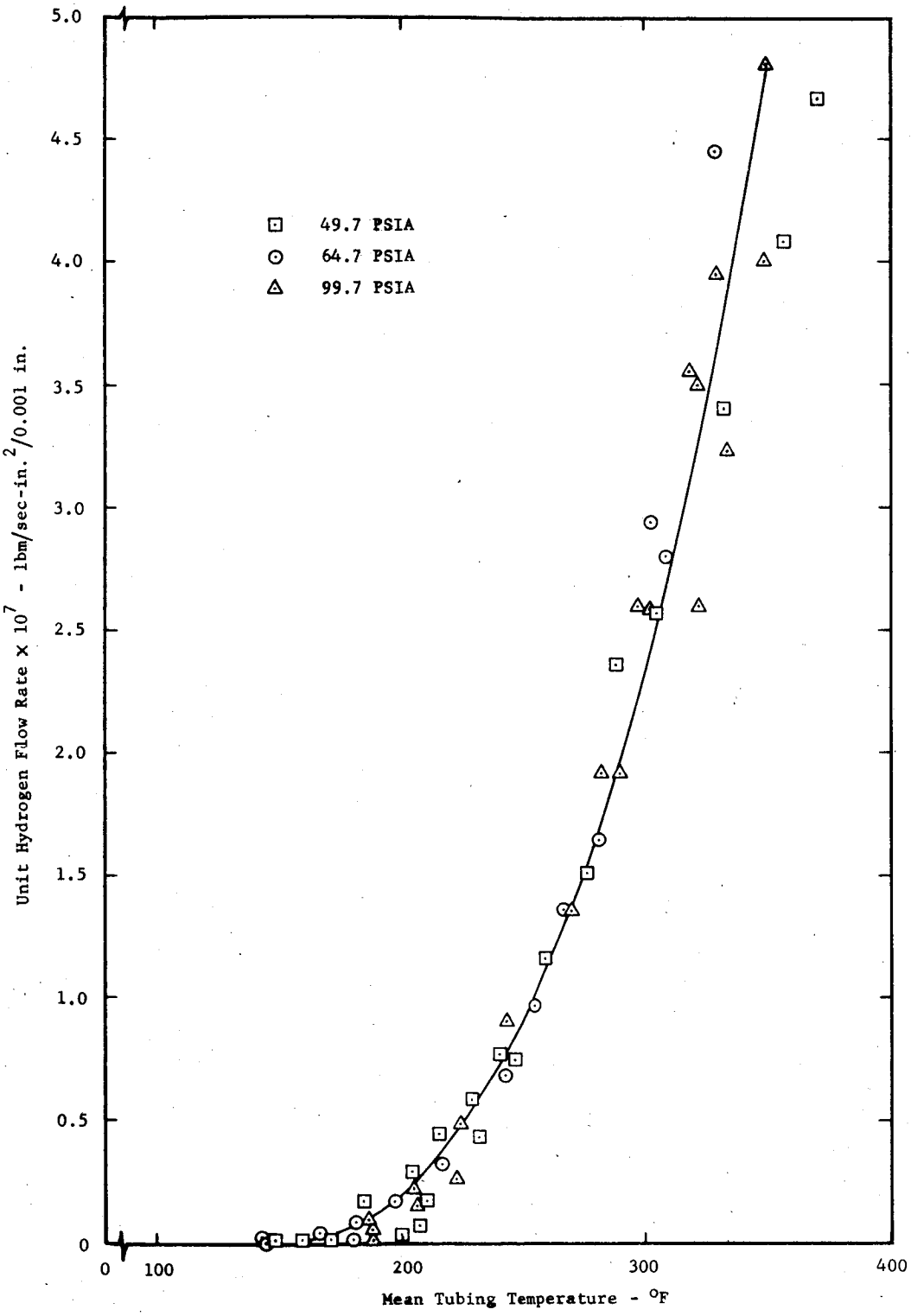

EFFECT OF MEAN TUBING TEMPERATURE ON HYDROGEN FLOW RATE
AT INDICATED PRESSURE DIFFERENTIALS
FOR 30-INCH DIFFUSION ELEMENT 12

FIGURE 11

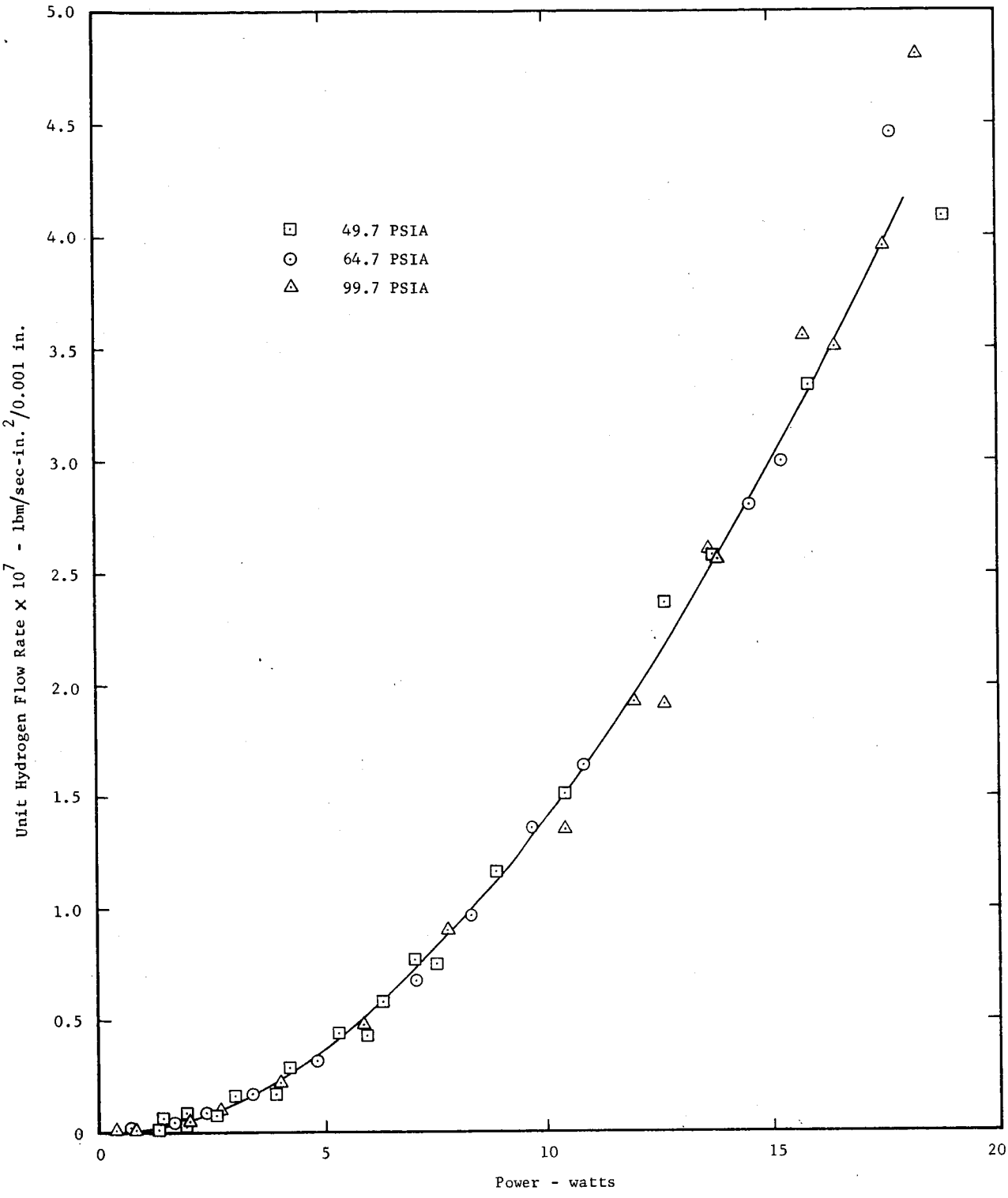

EFFECT OF DC POWER INPUT ON HYDROGEN FLOW RATE
AT INDICATED PRESSURE DIFFERENTIALS
FOR 30-INCH DIFFUSION ELEMENT 12

FIGURE 12

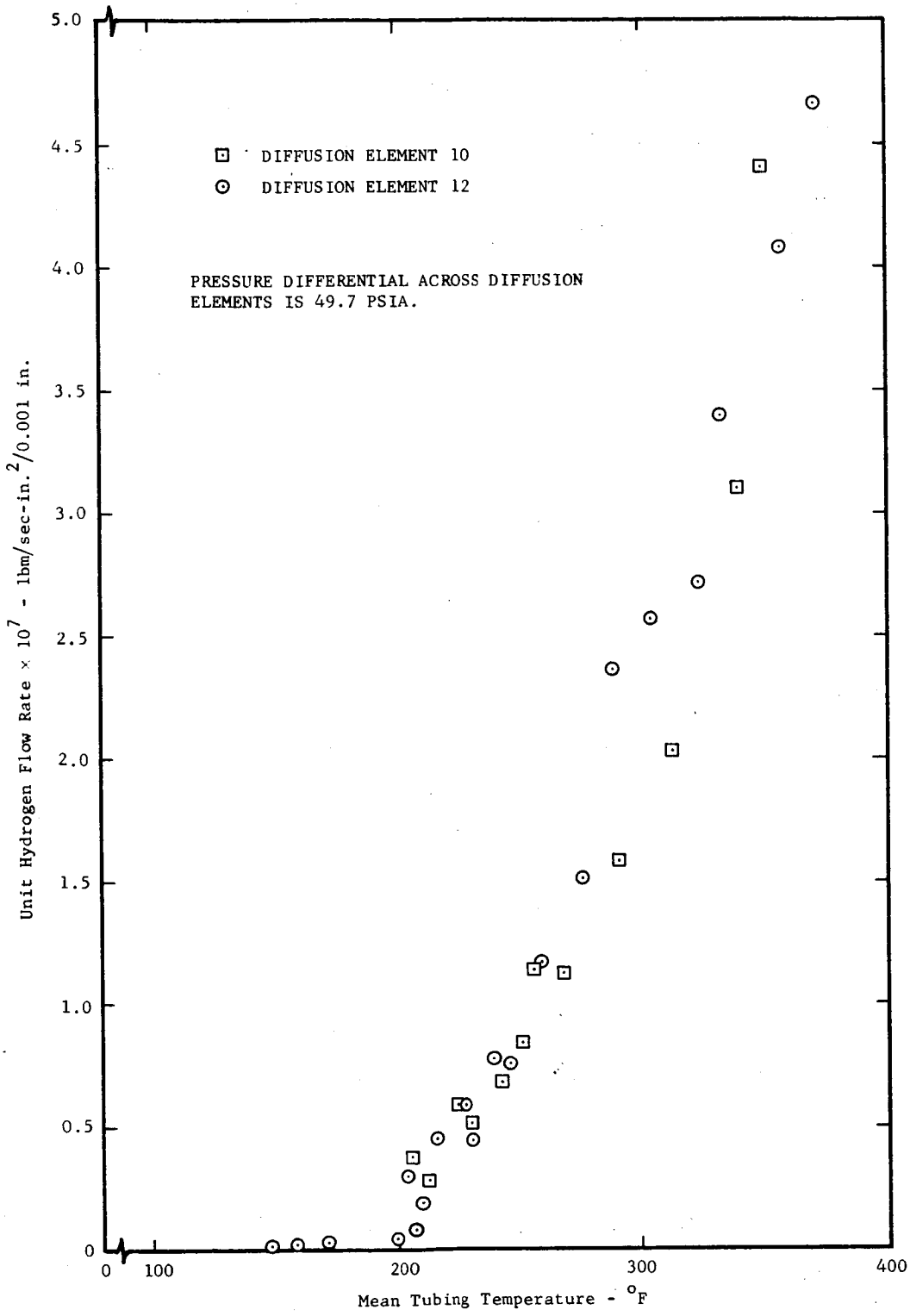

EFFECT OF TUBING TEMPERATURE ON HYDROGEN FLOW RATE FOR 30-INCH DIFFUSION ELEMENTS 10 AND 12

FIGURE 13

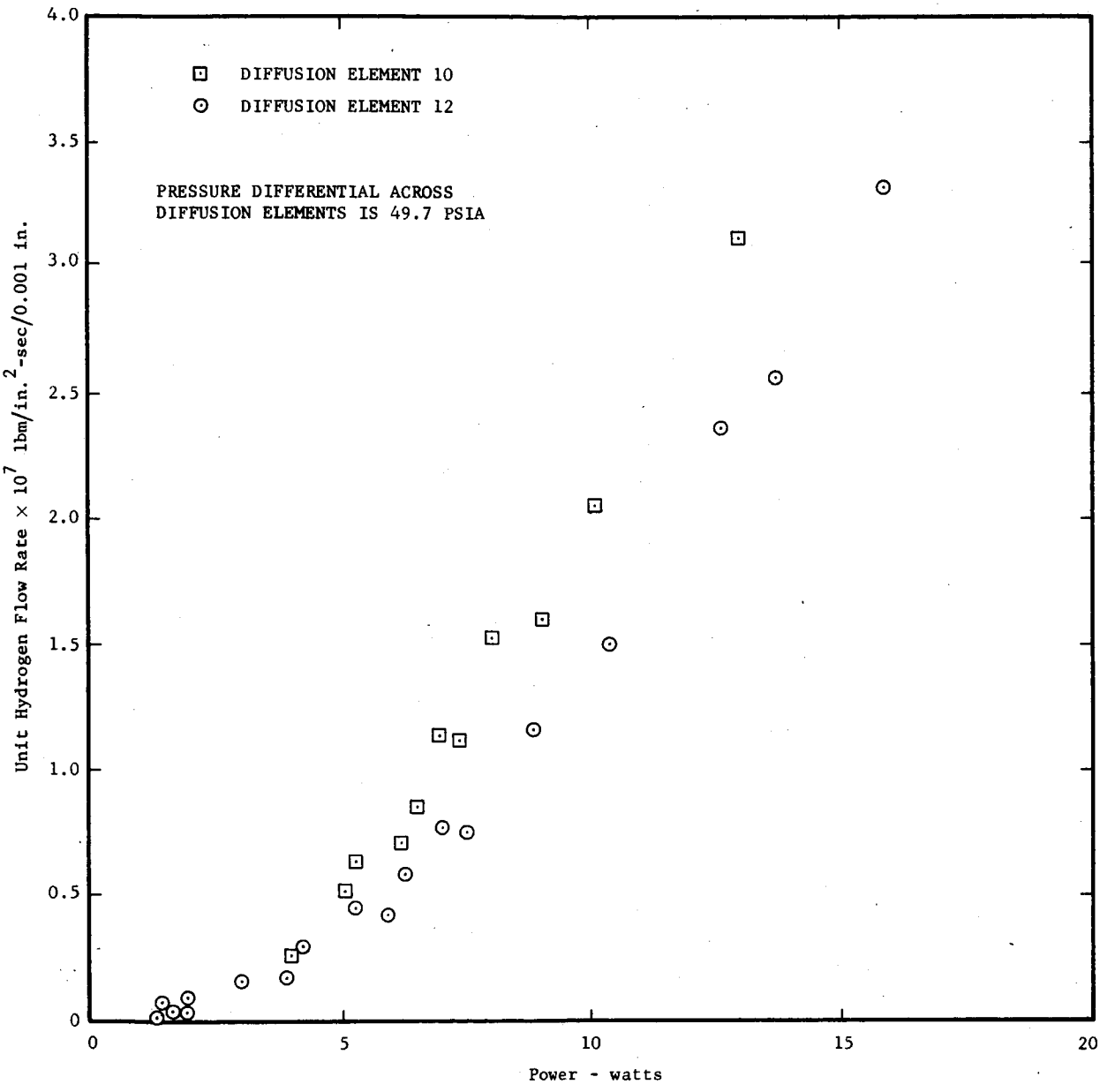

EFFECT OF DC POWER INPUT ON HYDROGEN FLOW RATE
FOR 30-INCH DIFFUSION ELEMENTS 10 AND 12

FIGURE 14

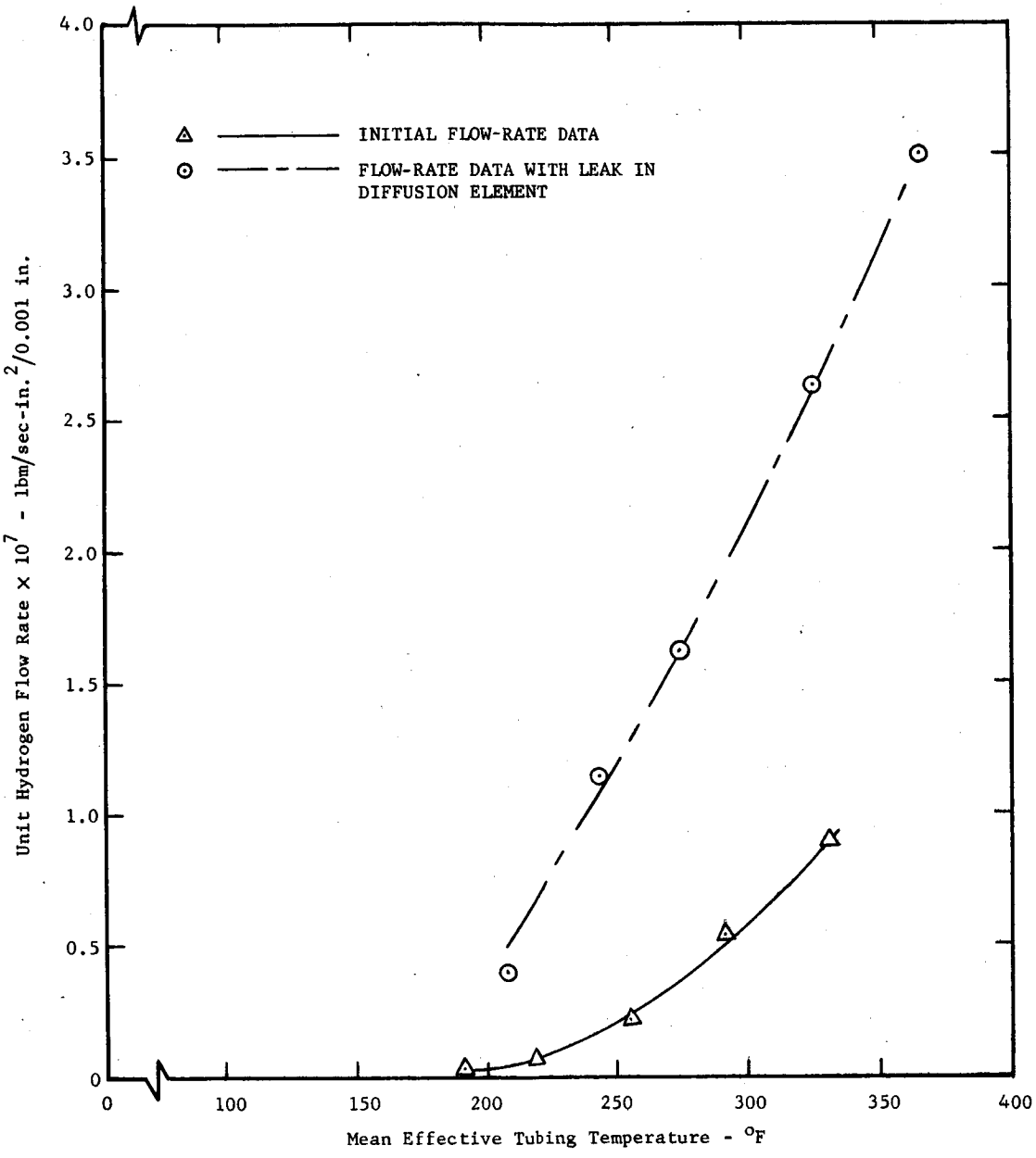

EFFECT OF MEAN TUBING TEMPERATURE ON HYDROGEN FLOW RATE FOR A 36-INCH DIFFUSION ELEMENT (13)

FIGURE 15

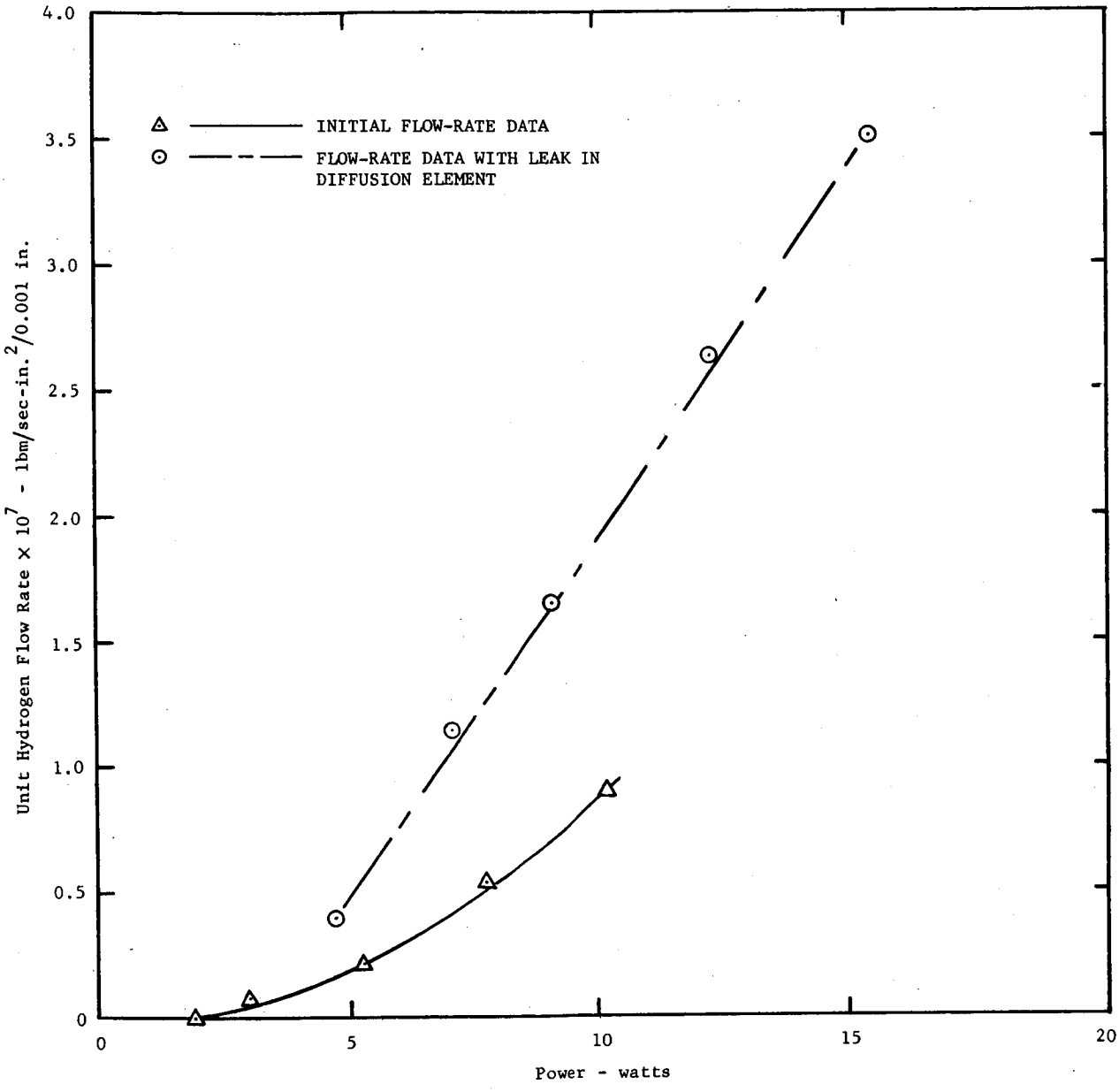

EFFECT OF DC POWER INPUT ON HYDROGEN FLOW RATE FOR A 36-INCH DIFFUSION ELEMENT (13)

FIGURE 16

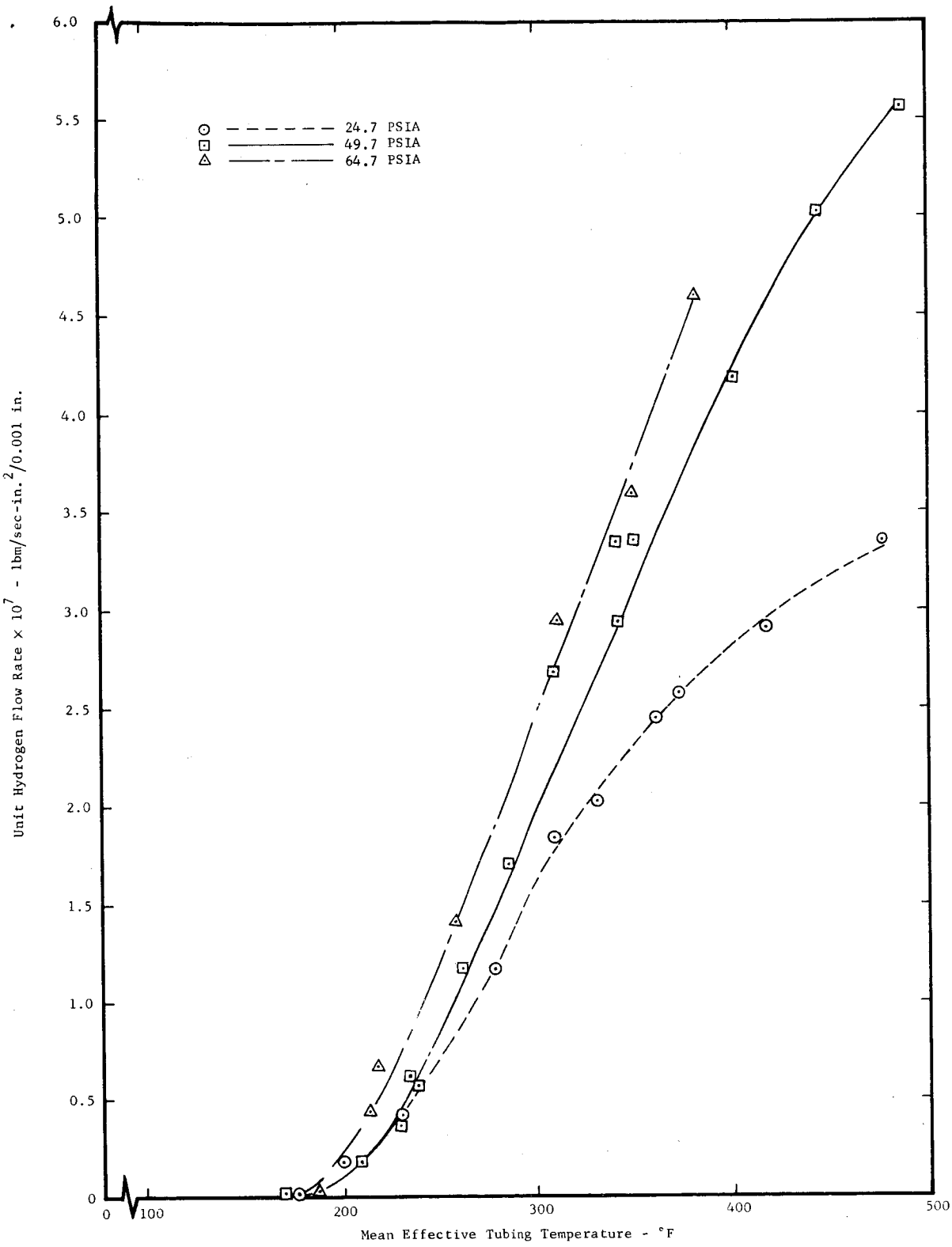

EFFECT OF MEAN TUBING TEMPERATURE ON HYDROGEN FLOW RATE AT INDICATED PRESSURE DIFFERENTIALS ACROSS A 34-INCH DIFFUSION ELEMENT (13)

FIGURE 17

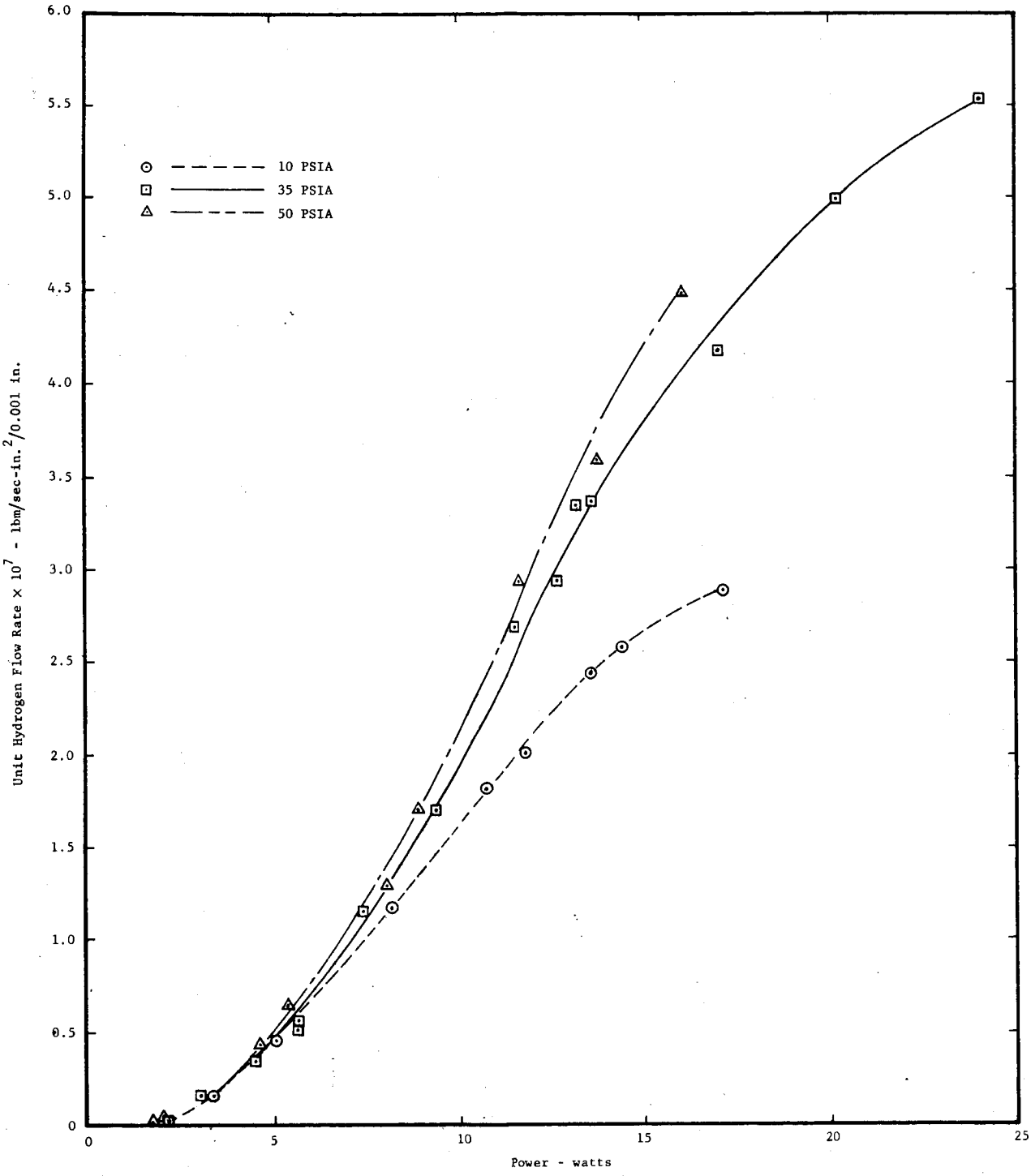

EFFECT OF DC POWER INPUT ON HYDROGEN FLOW RATE
AT INDICATED PRESSURE DIFFERENTIALS
ACROSS A 34-INCH DIFFUSION ELEMENT (13)

FIGURE 18

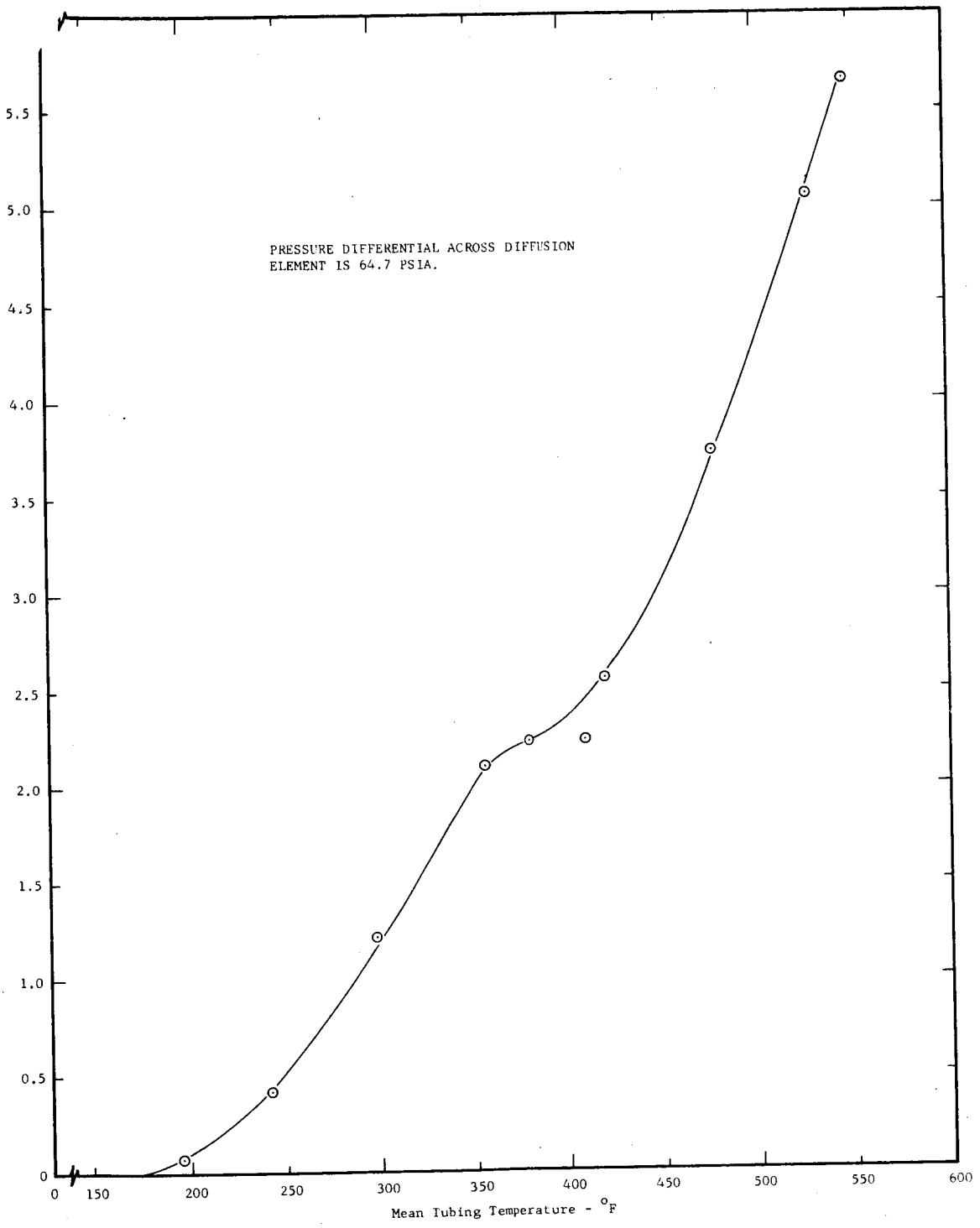

EFFECT OF MEAN TUBING TEMPERATURE ON HYDROGEN FLOW RATE FOR A 24-INCH DIFFUSION ELEMENT (15)

FIGURE 19

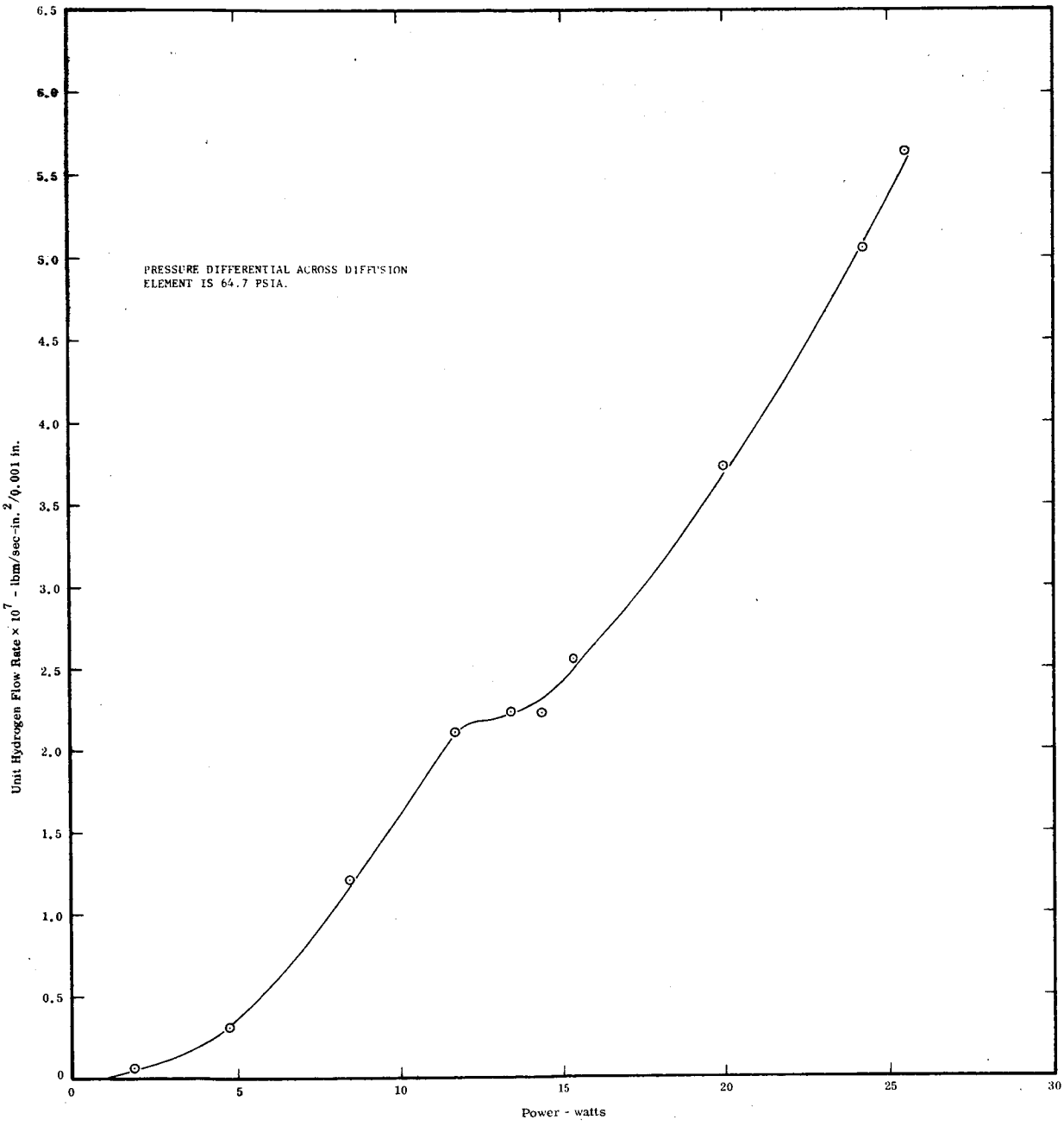

EFFECT OF DC POWER INPUT ON HYDROGEN FLOW RATE FOR A 24-INCH DIFFUSION ELEMENT (15)

FIGURE 20

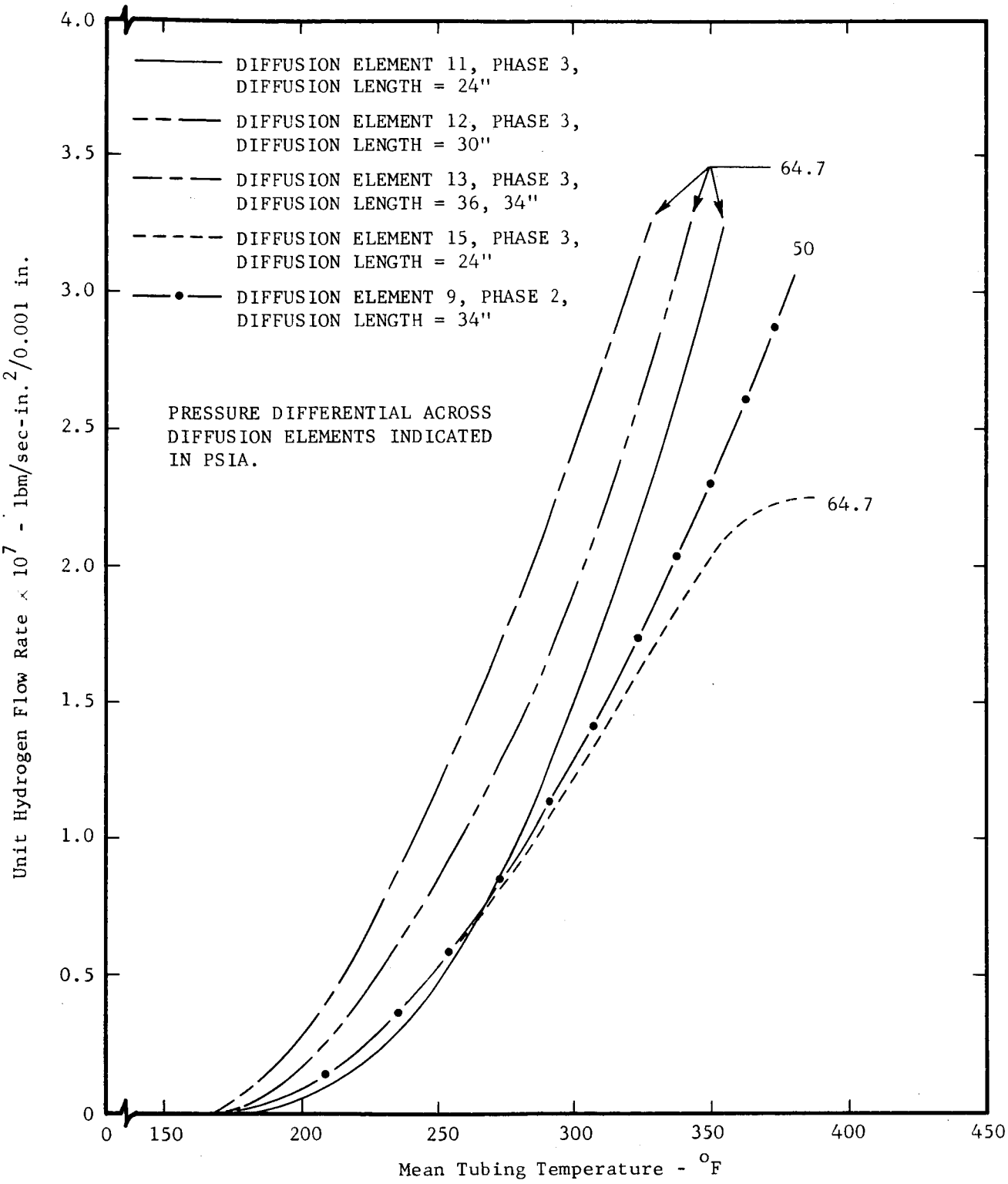

EFFECT OF MEAN TUBING TEMPERATURE ON HYDROGEN FLOW RATE FOR INDICATED DIFFUSION ELEMENTS AND TEST CONDITIONS

FIGURE 21

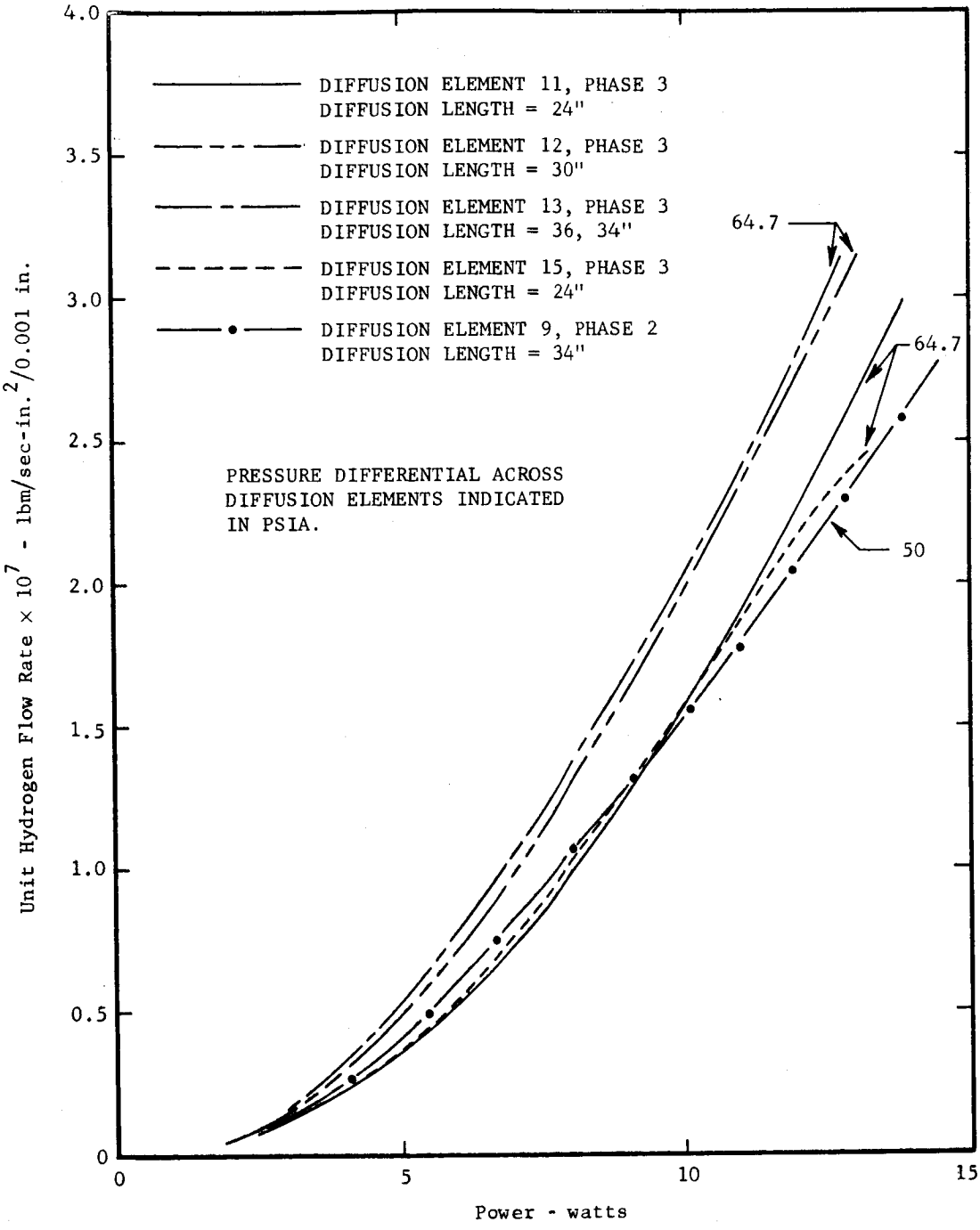

EFFECT OF DC POWER INPUT ON HYDROGEN FLOW RATE
FOR INDICATED DIFFUSION ELEMENTS AND TEST CONDITIONS

FIGURE 22

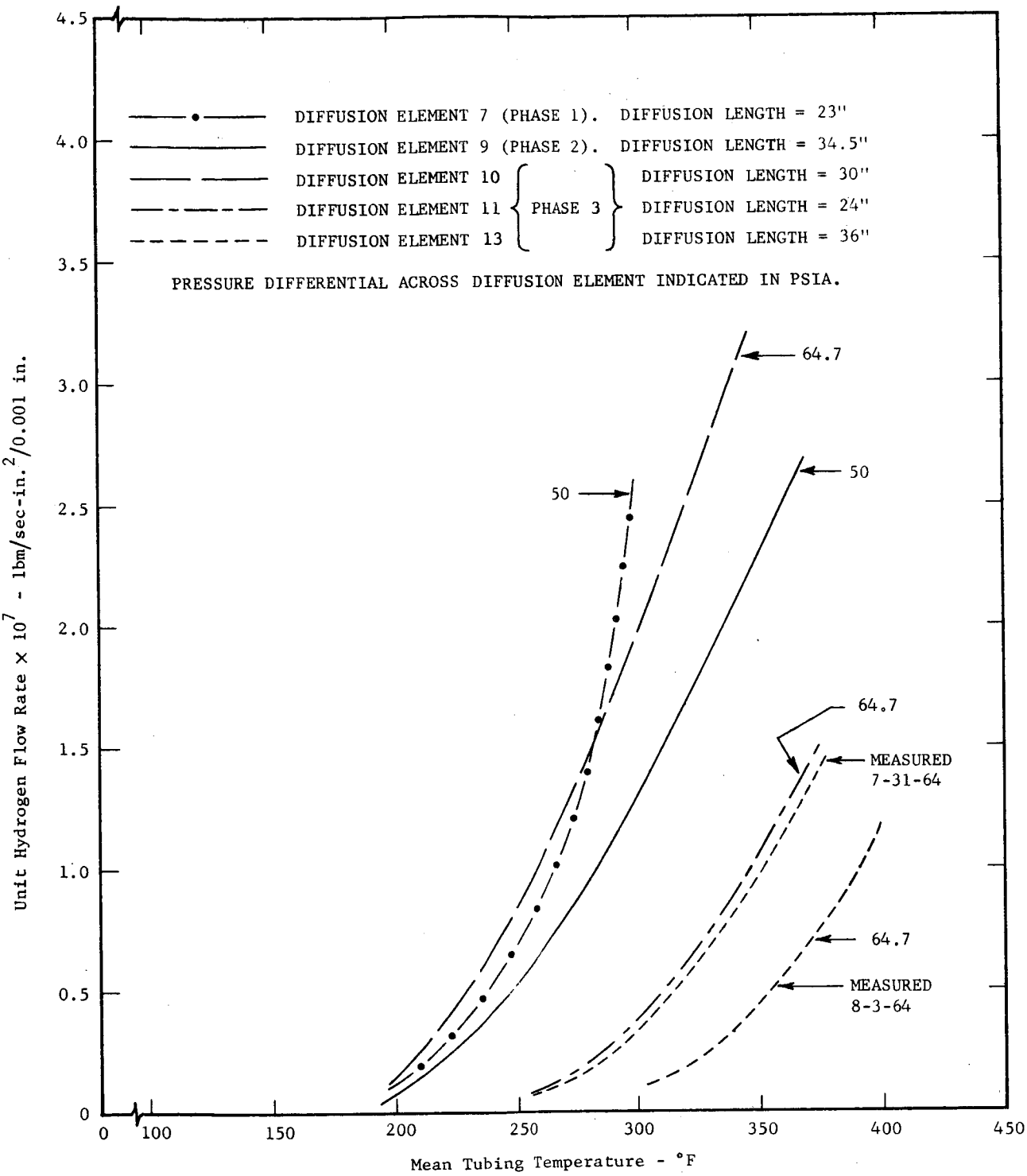

EFFECT OF MEAN TUBING TEMPERATURE ON HYDROGEN FLOW RATE FOR DIFFUSION ELEMENTS SUBJECTED TO THE INDICATED CONDITIONS

FIGURE 23

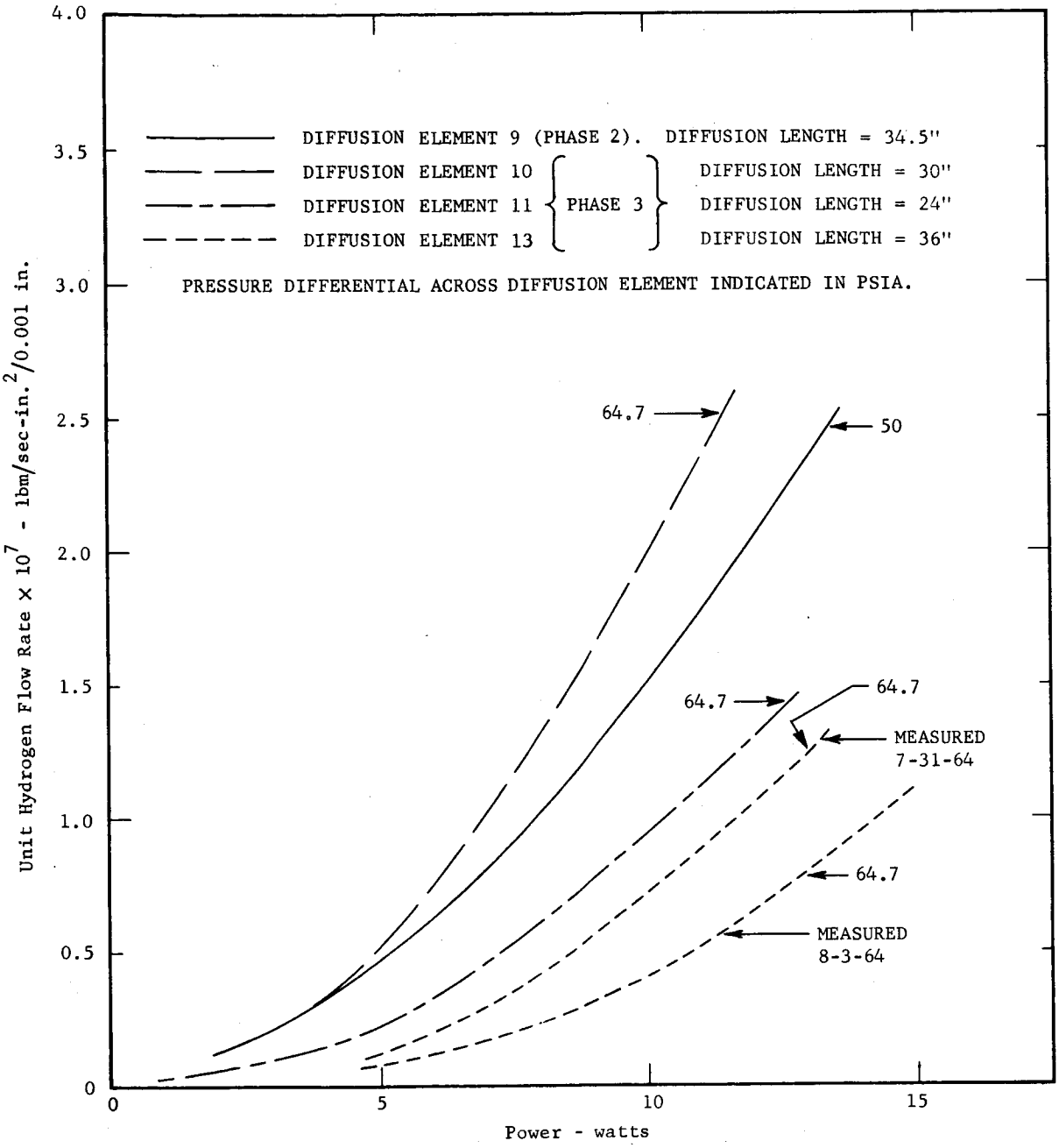

EFFECT OF DC POWER INPUT ON HYDROGEN FLOW RATE
FOR DIFFUSION ELEMENTS SUBJECTED TO THE INDICATED CONDITIONS

FIGURE 24

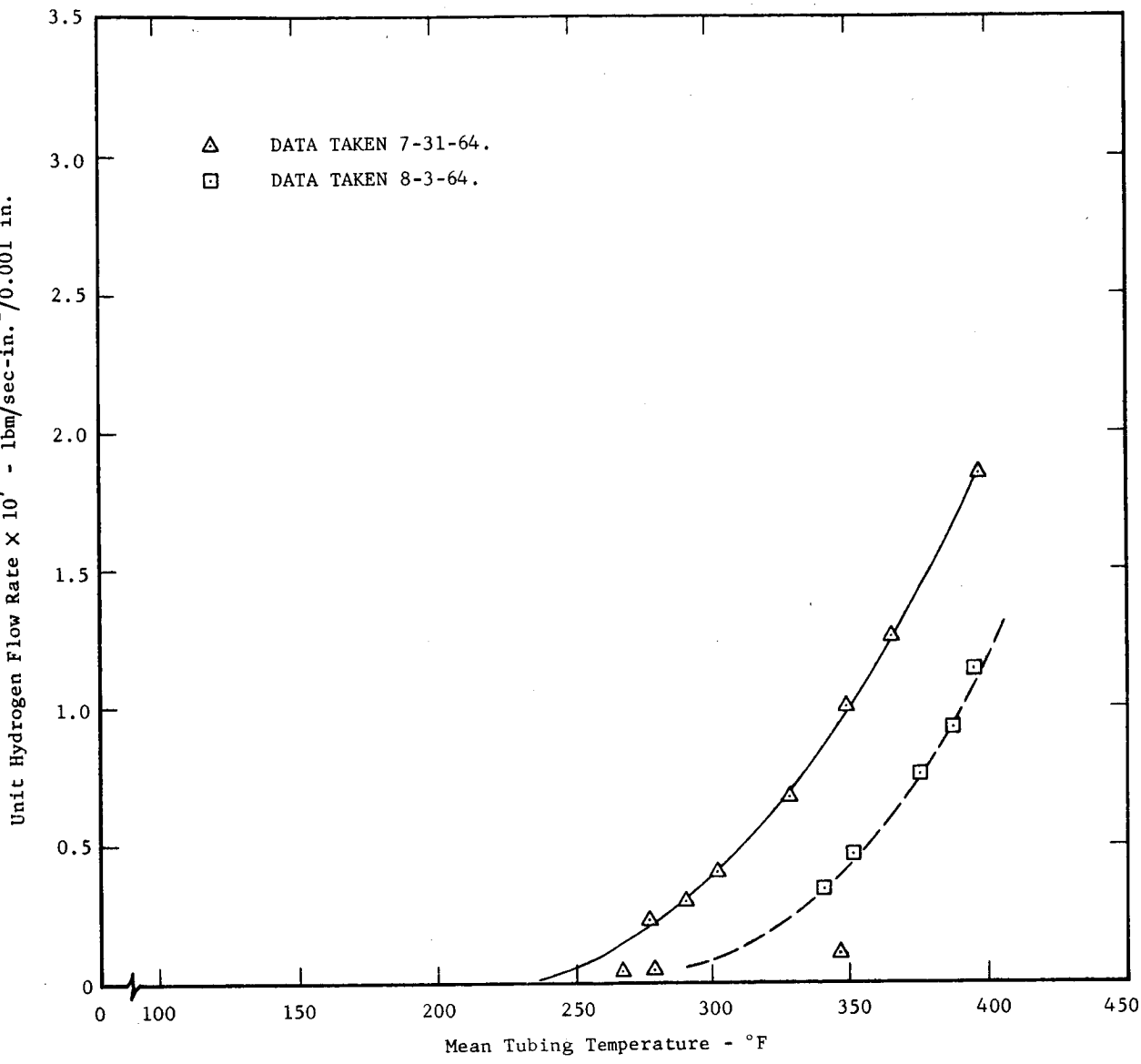

EFFECT OF MEAN TUBING TEMPERATURE ON HYDROGEN FLOW RATE FOR DIFFUSION ELEMENT 13

FIGURE 25

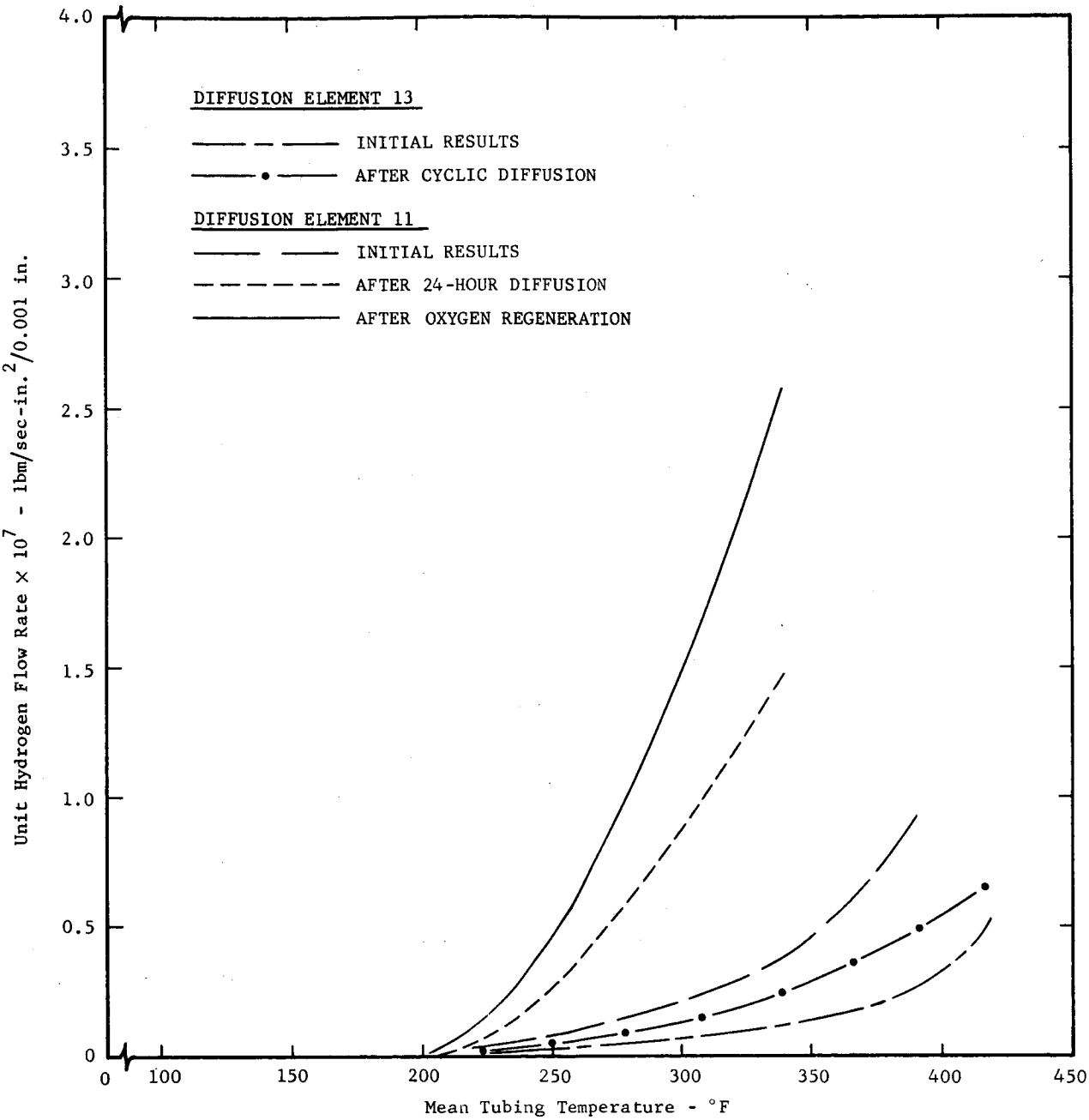

PERFORMANCE OF DIFFUSION ELEMENTS 11 AND 13
FOLLOWING APPLICATION OF INDICATED DECONTAMINATION METHODS

FIGURE 26

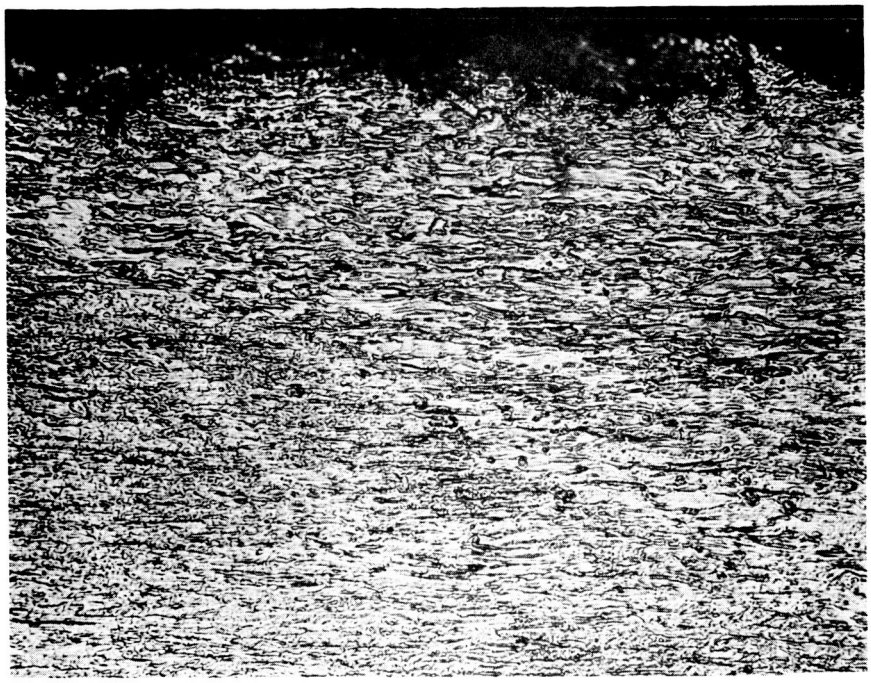

500× Neg. #5756

a. Shipment 1

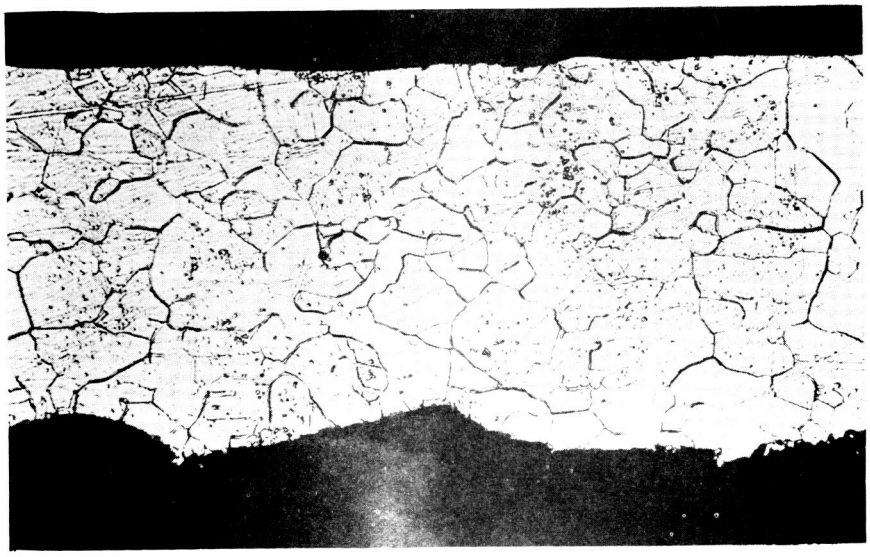

500× Neg. #5757

b. Shipment 2

PHOTOMICROGRAPHS OF UNTESTED PALLADIUM-SILVER-ALLOY TUBING, SHOWING VARIATION IN MATERIAL STRUCTURE OF THE TWO TUBING SHIPMENTS RECEIVED

FIGURE 27

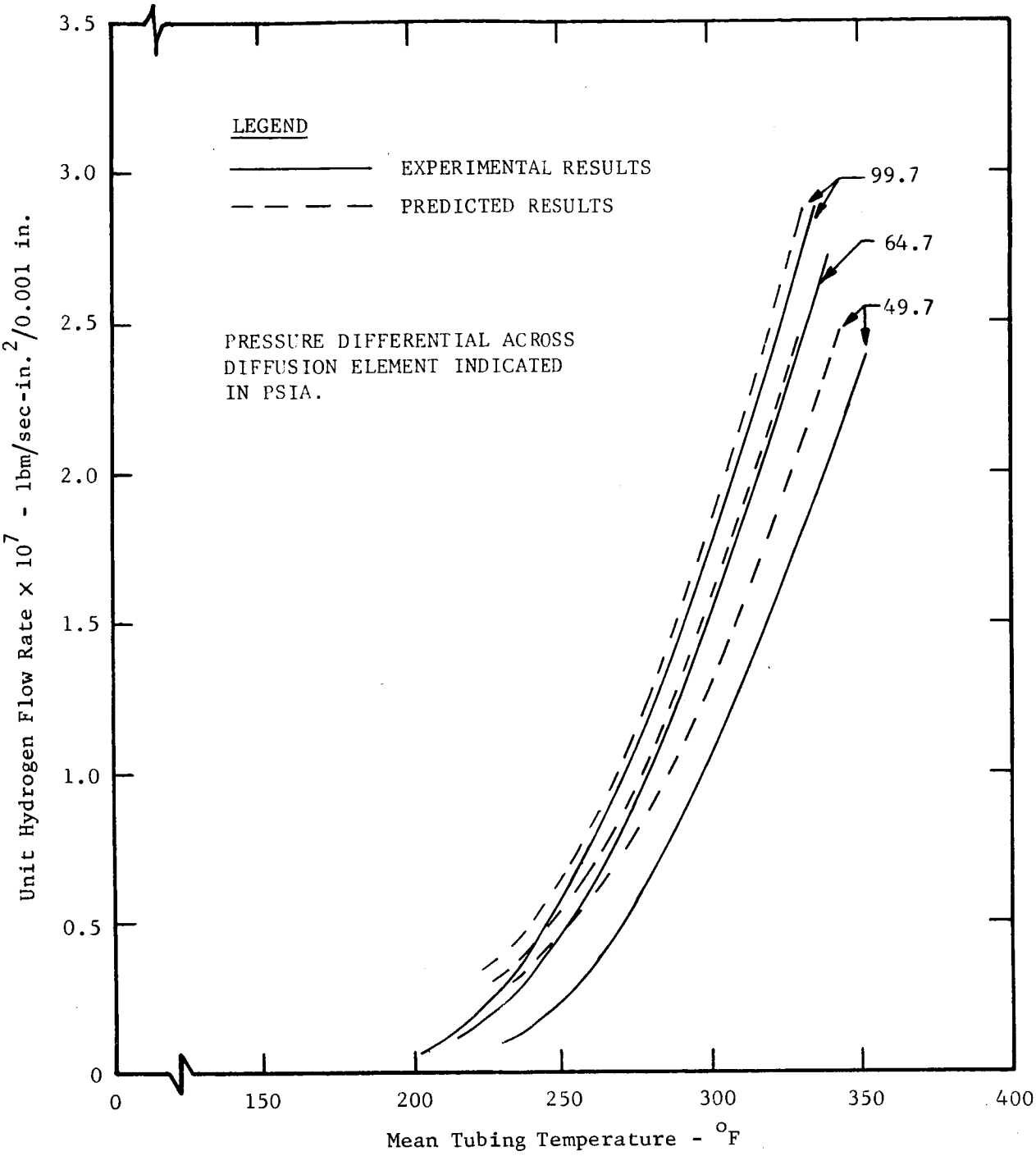

COMPARISON OF MEASURED HYDROGEN FLOW RATES WITH THOSE PREDICTED BY EQUATION 1 AT INDICATED PRESSURE DIFFERENTIALS FOR A 24-INCH DIFFUSION ELEMENT (11)

FIGURE 28

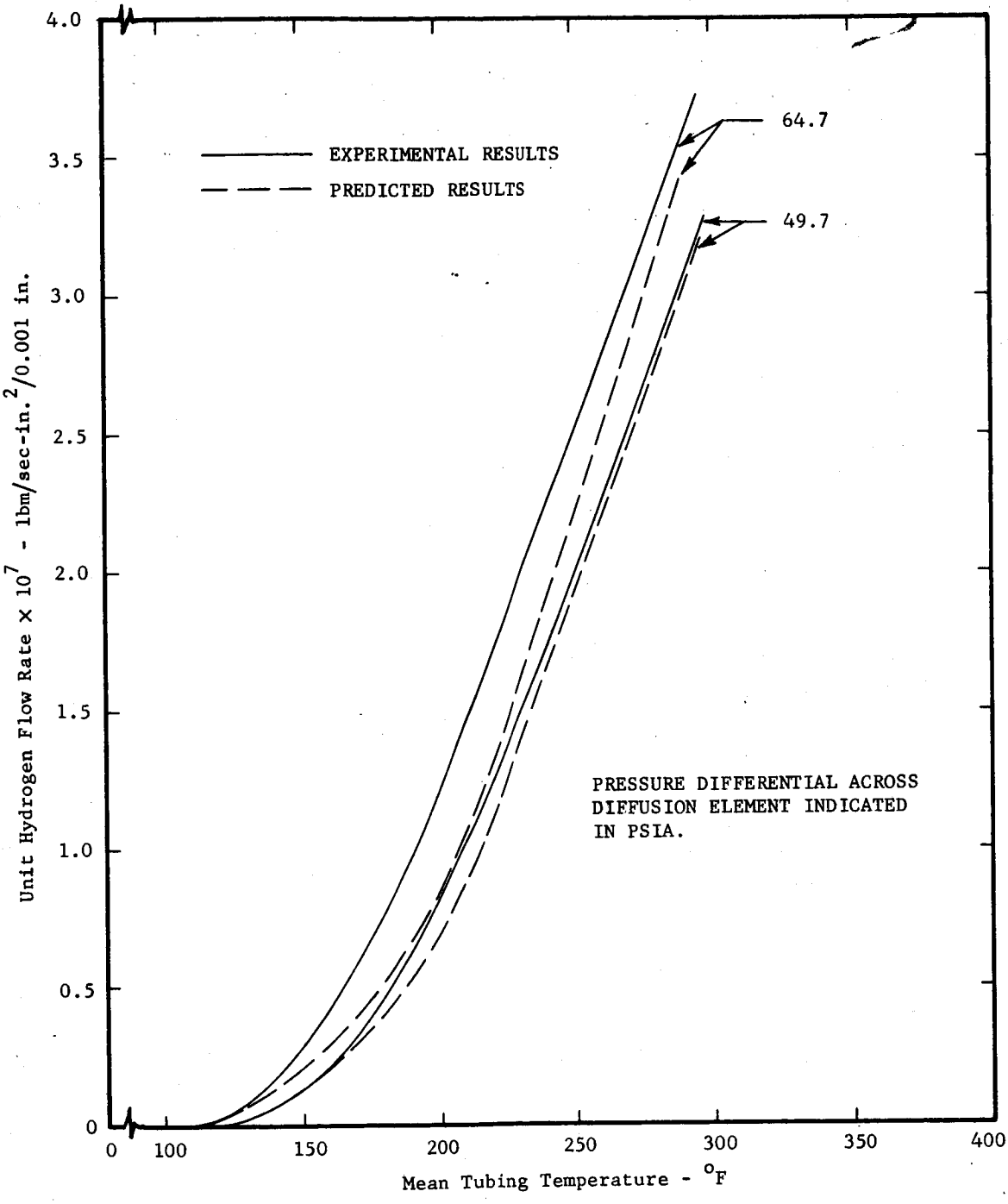

COMPARISON OF MEASURED HYDROGEN FLOW RATES
WITH THOSE PREDICTED BY EQUATION 1
AT INDICATED PRESSURE DIFFERENTIALS
FOR A 34-INCH DIFFUSION ELEMENT (13)

FIGURE 29

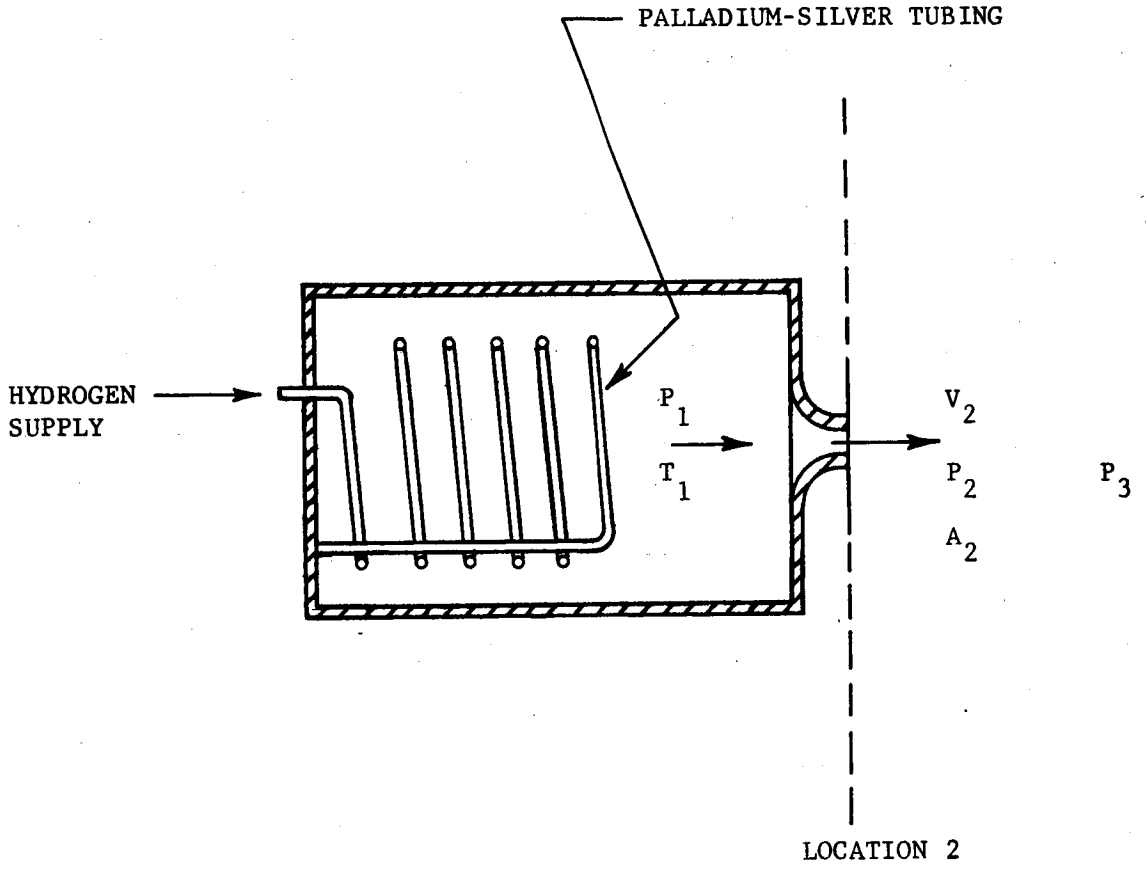

NOTES: $P_3 = 0$.
LOCATION 2 CORRESPONDS TO THROAT CONDITIONS.

DIAGRAMMATIC SKETCH FOR THRUST-LEVEL CALCULATIONS
(Symbols Are Defined in Nomenclature)

FIGURE 30

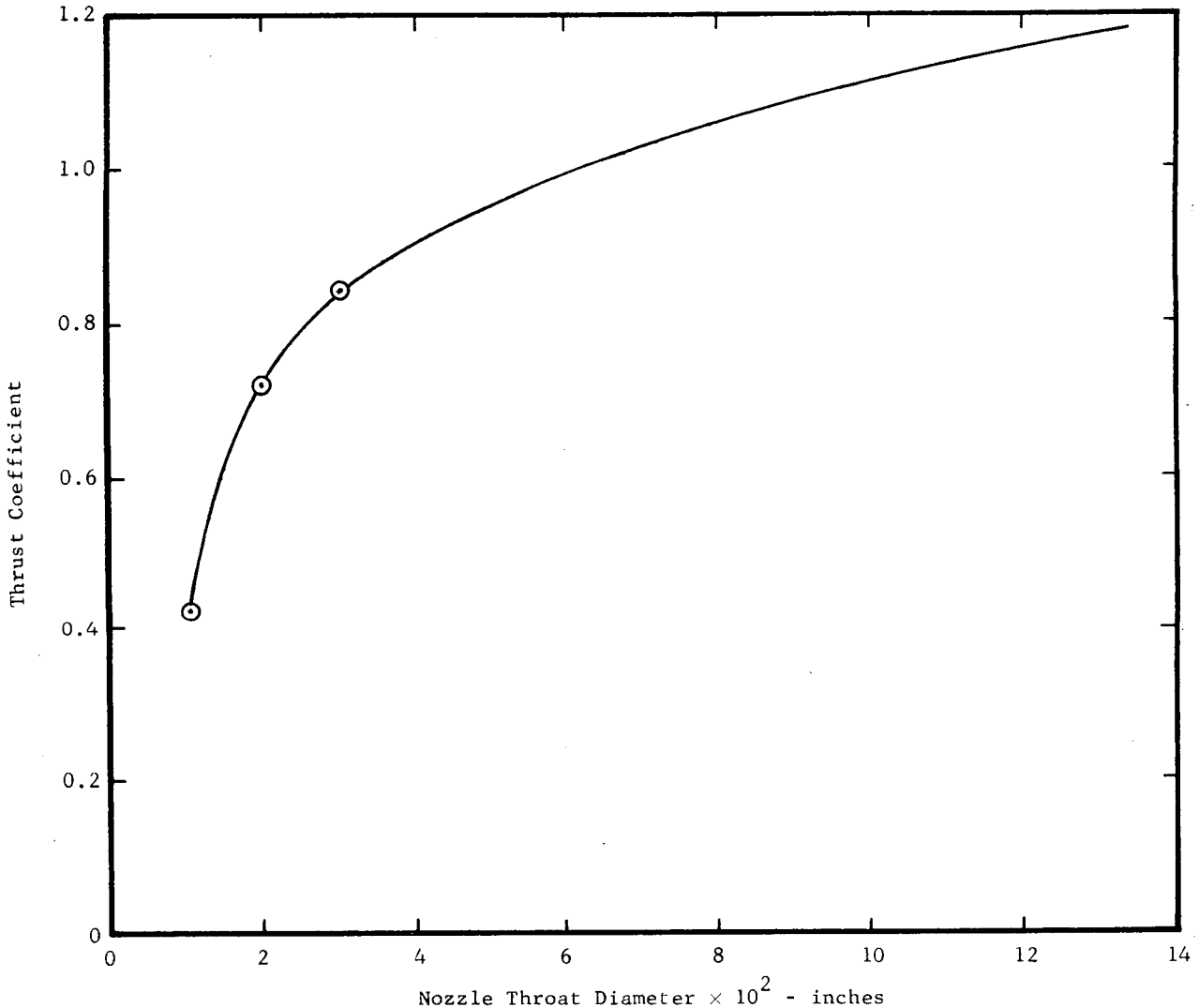

THRUST-COEFFICIENT VARIATION WITH NOZZLE THROAT DIAMETER FOR EXPANSION RATIO OF UNITY

FIGURE 31

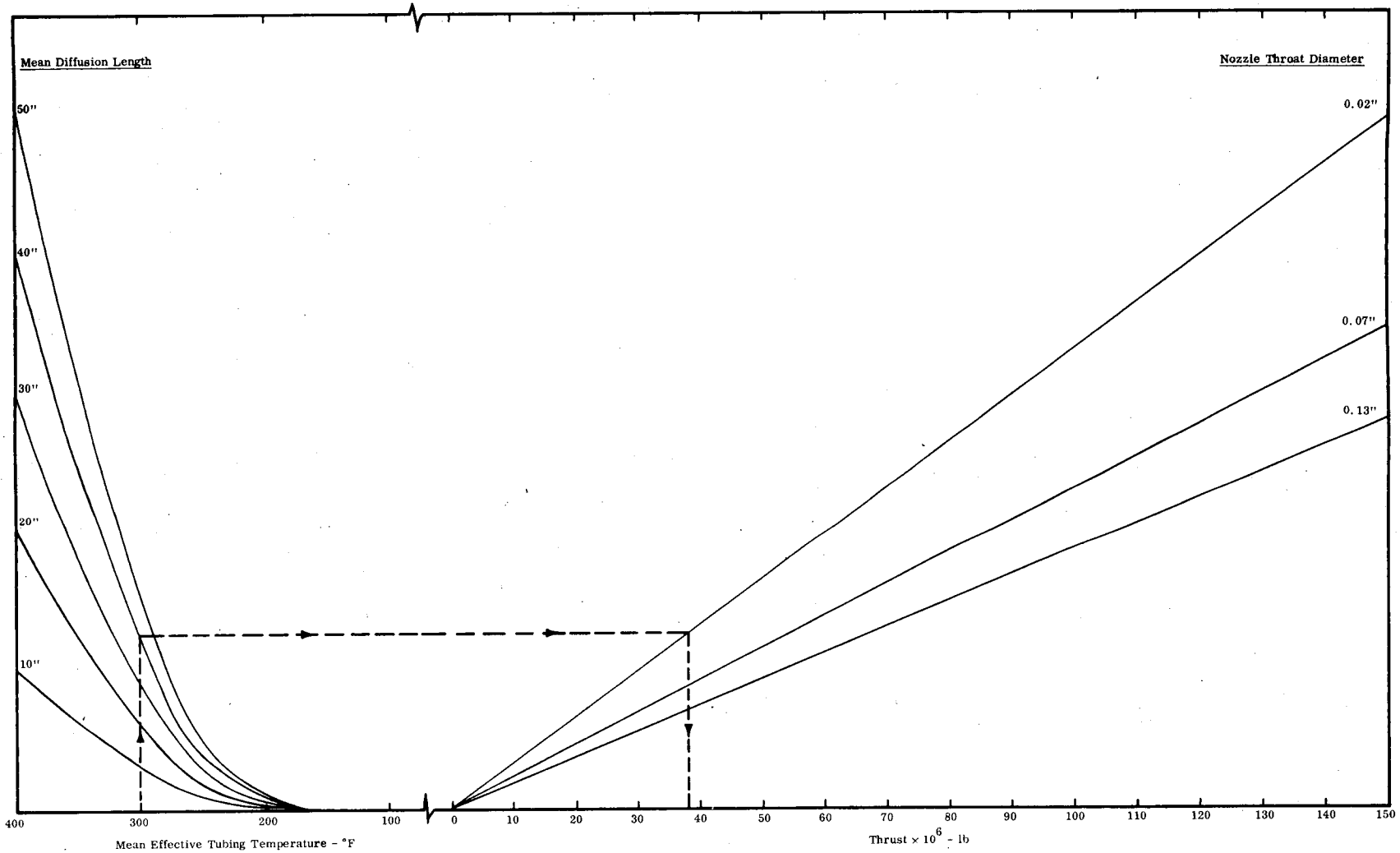

PERFORMANCE CURVES ILLUSTRATING THEORETICAL THRUST LEVELS PRODUCED BY DESCRIBED THRUSTER SYSTEM AS FUNCTIONS OF DIFFUSION-ELEMENT LENGTH, DIFFUSION-ELEMENT TEMPERATURE, AND CONVERGENT-NOZZLE THROAT DIAMETER

FIGURE 32

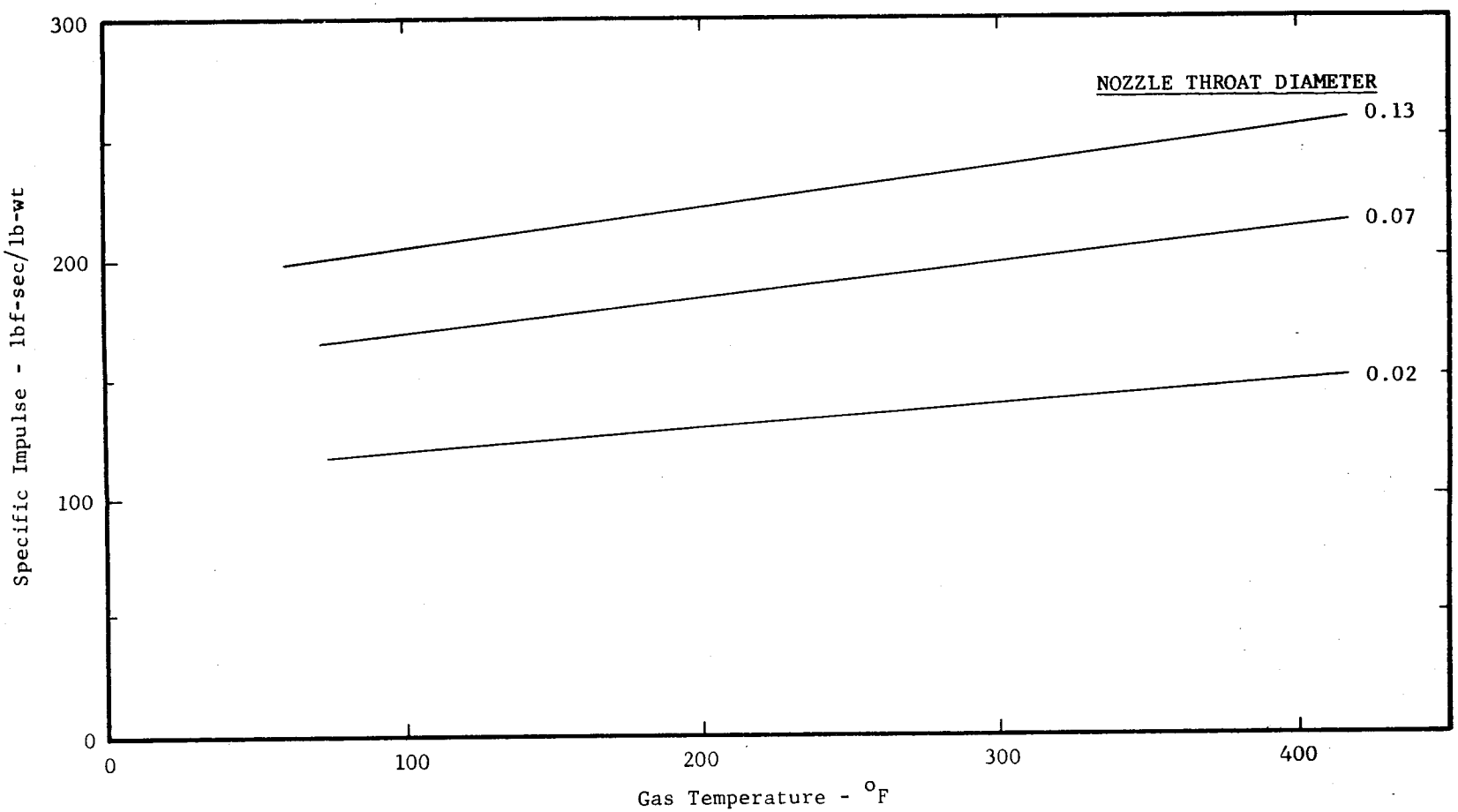

PERFORMANCE CURVES ILLUSTRATING THEORETICAL SPECIFIC IMPULSE PRODUCED BY DESCRIBED SYSTEM AS FUNCTIONS OF HYDROGEN-GAS TEMPERATURE AND NOZZLE THROAT DIAMETER

FIGURE 33

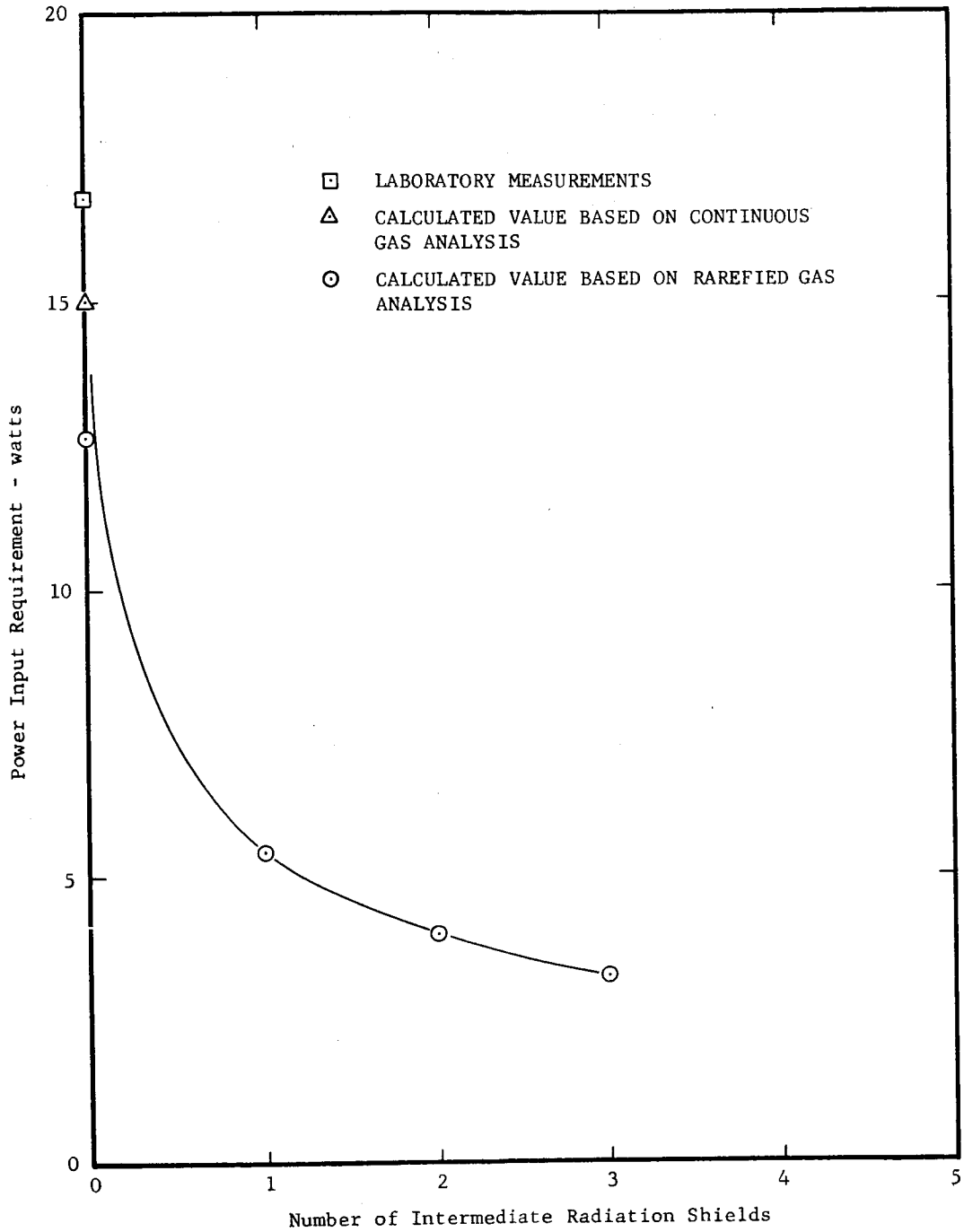

POWER REQUIREMENT AS A FUNCTION OF SHIELDING FOR A DIFFUSION THRUSTER SYSTEM EMPLOYING A 24-INCH ELEMENT AT 400°F

FIGURE 34

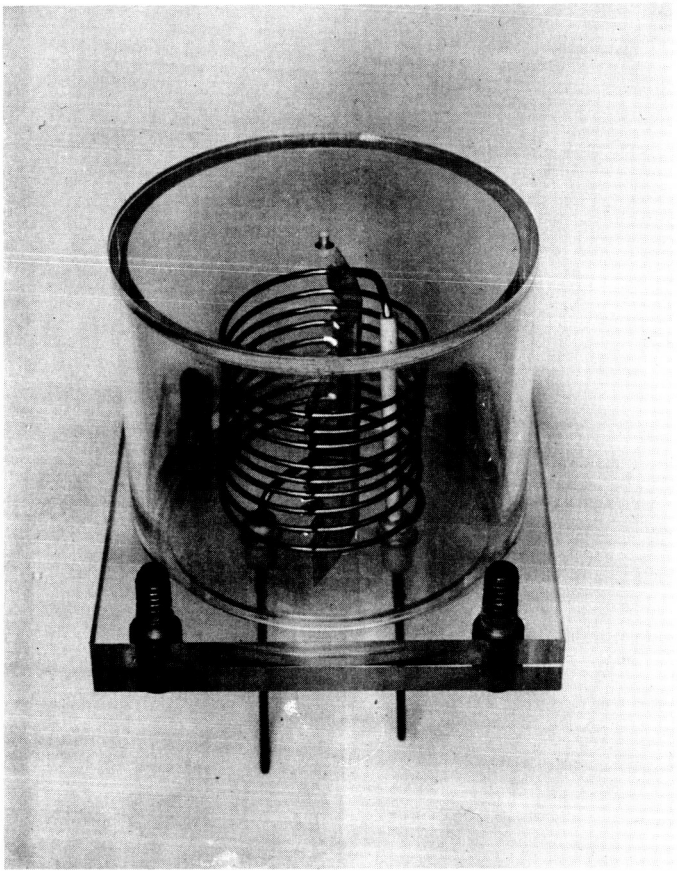

DISPLAY MODEL SHOWING GENERAL CONFIGURATION OF
BREADBOARD THRUSTER
(Thermal Insulation Not Shown)

FIGURE 35

PART NO.	ITEM	DIA "B"
8782-012	7	.020
8782-013	8	.070
8782-014	9	.130

PART NO.	ITEM	DIM "C"
8782-007	2	$2\frac{15}{32}$
8782-008	3	$2\frac{3}{16}$
8782-009	4	$1\frac{7}{8}$

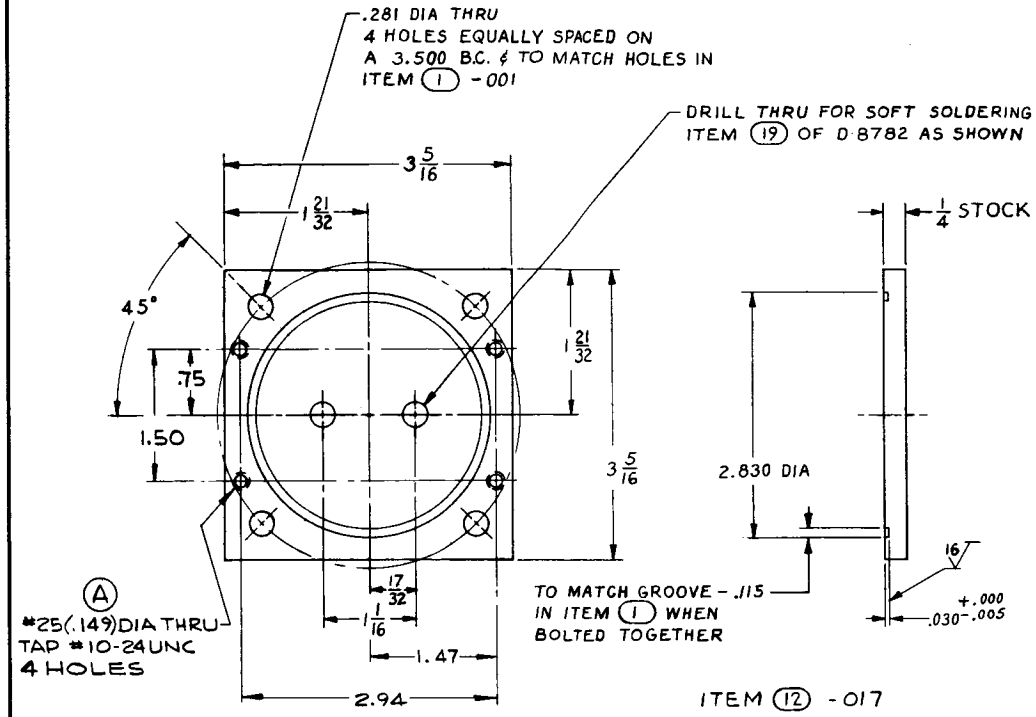

ITEM (12) -017

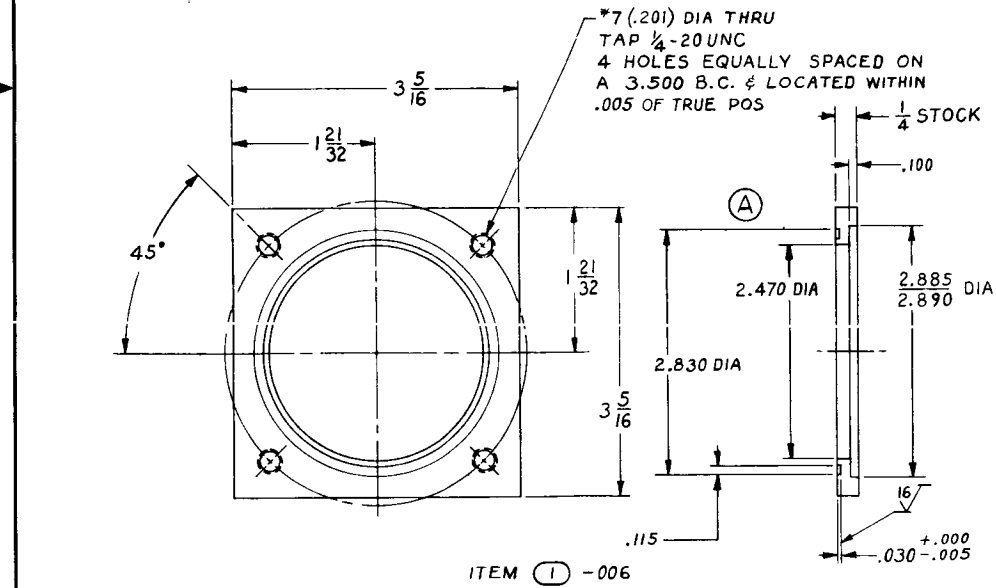

ITEM (1) -006

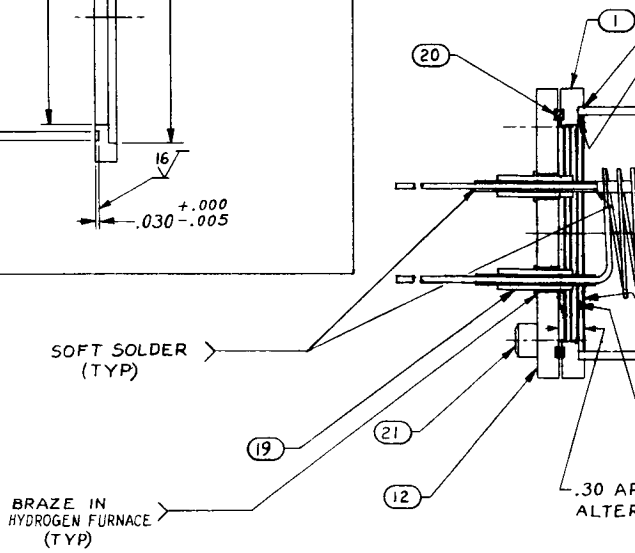

2. ALL MATERIAL AS SPECIFIED OR APPROVED EQUAL
1. ALL WELDED ¢ BRAZED JOINTS TO BE VACUUM TIGHT
NOTE:

2

E.O.(s) No. [ ] AMEND THIS DOCUMENT

REVISIONS				
SYM.	DESCRIPTION	DATE	DR. CHK	APPD.
A	E.O. 6204 INCORPORATED	4-26-65	[illegible]	[illegible]

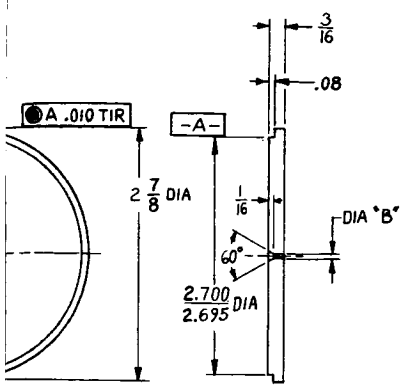

ITEM (7), (8) & (9)
-012, -013 & -014

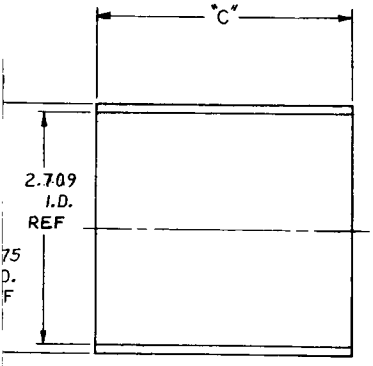

ITEM (2), (3) & (4)
-007, -008 & -009

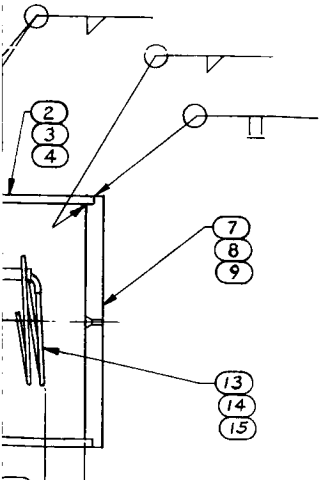

4 THK OF ITEM (22) & (23) (3)- 2 15/32 & (1) 2 11/16 DIA
Y INTERLEAVED AS SHOWN

QTY REQD	QTY REQD	QTY. REQD.	PART OR IDENTIFYING NO.	DWG. SIZE	NOMENCLATURE OR DESCRIPTION	MATERIAL, SPECIFICATION, OR NOTE		ITEM NO.
								24
A/R	A/R	A/R			FOIL	ALUMINUM		23
A/R	A/R	A/R			INSULATION	FIBER FRAX		22
4	4	4			SCREW HEX SOC HD	SST 1/4-20 UNC x 1/2 LG		21
1	1	1			"O" RING	RUBBER (MS 9021-146)		20
2	2	2			STR WALL INSUL-TUBE CTR COND (FEED THRU)	CERAMASEAL TERM. #800A0209-1		19
								18
								17
								16
1			8783-003	D	COIL ASSY			15
	1		8783-002	D	COIL ASSY			14
		1	8783-001	D	COIL ASSY			13
1	1	1	8782-017	D	FLANGE CAP	SST (TYPE 304)		12
								11
								10
1			8782-014	D	END CAP	SST (TYPE 304)		9
	1		8782-013	D	END CAP	SST (TYPE 304)		8
		1	8782-012	D	END CAP	SST (TYPE 304)		7
								6
								5
1			8782-009	D	BODY	SST (SCHEDULE 5S TYPE 304) PIPE 2.875 O.D. 2.709 I.D. .083 WALL		4
	1		8782-008	D	BODY	SST (SCHEDULE 5S TYPE 304) PIPE 2.875 O.D. 2.709 I.D. .083 WALL		3
		1	8782-007	D	BODY	SST (SCHEDULE 5S TYPE 304) PIPE 2.875 O.D 2.709 I.D. .083 WALL		2
1	1	1	8782-006	D	FLANGE RING	SST (TYPE 304)		1
-003	-002	-001	8782-	D	CANISTER ASSY			X

LIST OF MATERIAL OR PARTS LIST

NEXT ASSY. C-8784

UNLESS OTHERWISE SPECIFIED DIMENSIONS ARE IN INCHES
TOLERANCES ON
FRACTIONS ± 1/32 DECIMALS XX ± .01 XXX ± .005 ANGLES ± 1/2°
REMOVE ALL BURRS.
BREAK SHARP EDGES .015x45°
MACHINE FILLETS .01 R.
MACHINE FINISH 63 √ RMS.

MATERIAL: SEE ABOVE

DO NOT SCALE DRAWING

DR. C. LARCOM	2-25-65	
CHK. P.C. Bachmann	3-15-65	
MATL.		
REL.		
PROJ.		
PROJ.		
PROGRAM [illegible]	RELEASED 3-20-65	
APPROVED		
APPROVED		

American-Standard ADVANCED TECHNOLOGY LABORATORIES DIVISION MOUNTAIN VIEW, CALIFORNIA

CANISTER ASSY
H_2 DIFFUSION VALVE

CODE IDENT. NO.	SIZE	DRAWING NO.	REV.
02644	D	8782	A

SCALE 1/1 | JOB NO. 1230502 | SHEET 1 OF 1

ATL 16184-2/64

D 8782 A

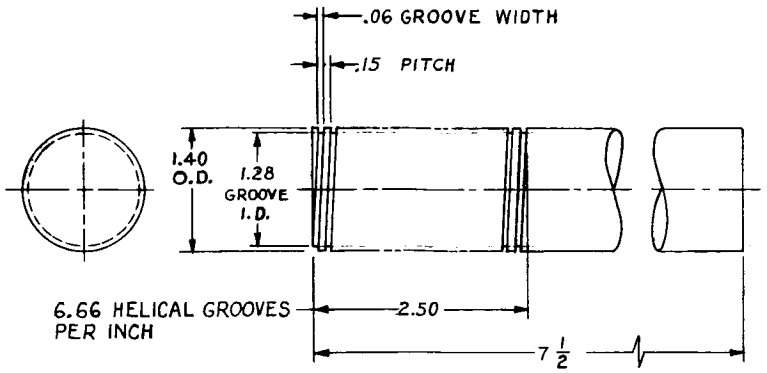

ITEM (16) -021

COIL FORM FOR ITEM (1) -006, (2) -007 & (3) -008

BRAZE

PART NO.	ITEM	DIM "D"
8783-006	1	1 3/8
8783-007	2	1 3/8
8783-008	3	1 1/16

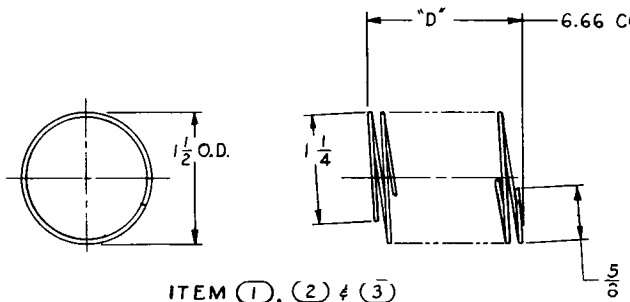

ITEM (1) -006, (2) -007 & (3) -008

PART NO.	ITEM	DIM "E"
8783-011	6	6
8783-012	7	5 9/16
8783-013	8	5 1/4

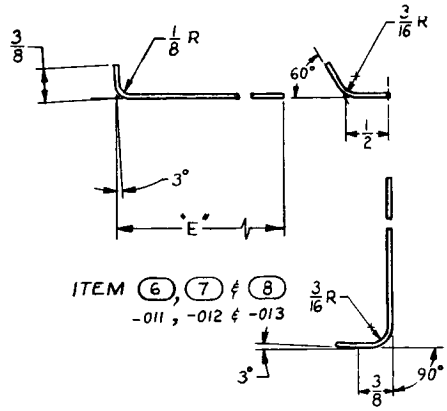

ITEM (6), (7) & (8) -011, -012 & -013

PART NO.	ITEM	DIM. "F"
8783-016	11	4 3/8
8783-017	12	3 13/16
8783-018	13	3 5/8

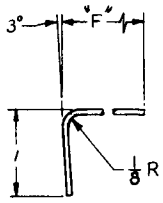

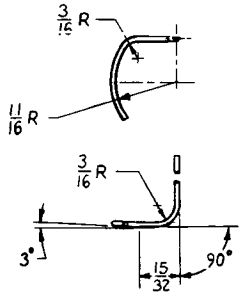

ITEM (11), (12) & (13) -016, -017 & -018

PART NO.	ITEM
8763-023	18
8763-024	19
8763-025	20

ITE

PART NO.	ITEM
8763-027	22
8763-028	23
8763-029	24

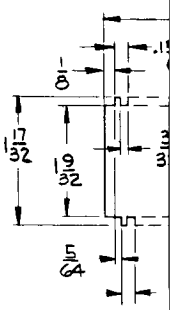

ITE

ALL MATERIAL AS SPECIFIED OR APPROVED EQUAL

NOTE:

2

E.O.(s) No. [ ] AMEND THIS DOCUMENT

REVISIONS				
SYM.	DESCRIPTION	DATE	DR. CHK	APPD.
A	E.O. 6205 INCORPORATED	4-22-65	EAM RCB	JC

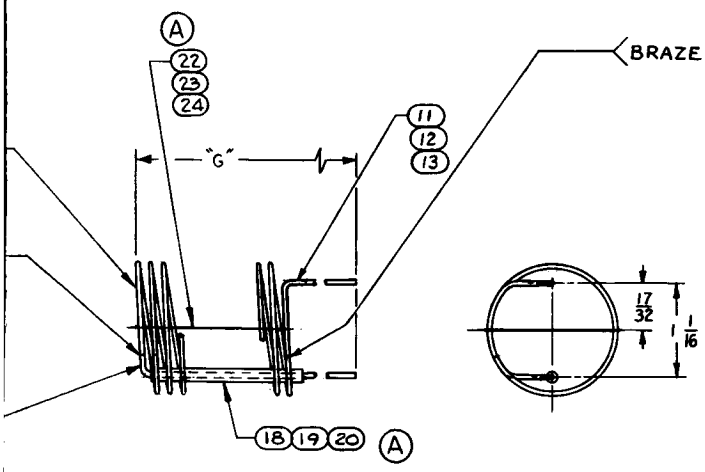

PART NO.	DIM "G" ± 1/8
8783-001	6 1/16
8783-002	5 1/2
8783-003	5 5/16

	QTY REQD	QTY REQD	QTY. REQD.	PART OR IDENTIFYING NO.	DWG. SIZE	NOMENCLATURE OR DESCRIPTION	MATERIAL, SPECIFICATION, OR NOTE		ITEM NO.
	1			8763-029	D	COIL SUPPORT	MICA .010 THK		24
A		1		8763-028	D	COIL SUPPORT	MICA .010 THK		23
			1	8763-027	D	COIL SUPPORT	MICA .010 THK		22
									21
A	3			8763-025	D	INSULATION TUBE	ALUMINA 1/8 O.D. x 1/16 I.D.		20
		3		8763-024	D	INSULATION TUBE	ALUMINA 1/8 O.D. x 1/16 I.D.		19
			3	8763-023	D	INSULATION TUBE	ALUMINA 1/8 O.D x 1/16 I.D.		18
									17
	—1—			8783-021	D	COIL FORM	LINEN PHENOLIC		16
									15
									14
	1			8783-018	D	COIL EXTENSION	SST .062 O.D. x .008 WALL		13
		1		8783-017	D	COIL EXTENSION	SST .062 O.D. x .008 WALL		12
			1	8783-016	D	COIL EXTENSION	SST .062 O.D. x .008 WALL		11
									10
									9
	1			8783-013	D	COIL EXTENSION	SST .062 O.D. x .008 WALL		8
		1		8783-012	D	COIL EXTENSION	SST .062 O.D. x .008 WALL		7
			1	8783-011	D	COIL EXTENSION	SST .062 O.D. x .008 WALL		6
									5
									4
	1/30"			8783-008	D	COIL	PALLADIUM SILVER ALLOY .045 O.D. x .003 WALL		3
A		1/40"		8783-007	D	COIL	PALLADIUM SILVER ALLOY .045 O.D x .003 WALL		2
			1/50"	8783-006	D	COIL	PALLADIUM SILVER ALLOY .045 O.D. x .003 WALL		1
	-003	-002	-001	8783-	D	COIL ASSY			X

LIST OF MATERIAL OR PARTS LIST

NEXT ASSY. D-8782

UNLESS OTHERWISE SPECIFIED DIMENSIONS ARE IN INCHES
TOLERANCES ON
FRACTIONS ± 1/32 DECIMALS XX ± .01 XXX ± .005 ANGLES ± 1/2°
REMOVE ALL BURRS. BREAK SHARP EDGES .015x45° MACHINE FILLETS .01 R.
MACHINE FINISH 63 √ RMS.

MATERIAL: SEE ABOVE

DO NOT SCALE DRAWING

DR. C. LARCOM	2-24-65	
CHK. R.C. Baelmann	3-15-65	
MATL.		
REL.		
PROJ.		
PROJ.		
PROGRAM	RELEASED 3-30-65	
APPROVED		
APPROVED		

American-Standard — Advanced Technology Laboratories Division, Mountain View, California

COIL ASSY
H_2 DIFFUSION VALVE

CODE IDENT. NO.	SIZE	DRAWING NO.	REV.
02644	D	8783	A

SCALE 1/1 | JOB NO. 1230502 | SHEET 1 OF 1

ATL 1838-4-2/64

D | 8783 | A

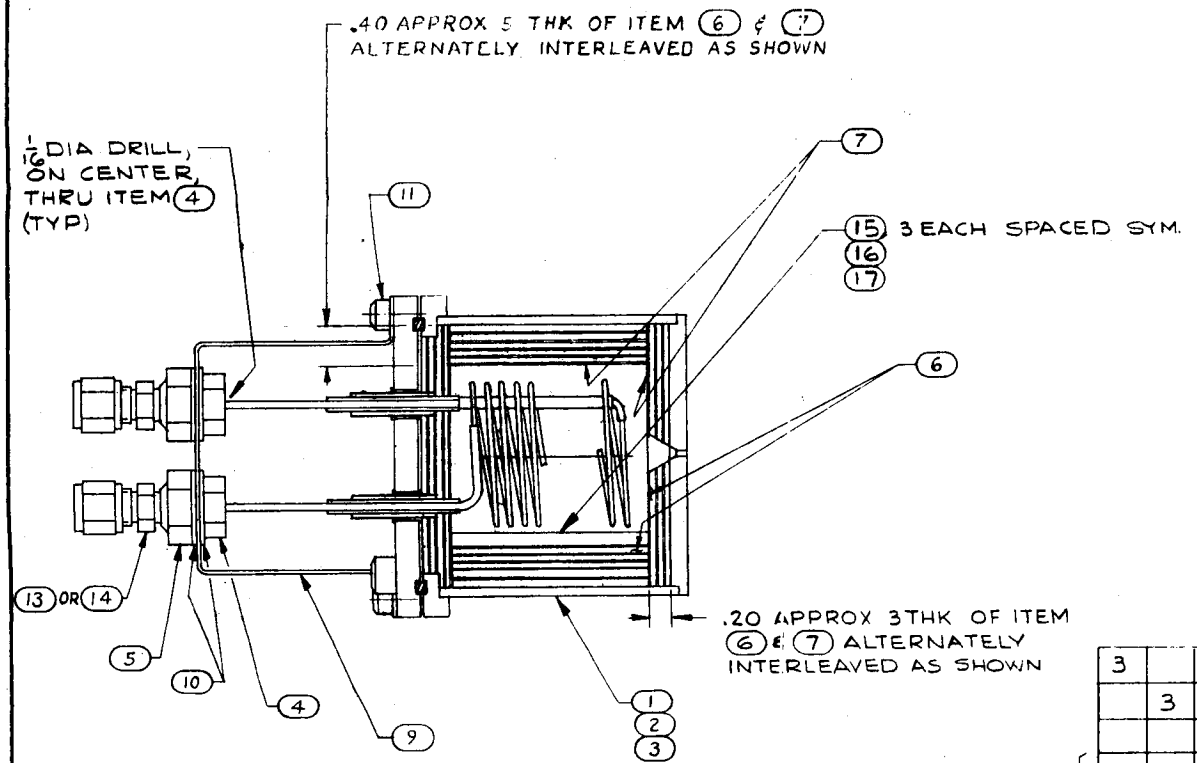

REQD	REQD	REQD	PART NO.	DWG SIZE	NAME OR DESCRIPTION	MATERIAL & MATL SPEC.	FIND NO
3			8784-012		INSULATION TUBE	ALUMINA 1/8 O.D. x 1/16 I.D. x 1 3/4 LG	17
	3		8784-011		INSULATION TUBE	ALUMINA 1/8 O.D. x 1/16 I.D. x 1 7/8 LG	16
		3	8784-010		INSULATION TUBE	ALUMINA 1/8 O.D. x 1/16 I.D. x 2 LG	15
2	2	2	IMPERIAL *768F	–	CONNECTOR 1/8 NPT FOR 1/8 O.D. TUBING	BRASS	14
2	2	2	IMPERIAL *68F	–	CONNECTOR 1/8 NPT FOR 1/8 O.D. TUBING	BRASS	13
							12
4	4	4		–	SCREW HEX SOC HD	SST 10-24 UNC x 1/4 LG	11
4	4	4		–	WASHER	NYLON 3/4 O.D. x 17/32 I.D. x 1/16 THK	10
1	1	1	8796-001	B	BRACKET		9
							8
A/R	A/R	A/R		–	FOIL	ALUMINUM	7
A/R	A/R	A/R		–	INSULATION	FIBER FRAX	6
2	2	2	IMPERIAL *111B	–	LOCK NUT	BRASS	5
2	2	2	IMPERIAL *188D	–	PLUG	BRASS	4
1			8782-003	D	CANISTER ASSY		3
	1		8782-002	D	CANISTER ASSY		2
		1	8782-001	D	CANISTER ASSY		1
-003	-002	-001	8784-	C	H_2 DIFFUSION VALVE ASSY		

OPTIONAL: ONE OR THE OTHER

2. UNIT TO BE VACUUM TIGHT
1. ALL MATERIAL AS SPECIFIED OR APPROVED EQUAL

NOTE:

UNLESS OTHERWISE NOTED
DIMENSIONS ARE IN INCHES
TOLERANCES: FRACTIONS ± 1/32 · DECIMALS XX ± .01 XXX ± .005 · ANGLES ± 1/2°
REMOVE ALL BURRS.
BREAK SHARP EDGES..015 X 45°
MACHINE FILLETS .01 R
MACHINE FINISH 63 RMS
DO NOT SCALE DRAWING

MATERIAL &/OR HEAT TREAT: SEE ABOVE
NEXT ASSY

APPROVALS
DRAWN—DATE C. LARCOM 2-26-65
CHECK—DATE 3/19/65
APPD—DATE 3/15/65
APPD—DATE

H_2 DIFFUSION VALVE ASSY

CONTRACT NUMBER
SCALE 1/1 | JOB NO 1230502 | DWG INDEX

ADVANCED TECHNOLOGY LABORATORIES
A DIVISION OF AMERICAN-Standard
369 WHISMAN ROAD MOUNTAIN VIEW, CALIF.

DWG SIZE C 8784 | REV LTR A
SHEET 1 OF 1

ATL-10 REV. 10/28/65

C 8784 A

APPENDIX A

RELATIONSHIP BETWEEN DIFFUSION AND PERMEATION

Throughout this report, the terms diffusion and permeation are used interchangeably to describe the mass transfer of hydrogen gas through the wall of palladium-silver-alloy tubing. The following discussion indicates the relationship between the two terms and justifies this terminology.

The rate at which a gas diffuses through a metal can be shown to depend upon the concentration gradient of the gas in the metal along the flow direction x as given by Fick's law:[8,16]

$$\frac{\partial c}{\partial \tau} = \frac{D \partial^2 c}{\partial x^2} \quad , \tag{A-1}$$

where $\frac{\partial c}{\partial \tau}$ = rate of change of concentration of component per unit volume,

$\frac{\partial c^2}{\partial x^2}$ = change with respect to flow direction of the concentration profile.

For steady-state diffusion through a plane membrane, equation A-1 can be integrated to give the mass transfer rate per unit area of the diffusion gas (ref.Figure A-1):

$$\frac{\dot{m}}{A} = \frac{\bar{D}}{\ell}(c_1 - c_2) \quad . \tag{A-2}$$

In certain engineering applications, however, it is more convenient to express rates of transfer in terms of partial pressures on the two side of the membrane $(p_1 - p_2)$, rather than in terms of the surface concentrations $(c_1 - c_2)$, which are usually quite difficult to measure. A new parameter called permeability is then used and is defined as:

$$P = \frac{\dot{m}/A}{(p_1 - p_2)/\ell} \quad . \tag{A-3}$$

Comparison of equations A-2 and A-3 suggests that if a relationship (called sorption isotherms) between the partial pressure and the surface concentration is known, p may be expressed as a function of the diffusion coefficient D. The relationship can be obtained either from experimental measurements or, where applicable, from Henry's law:

$$P = C_3 c \quad . \tag{A-4}$$

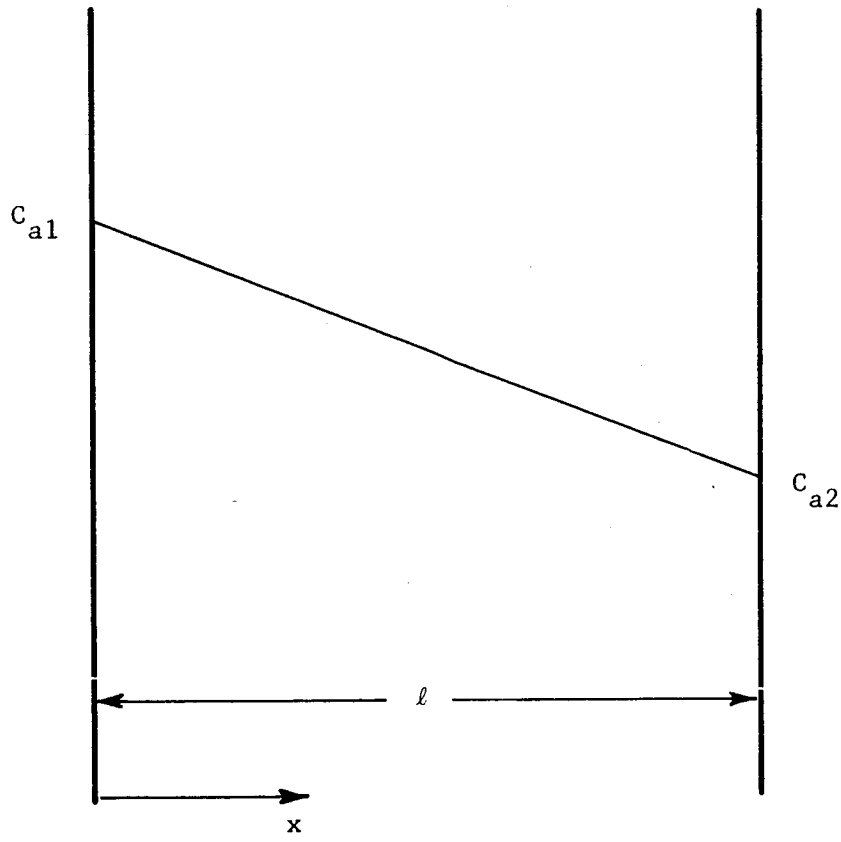

STEADY-STATE-CONCENTRATION DISTRIBUTION IN A PLANE MEMBRANE

FIGURE A-1

APPENDIX B

SAMPLE CALCULATION OF HYDROGEN FLOW RATES

Based on the procedures described in Section I. of this report, ultra-pure hydrogen gas is diffused through the palladium-silver-alloy diffusion element and caused to flow into the collection vessel. Representative test data and a hydrogen-flow-rate calculation are presented below

1. Test Data

   a) Dimensions of diffusion element: 24" × 0.045" OD × 0.003" wall.

   b) Pressure drop across diffusion element: 64.7 psia.

   c) Power input to maintain diffusion-element temperature: 9.9 watts.

   d) Mean temperature of diffusion element: 300°F.

   e) Temperature of collection vessel and McLeod gages: 80°F.

   f) Pressure upstream of orifice: 0.73×10^{-3} torr.

   g) Initial pressure in collection vessel: 0.181×10^{-3} torr.

   h) Pressure in collection vessel after 30 seconds of hydrogen gas accumulation: 0.928×10^{-3} torr.

2. Calculation

$$\dot{m} = \frac{\Delta P V}{R T \Delta \tau} \quad , \tag{B-1}$$

$$\dot{m} = \frac{(0.928 - 0.121)(1.067)(2117)}{767\,(540)(30)(760)} \quad ,$$

where 760 mm Hg = 2117 lbf/ft^2

$$\dot{m} = 1.77 \times 10^{-7} \text{ lbm/sec} = \text{average total mass flow rate.}$$

For unit mass flow rate:

$$M = \frac{\dot{m}}{A/h} = \frac{1.77 \times 10^{-7}}{2\,(0.0225)/3} = 1.57 \times 10^{-7} \text{ lbm/sec-in.}^2/0.001 \text{ in.}$$

APPENDIX C

DETERMINATION OF EMPIRICAL RELATIONSHIP

A form of the basic permeability equation can be expressed as:[3]

$$\dot{M} = \frac{A}{h} C_1 e^{-C_2/T} (\Delta P)^n \quad . \quad * \qquad \text{(C-1)}$$

The term C_1 is a characteristic constant of the gas-metal system. The term C_2 is a constant defined by:[7]

$$C_2 = \frac{E_o}{2 R_o} \quad , \qquad \text{(C-2)}$$

where $E_o/2$ = heat of diffusion in gram-calories per gram-atom.

The reciprocal nature between the unit mass flow rate and the diffusion-element thickness indicated by equation C-1 has been well established for numerous gas-metal systems including a hydrogen-palladium system.[1,3] Therefore, additional investigation of this reciprocal trend was not conducted.

Figure C-1 shows unit hydrogen flow rate as a function of the reciprocal of the mean tubing temperature expressed in absolute units. The points on Figure C-1 do not represent actual measured data points. However, they were taken directly from the experimental results presented in Figure 7 for a 24-inch diffusion element (11). This approach was used in the construction of Figure C-1 to eliminate any influence of the original data scatter (see Figure 7).

From Figure C-1, the following relationship was determined:

$$\dot{M} \propto e^{-11,120/T} \quad . \qquad \text{(C-3)}$$

Figure C-2, plotted from information in Figure C-1, relates the unit hydrogen flow rates to the effective pressure differential across the diffusion element. Due to both the scarcity and the scatter of the results indicated in Figure C-2, it is difficult to validly establish an empirical relationship between the unit flow rates and the

---

* Symbols defined in Nomenclature except as noted.

pressure differential across the diffusion element. However, other investigators found that, generally, for gas-metal systems, n in equation C-1 is equal to 0.050 ± 0.01.[1,3,16,17] This trend is also suggested by the curve drawn on Figure C-2.

By substituting the above results into equation C-1, the value of C_1 was determined for typical experimental conditions. Equation C-1 then took the following form:

$$\dot{M} = \frac{3.82 \times 10^{-2} \, A \, e^{-11,120/T} \sqrt{\Delta P}}{h} \quad . \tag{C-4}$$

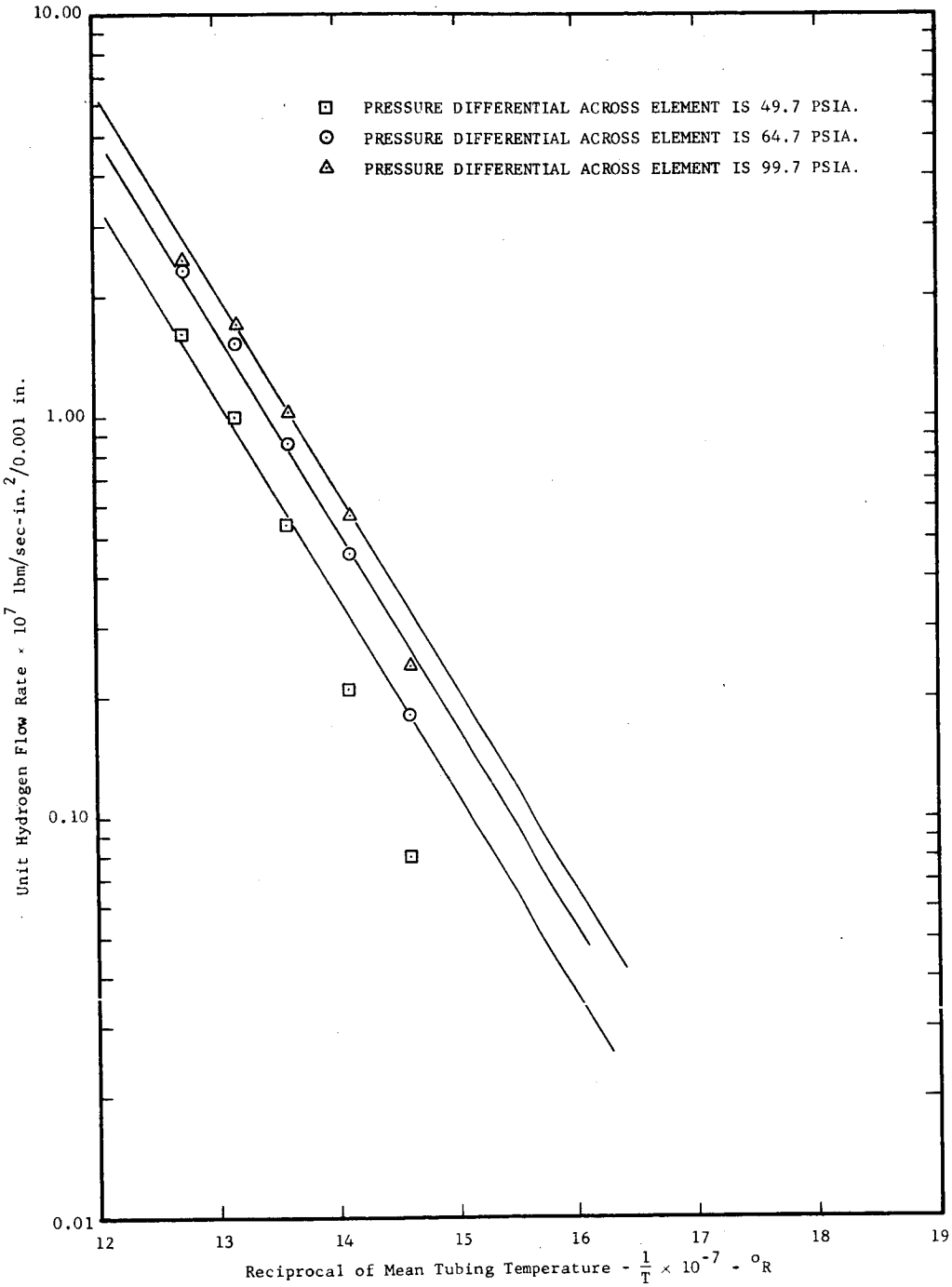

EFFECT OF RECIPROCAL OF MEAN TUBING TEMPERATURE
ON UNIT HYDROGEN FLOW RATE
AT INDICATED PRESSURE DIFFERENTIALS
FOR A 24-INCH DIFFUSION ELEMENT

FIGURE C-1

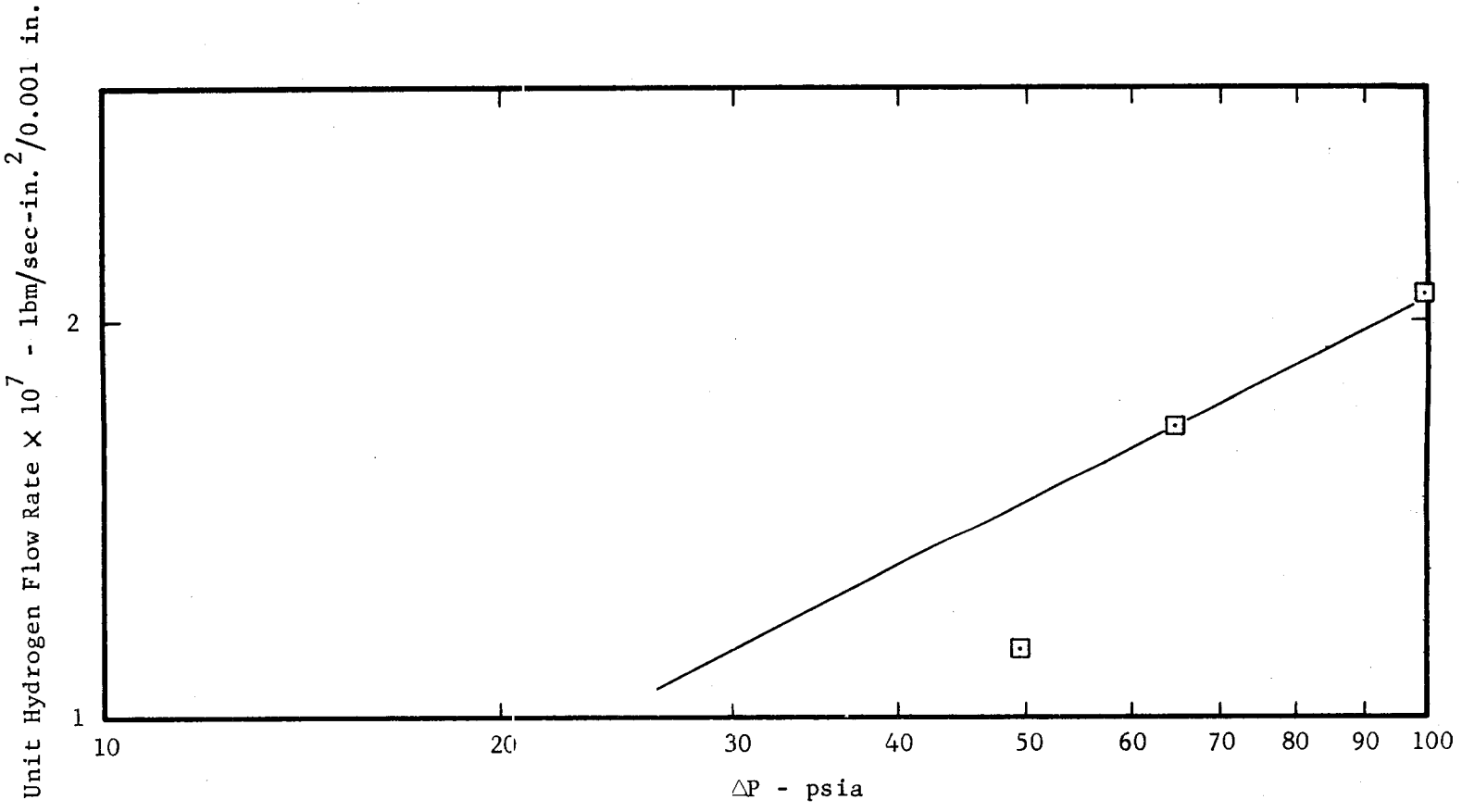

EFFECT OF PRESSURE DIFFERENTIAL ACROSS DIFFUSION ELEMENT ON UNIT HYDROGEN FLOW RATE FOR A 24-INCH ELEMENT

FIGURE C-2

APPENDIX D

ANALYTICAL APPROACH USED FOR POWER INPUT STUDIES

1. Power Requirement for Laboratory Diffusion System

A sketch of the applicable part of the laboratory diffusion system and the heat-loss mechanisms considered in this analysis are shown in Figure D-1a. A heat balance on an equivalent thruster configuration would include:

$$P = \sum q_l = q_r + q_c + q_{cd} + q_h \quad . \tag{D-1}$$

Equation D-1 indicates that the power input depends on the heat loss due to radiation from the diffusion element to the radiation shields, convection from the diffused-hydrogen gas to the radiation shield, conduction losses along the diffusion-element length, and the heat input required to raise the temperature of the hydrogen gas from ambient to the specified temperature of the diffusion element. Radiation from the diffused-hydrogen gas to the radiation shield was excluded in this analysis because hydrogen gas is almost transparent to thermal radiation.

Using equation D-1, the power requirement was calculated for a 24-inch diffusion element operating at a pressure differential of 64.7 psia across the element and at a mean tubing temperature of 400°F. Figure D-1b illustrates the system and the various sections employed in this analysis. The methods used for determining heat losses are discussed below.

a. Radiation Heat Loss

The magnitude of radiation heat loss can be evaluated by:[18]

$$q_r = \sigma f_{1-2} A_1 (T_1^4 - T_2^4) \quad , \tag{D-2}$$

where f_{1-2} is the gray-body radiation shape factor between the diffusion element and the radiation shield and accounts for both geometry and emissivity effects. In general, the determination of shape factors for all but the most simple geometric configurations is complex. This is especially true for gray-body radiant exchange between a helical cylindrical shape encompassed by a hollow cylinder. However, the complexity of this shape-factor calculation can be reduced significantly while still preserving a first-approximation estimate of the radiant exchange, if the shape factor

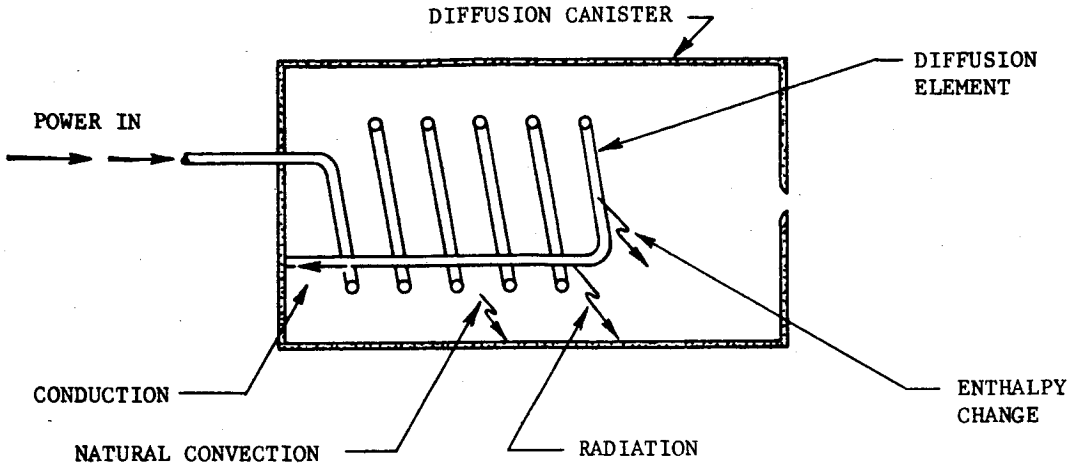

a. Heat-Loss Mechanisms

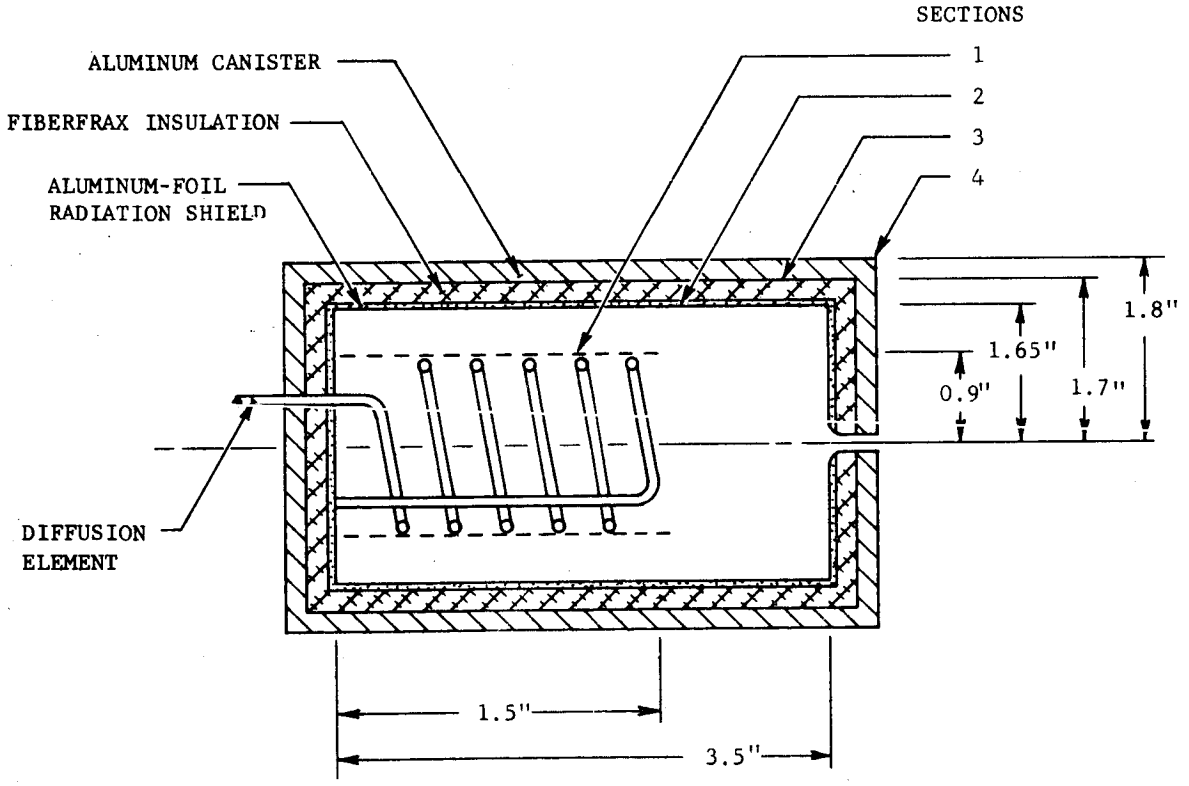

b. System Description and Geometry

DIAGRAMMATIC SKETCH OF LABORATORY DIFFUSION-CANISTER CONFIGURATION FOR POWER-REQUIREMENT CALCULATIONS

FIGURE D-1

is described in terms of radiation between two gray-body concentric cylinders. For such an application, the shape factor reduces to:[18]

$$f_{1-2} = \frac{1}{\frac{1}{\epsilon_1} + \frac{A_1}{A_2}\left(\frac{1}{\epsilon_2} - 1\right)} \quad . \tag{D-3}$$

Since this modified form of the shape factor can be easily calculated, it remains only to determine the radiation-shield temperature (T_2) in order to evaluate the radiant heat exchange. Direct measurement of the shield temperature resulted in a maximum value of 130°F.

An effort was also made to calculate a value of the shield temperature (T_2) based on applying a heat balance across the canister section of the diffusion system (ref. Figure D-1b, sections 1 through 4). The heat balance took the following form:

$$\sigma f_{1-2} A_1 (T_1^4 - T_2^4) = \frac{[2\pi k_\ell]_{2-3}}{\ln (r_3/r_2)} (T_2 - T_3) = \frac{[2\pi k_\ell]_{3-4}}{\ln (r_4/r_3)} (T_3 - T_4) \quad . \tag{D-4}$$

The thermal conductances can be evaluated from the material properties and system dimensions, and the temperature of the outer wall of the canister can be measured. Solving these simultaneous equations (equation D-4) will eliminate T_3, resulting in a value of T_2 equal to approximately 115°F, which agrees favorably with the measured value. The use of equation D-2 resulted in a value of 6.5 watts for the radiant exchange between the diffusion element and the radiation shield for the stated operating conditions and the assumed shape-factor geometry.

b. Convection Heat Loss

The convection heat transfer between the diffused-hydrogen gas and the cylindrical aluminum-foil radiation shield can be estimated by considering only natural-convection heat transfer (stagnation-chamber conditions), which can be described in terms of natural-convection exchange for short vertical plates or tubes. While forced-convection heat losses will occur in the orifice region of the canister, this contribution to the over-all heat loss is quite small and will be neglected. The convection heat transfer can thus be expressed by:[19]

$$q_c = h_c A_2 (T_g - T_2) \quad , \tag{D-5}$$

where h_c is strongly dependent on the properties of the diffused-hydrogen gas evaluated at the canister-chamber pressure and the arithmetic-mean temperature between the gas and the shield surface.

Extensive natural-convection heat-transfer data have been collected for short vertical plates and tubes (0.5 to 12 inches).[19] This data can be best correlated and utilized in terms of the dimensionless functions of Prandtl, Grashof, and Nusselt numbers, which are defined respectively by:

$$Pr = \frac{\mu c_p}{k} \quad . \tag{D-6}$$

$$Gr = \frac{\rho^2 g \beta (T_2 - T_g) \ell^3}{\mu^2} \quad . \tag{D-7}$$

$$Nu = \frac{h_c \ell}{k} \quad . \tag{D-8}$$

Of the parameters shown in equations D-6 through D-8, the gas temperature, T_g, is the most difficult to evaluate accurately due to radiation heating of the gas-temperature thermocouple by the diffusion element. An attempt was made to hold this heating effect to a minimum during gas-temperature measurement by appropriate thermocouple shielding. A number of gas-temperature measurements were made at various points in the diffusion canister. The measurement was found to vary between approximately 210 and 390°F, depending on the proximity of the measuring thermocouple to the diffusion element. A value of 300°F was therefore chosen for the effective free-stream gas temperature.

Determination of the heat-transfer coefficient involved first evaluating the Prandtl and Grashof numbers for the test conditions. This process fixes the value of the Nusselt number, which can then be determined from the literature. Magnitudes of the Prandtl, Grashof, and Nusselt numbers were found to be 0.731, 0.00945, and 1.121, respectively. Using the convection heat-transfer coefficient from equation D-8, equation D-5 resulted in natural-convection heat transfer equal to 7.76 watts.

c. Conduction Heat Loss

Conduction heat loss along the length of the diffusion element can be expressed in terms of the Fourier conduction law in one dimension:[18]

$$q_{cd} = k A \frac{dT}{dx} \quad . \tag{D-9}$$

The magnitude of this heat-loss mode was found to be negligible because 1) significant temperature gradients were eliminated by the presence of the stainless-steel transition tubing between the hydrogen gas supply and the diffusion element, and 2) the cross-sectional area available for heat conduction was very small (4.0×10^{-4} in.^{2}).

d. Enthalphy Change

The amount of heat required to raise the hydrogen gas temperature from ambient (i.e., storage temperature) to the specified diffusion-element temperature can be determined by again applying the first law of thermodynamics across a section of the diffusion-element-tubing wall. This energy balance reduces to[18]

$$q_h = \dot{m} c_p (T_1 - T_a) = \Delta H \quad , \tag{D-10}$$

which is the change in enthalpy of the hydrogen gas. The value of $\dot{m}$ (total hydrogen mass flow rate) can be determined from the experimental data. The enthalpy change was computed to be 0.77 watt.

2. Power-Optimization Analysis

In the analysis described in Section III. D. 2., the dimensions of both the diffusion element and the thruster body were identical to diffusion element 10 and the laboratory diffusion canister (see Figure D-1). The calculations described were made for the above system with the addition of 1, 2, and 3 intermediate radiation shields evenly spaced between the element and the interior of the diffusion canister.

Before actual heat-transfer magnitudes could be evaluated for the different insulation designs, the temperature of the intermediate shields had to be estimated. The method used to calculate these temperatures is identical to that described in 1.a. above.

Radiation heat-transfer rates were estimated for the various shielding configurations using the techniques described in 1.a. above. The evaluation of the natural-convection

effects did not make use of the conventional techniques for natural-convection heat-transfer calculations (see 1.b.). Instead, the approach consisted of applying relationships correlated to experimental studies of natural convection from heat wires in gases at pressures varying between 5×10^{-2} and 760 torr.[19] This type of analysis defines a fictitious Nusselt number (Nu*):[19]

$$\frac{2}{Nu} = \frac{2}{Nu^*} + \frac{8\gamma\lambda}{\alpha Pr(\gamma + 1)d} - \ln\left(\frac{1 + 2\lambda}{d}\right) \quad . \tag{D-11}$$

The observed Nusselt number (Nu) becomes equal to Nu* when rarefied-gas effects are absent. In the presence of natural convection, values of Nu* can be determined by:

$$\frac{2}{Nu^*} = \ln\left[1 + \frac{6.82}{(Gr\ Pr)^{1/3}}\right] \quad , \tag{D-12}$$

for $10^{-8} \leq Gr\ Pr \leq 10^{-1}$.

The Nusselt number can be determined from equation D-11. The convection heat-transfer coefficient, determined from equation D-8, is then substituted into equation D-5 to evaluate the natural-convection heat loss.

NOMENCLATURE

A = area (in.^{2})

C = constant

c = mass concentration per unit volume (lbm/in.^{3})

c_p = specific heat at constant pressure (Btu/lbm-°R)

C_F = thrust coefficient

D = diffusion coefficient (ft^2/hr)

d = diameter (in.)

E_o = heat of diffusion (gram-calories/mole)

F = thrust (lbf)

f_{1-2} = gray-body radiation shape factor between diffusion element and radiation shield

g = acceleration due to gravity = 32.2 ft/sec^2

g_c = gravitational conversion factor = 32.2 lbm-ft/lbf-sec^2

H = total enthalpy (Btu)

h = wall thickness (in.)

h_c = convective heat-transfer coefficient (Btu/hr-ft^2-°F)

I_s = specific impulse (lbf-sec/lb-wt)

k = thermal conductivity (Btu/ft-hr-°F)

ℓ = length (in.)

$\dot{M}$ = unit mass flow rate (lbm/sec-in.^{2}/0.001 in.)

$\dot{m}$ = total mass flow rate (lbm/sec)

n = exponential power

P = permeability coefficient (ft^2/hr); power (watt); gas pressure (psia)

q = heating rate (watts)

R = gas constant for hydrogen = 778 ft-lbf/lbm-°R

R_o = universal gas constant = 1545 ft-lbf/mole-°R

T = temperature (°F; °R)

U = mean molecular velocity = $\sqrt{8/\pi g_c RT}$ (ft/sec)

V = velocity (ft/sec); volume (cubic ft)

$\dot{w}$ = total weight flow rate (lb-wt/sec)

x = coordinate direction

α = accommodation coefficient = actual energy change/ideal energy change

β = coefficient of thermal expansion (1/°F)

γ = ratio of specific heats at constant pressure and volume

Δ = change between two points or sections

ϵ = total emissivity

λ = mean free path (ft)

μ = viscosity (lbf-sec/ft^2)

ρ = density (lbm/ft^3)

σ = Stefan-Boltzmann constant = 0.1714×10^{-8} Btu/ft^2-°R^4-hr

τ = time (sec)

Dimensionless Groups

Gr = Grashof number

K = Knudsen number

M = Mach number

Nu = Nusselt number

Nu* = fictitious Nusselt number

Pr = Prandtl number

Re = Reynolds number

Subscripts

a = ambient

c = convection

cd = conduction

g = gas

h = enthalpy

l = loss

r = radiation

t = throat

1 = section 1

2 = section 2

3 = section 3

4 = section 4

} Ref. Figure D-1.

REFERENCES

1. "Research on Diffusion of Hydrogen Through Palladium," Advanced Technology Laboratories, A Division of American-Standard, First Phase Report, ATL-D-943, 21 December 1962.
2. "Research on Diffusion of Hydrogen Through Palladium," Advanced Technology Laboratories, A Division of American-Standard, Second Phase Report, ATL-D-1136, 28 October 1963.
3. W. Jost, Diffusion, New York, Academic Press, Inc. (1952).
4. Colin J. Smithells, Metal Reference Book, Vol. II, New York, Interscience Publishing, Inc. (1955).
5. R. Rubin, "Purification of Hydrogen by Permeation Through Palladium and Palladium-Silver Alloys," Englehard Industries, Inc., Technical Bulletin, Vol. II, No. 1, June 1961.
6. "Tube Laboratory Manual," Research Laboratory of Electronics, Massachusetts Institute of Technology (1956).
7. S. Dushmann and J. Lafferty, Scientific Foundations of Vacuum Technique, 2nd Edition, New York, John Wiley and Sons (1962).
8. W. Rohsenow and H. Choi, Heat Mass and Momentum Transfer, New York, Prentice Hall, Inc. (1961).
9. A. H. Shapiro, The Dynamics and Thermodynamics of Compressible Fluid Flow, Vol. I, New York, Ronald Press Co. (1953).
10. G. P. Sutton, Rocket Propulsion Elements, New York, John Wiley and Sons (1958).
11. B. E. Tinling, "Measured Steady State Performance of Water Vapor Jets for Use in Space Vehicle Attitude Control Systems," NASA TN D-1302 (1962).
12. "Hydrogen Purification Technical Data Sheet," J. Bishop and Co., Malvern, Pa., June 1961.
13. R. G. Folson, "Nozzle Characteristics in High Vacuum Flows - Rarefied Gas Dynamics," Transactions of the ASME, August 1952.
14. M. W. Milligan, "Nozzle Characteristics in the Transition Regime Between Continuum and Free Molecular Flow," AIAA Journal, 2, No. 6, June 1964.
15. B. Dayman, "Simplified Theoretical Estimates of Thrust Losses in Miniature Nozzles," Internal Memorandum, JPL CP-1, California Institute of Technology, April 1961.
16. R. E. Treyhal, Mass-Transfer Operations, New York, McGraw-Hill Book Co., Inc. (1955).
17. "Investigation of Static (Valveless) Flow Control of Gases," Advanced Technology Laboratories, A Division of American-Standard, Summary Report, ATL-453, September 30, 1960.

REFERENCES
(concl.)

18. W. H. Giedt, Principles of Engineering Heat Transfer, New York, D. Van Nostrand Co., Inc. (1957).

19. W. H. McAdams, Heat Transmission, 3rd Edition, New York, McGraw-Hill Book Co., Inc. (1954).

DISTRIBUTION

	No. of Copies
Headquarters National Aeronautics and Space Administration Washington 25, D. C.	
REC - Mr. Carl Janow	3
RPL - Mr. F. Compitello	2
MAT - Mr. M. Malamut	2
RC - Mr. J. Sloop	1
Headquarters National Aeronautics and Space Administration Technical Information Division, Code AFSS-L 400 Maryland Avenue, S. W. Washington 25, D. C.	2
NASA Goddard Space Flight Center Greenbelt, Maryland	
Mr. Dave Sudduth	2
Mr. Wm. Isley	1
Mr. J. Fedor	1
Mr. R. Darcey	1
NASA Western Operations Office 150 Pico Boulevard Santa Monica, California	
Technical Division, Mr. P. Pomerantz	2
Contracting Officer	1
Technical Library	1
NASA George C. Marshall Space Flight Center Huntsville, Alabama	
Technical Library	2
Mr. A. Krupnick	1
NASA Ames Research Center Moffett Field, California	
Technical Library	2
Mr. G. Kanning	2
NASA Langley Research Center Langley Station Hampton, Virginia	
Technical Library	2

	No. of Copies
NASA Lewis Research Center 21000 Brookpark Road Cleveland 35, Ohio	
Mr. I. Johnsen	2
Mr. H. Childs	1
Technical Library	2
NASA Manned Spacecraft Center Houston 1, Texas	
Mr. J. G. Thibodaux	1
Mr. H. Pohl	1
C. Yodzis	1
Technical Library	2
Liquid Propellant Information Agency The Johns Hopkins University Silver Spring, Maryland	2
Jet Propulsion Laboratory 4800 Oak Grove Drive Pasadena, California	
Mr. Edgar Koch	1
Mr. Benn Martin	1
Mr. R. G. Forney	1
Mr. R. Rose	1
Technical Library	2
Advanced Research Projects Agency Washington 25, D. C.	
Mr. Fred A. Koether	2
Central Intelligence Agency 2430 East Street, N. W. Washington 25, D. C.	
OCD, Standard Dist.	2
Office of the Director of Defense Research and Engineering Washington 25, D. C.	
Mr. H. Schulz	2
National Bureau of Standards Washington 25, D. C.	
Dr. Beckett	1
Commander Aeronautical Research Laboratory Wright-Patterson AFB, Ohio	
ARC, Mr. Karl Scheller	2

	No. of Copies
AF Office of Scientific Research Washington 25, D. C. SRHP, Dr. J. F. Masi	2
Commander AFSC Foreign Technology Division Wright-Patterson AFB, Ohio FTD (TD-E3b)	2
Defense Document Center Cameron Station Alexandria, Virginia 22314	2
Air Force Flight Test Center Edwards AFB, California Curt Lundblad	2
Department of the Army Office Chief of Ordnance Washington 25, D. C. ORDTU, Mr. H. Jersin	2
Commanding Officer Army Research Office (Durham) Box CM, Duke Station Durham, North Carolina Technical Library	2
Commanding Officer Picatinny Arsenal Liquid Rocket Propulsion Laboratory Dover, N.J. Technical Library	2
Bureau of Naval Weapons Department of the Navy Washington 25, D. C. RMMP-24	2
Commander U.S. Naval Ordnance Test Station China Lake, California Mr. Powell Jenkins	2

	No. of Copies
Director (Code 6180) U. S. Naval Research Laboratory Washington 25, D. C.	
Mr. H. W. Carhart	1
Technical Library	2
Department of the Navy Office of Naval Research Washington 25, D. C.	
Power Branch	1
Aerojet-General Corporation Sacramento Plants, P. O. Box 1947 Sacramento 9, California	
Mr. R. G. Weitz Head, Technical Information Office	1
Aeronutronic Division of Philco Ford Road Newport Beach, California	
Library	1
Air Reduction Company, Inc. Murray Hill, New Jersey	
Mr. Fred Balcar	1
Armour Research Foundation Illinois Institute of Technology Chicago, Illinois	
Mr. C. K. Hersh, Chemistry Division	1
Bell Aerosystems Box 1 Buffalo 5, New York	
Mr. T. Reinhardt	1
General Electric Company Rocket Propulsion Units Building 300 Cincinnati 15, Ohio	
Library	1
Marquardt Corporation 16555 Saticoy Street Van Nuys, California	
Mr. F. Morris	1

	No. of Copies
New York University Dept. of Chemical Engineering New York 53, New York Mr. P. F. Winternitz	1
Purdue University Lafayette, Indiana Mr. M. J. Zucrow	1
Reaction Motors Division Thiokol Chemical Corporation Denville, New Jersey Library	1
Rocketdyne North American Aviation, Inc. 6633 Canoga Avenue Canoga Park, California Mr. J. Silverman	1
TRW Redondo Beach, California Library	1
Thiokol Chemical Corporation Redstone Division Huntsville, Alabama Technical Director	1
Air Products and Chemicals, Inc. P.O. Box 538 Allentown, Pennsylvania Dr. Clyde McKinley	1
Aerospace Corporation P.O. Box 95085 Los Angeles 45, California Dr. D. H. Loughridge Dir. Applied Res. Management	1
United Technology Corporation P.O. Box 358 Sunnyvale, California Technical Library	1
Dr. Robert Cannon Department of Aeronautics & Astronautics Stanford University Stanford, California	1

	No. of Copies
Dr. J. Lowen Shearer Pennsylvania State University University Park, Pennsylvania	1
Mr. George Work Hughes Research Laboratory Malibu, California	1
Mr. Utter Hughes Aircraft Company Culver City, California	1
ATD Files	61